Nuno Ricardo Pereira Bastos

Controlo de uma plataforma servo-hidráulica com cinemática paralela para estampagem incremental

Control of a servo-hydraulic platform using parallel kinematics for incremental forming

Nuno Ricardo Pereira Bastos

Controlo de uma plataforma servo-hidraulica com cinemática paralela para estampagem incremental

Control of a servo-hydraulic platform using parallel kinematics for incremental forming

Dissertação apresentada à Universidade de Aveiro para cumprimento dos requesitos necessários à obtenção do grau de Mestre em Engenharia Mecânica, realizada sob a orientação científica dos Doutores Jorge Augusto Fernandes Ferreira, e Ricardo José Alves de Sousa, ambos Professores Auxiliares do Departamento de Engenharia Mecânica da Universidade de Aveiro.

O júri / The jury

Presidente / President

Prof.Doutora Mónica Sandra Abrantes de Oliveira Correia
Professora Auxiliar do Departamento de Engenharia Mecnica da Universidade de Aveiro

Vogais / Committee

Prof. Doutor António Manuel Ferreira Mendes Lopes
Professor Auxiliar do Departamento de Engenharia Mecânica da Faculdade de Engenharia da Universidade do Porto

Prof. Doutor Jorge Augusto Fernandes Ferreira
Professor Auxiliar do Departamento de Engenharia Mecânica da Universidade de Aveiro (Orientador)

Agradecimentos / Acknowledgements

Primeiramente gostaria de agradecer aos meus orientadores, o Professor Jorge Ferreira e o Professor Ricardo Sousa, por todo o apoio e disponibilidade prestado durante toda esta árdua maratona designada de dissertação de mestrado.

A todos os meus Professores com quem direta e indiretamente estive envolvido no meu percurso académico, por me terem transmitido os seus vastos conhecimentos, por me transformarem numa pessoa com formação e terem contribuído para o meu crescimento como indivíduo. Um agradecimento especial à diretora de Curso, a Professora Mónica Oliveira pelo esforço conjunto durante a minha atividade na Comissão de Curso do MIEM, sempre zelando pelo melhor dos interesses dos alunos. Também um agradecimento ao Mestre António Festas.

Um especial obrigado ao Miguel Martins, tanto a nível profissional como pessoal pela colaboração e conselhos prestados durante a primeira fase da minha dissertação e por toda a alegria por ele proporcionada. Uma palavra de agradecimento também ao colega João Sá de Farias pela sua boa disposição e pelo conhecimento transmitido. Ao pessoal do GRIDS pelo companheirismo durante esta etapa.

Os meus colegas de curso e de infância um especial agradecimento, por terem estado presentes na minha vida durante estes anos e ter partilhado experiências inesquecíveis.

Por último, mas no menos importante, agradecer à minha família pelo apoio prestado durante toda a minha vida. Também um agradecimento especial ao meu irmão e à minha cunhada por terem me suportado de forma relevante todo o meu percurso académico e me terem tornado numa pessoa mais responsável.

Palavras-chave

Plataforma de Gough-Stewart; Estampagem Incremental; Cinemática Paralela; Controlo de Posição; Controlo de Velocidade; Controlador lógica difusa, PID.

Resumo

SPIF-A é um projecto inovador sobre uma plataforma de Gough-Stweart com cinemática paralela para estampagem incremental que abrange inumeras áreas da engenharia. É um trabalho de longa data composto por uma equipa de profissionais entre professores, estudantes e investigadores que visa estimular o conhecimento científico. A estampagem incremental está muito em voga uma vez que as suas vantagens são tremendas. Dentro desta, destaca-se a estampagem incremental de alta velocidade.

O objetivo é então o contrôlo de uma plataforma Gough-Stewart, planeamento e execução de trajetórias ISO. Para isso, é feita uma revisão do estado da arte sobre estampagem incremental, plataformas paralelas, cinemática paralela e teoria de controladores. São desenvolvidos e implementados controladores de posição e definidas trajetórias para um manipulador de 6 graus de liberdade. São levados a cabo testes de precisão e fiabilidade do hardware do manipulador tendo em vista a sua melhoria futura.

Uma série de controladores, baseados em lógica difusa e um controlador PID linear, foram estudados e testados durante a implementação do novo hardware na plataforma tendo em conta a melhoria de todo o seu sistema de controlo.

Keywords Gough-Stewart Plataform; Incremental Forming; Parallel Kinematics; Position Control; Velocity Control; Fuzzy Logic Controller, PID.

Resumo

SPIF-A is an innovative project about Gough-Stewart platform using parallel kinematics for incremental forming that is supported by different fields of engineering. It is a long term work composed by a professional team that includes professors, students and researchers fancying to improve and contribute for scientific knowledge. Incremental forming is emerging due to its useful advantages, highlighting the high-speed machining.

The objective is the control of a Gough-Stewart platform, planning and execution of G-code trajectories. Thereunto, a state-of-the-art regarding incremental forming, parallel platforms, parallel kinematics and control theory is carried out. Position controllers and trajectory planning are developed and implemented for a 6 degree-of-freedom manipulator. Accuracy and reliability tests are done to consummate an hardware improvement.

Some types of controllers, based in fuzzy logic and one linear PID, were studied and executed on this platform in order to improve its control system.

"Failure is the condiment that gives success its flavor."

Truman Capote
(September 30th 1924 — August 25th 1984)

Contents

List of Tables

List of Figures

List of Acronyms

ADC Analog Digital Conversion

CAD Computer Aided Design

CAM Computer Aided Manufacturing

CNC Computer Numerical Control

DOF Degree-of-Freedom

FIS Fuzzy Inference System

FLC Fuzzy Logic Controller

FMS Force Measuring System

GCS Global Coordinate System

GUI Guide User Interface

ISF Incremental Sheet Forming

LC Load Cells

LCS Local Coordinate System

MIMO Multiple Input Multiple Output

MISO Multiple Input Multiple Output

PID Proportional-Integral-Derivative

PKM Parallel Kinematics Machine

RC Resistor-Capacitor

SKM Serial Kinematics Machine

SPIF Single Point Incremental Forming

SPIF-A Single Point Incremental Forming - Aveiro

SIMO Simple Input Multiple Output

SISO Single Input Single Output

TCP/IP Transmission Control Protocol - Internet Protocol

UPS Universal-Prismatic-Spherical

List of Symbols

P_{req} - Power Required

Q_t - Flow Rate

P_t - Pressure

η_t - Efficiency

A_c - Cylinder Bore Area

v_{max} - Maximum Velocity

d_{bore} - Bore Diameter

$\dot{m}_{wcs}$ - Flow (worse case scenario)

w_c - Cut-off Frequency

f_c - Cut-off Frequency

R_{rc} - Resistor in RC Circuit

C_{rc} - Capacitor in RC Circuit

kr_{top} - Circumference Radius in Top Platform

kr_{bot} - Circumference Radius in Bottom Platform

θ_{top} - Vertex Angles in Top Platform

θ_{bot} - Vertex Angles in Bottom Platform

K_{top} - Vertex Points in Top Platform

K_{bot} - Vertex Points in Bottom Platform

R_{top} - Top Platform Transformation Matrix

C_{3D} - Desired Three Dimensional Coordinate

ZP - Zero Part Offset

α - Yaw Euler Angle

β - Pitch Euler Angle

γ - Roll Euler Angle

R_{RPY} - Euler Transformation Matrix

h_i - Distance between top and bottom platform

L_t - Tool Length

h_t - Spindle System Length

F_{pos} - Fake Position

R_{pos} - Real Position

C_L - Cylinder Length

L_i - Actuator Length

C_i - Initial Cylinder Length

J^{-1} - Inverse Jacobian Matrix

F_{ef} - End-Effector Forces

σ_{af} - Actuator Forces

K_e - Error Gain

K_{de} - Error Derivative Gain

KU - Ultimate Gain

Chapter 1

Introduction

A brief summary and contextualization of the project where this thesis is inserted. Here, goals and achievements are explained and, at the end, there are given some orientations for reading the present document attached with a brief synthesis on the top of every chapter.

Perhaps, the first example of a human made device designed to manage power is the hand axe, made by chipping flint to form a wedge. The idea of a simple machine originated with the Greek philosopher Archimedes around the 3rd century BC, whos studied the Archimedean simple machines: lever, pulley, and screw [1].

Since the industrial revolution, there is a demanding for product quality and reducing manufacturing costs. The product quality entirely depended of the craftsman's skill, and the product cost is high. Ford Motor Company in 1905 introduced the concept of *mass production*. In this environment most of the manufacture is carried out by specialized machines that drastically reduces the production time and cost. The term *Hard Automation* explains the fact that every time a new model sets in, all the production line needs to stop and retooled inducing extra expenses. *Robot manipulators* have been introduced by manufacturing industries in order to perform predetermined (Programmed) tasks or multitasks. Once these machines are computerized and controlled by microprocessors, each time the model changes all the manipulators are quickly reprogrammed to do new tasks without the need for machinery replacement. This type of automation is called *Flexible Automation*.

1.1 The SPIF-A Project

The Division of Plastic Forming Simulation (DiPForm) from University of Aveiro is developing a machine [2] since 2010 in order to do single point incremental forming (SPIF) operations. The team is composed by students and teachers/researchers working in different areas of engineering.

In 2010, Sonia Marabuto gave the very first impulse of the project by studying the development of a machine for SPIF operations [4]. Other kind of research was done by

Miguel Martins by projecting and build a machine for incremental forming [6] shared by José Sena who have simulated and studied SPIF operations on ABAQUS software [7]. Later, João Torrão steps into the project and develops/execute the first controller [5].

This machine, so as the project, is denominated by Single Point Incremental Forming - Aveiro, since it is being carried out at the Department of Mechanical Engineering of the University of Aveiro.

This machine is custom made using a Gough/Stewart platform with six cutting edge hydraulic cylinders providing 6 degrees of freedom (DOF) and being capable of apply high loads [2]. Since its beginning, many technologies have been implemented and upgraded to increase the performance of doing SPIF operations.

1.2 Motivation and Goals

On the last several years, parallel platforms have been used to perform many kinds of different processes due to its flexibility and strength. This type 6 DOF manipulator is being studied by many authors and it is considered multifaceted.

The motivation for this work lies on the capability of taking the advantage of using parallel platforms to do SPIF operations by improving its current kinematics control and implement other types of controllers and hardware upgrades. Therefor, the initial goals outlined for this thesis are:

- Improvement on the inverse and forward kinematic system in order to perform 6 DOF operations.
- Design a new controller to improve position accuracy regarding working loads.
- Generate and execute 3D trajectories from CAD/CAM software.
- Trajectory evaluation using forward kinematics.
- Implement of hardware upgrades on the present machine.

1.3 Reading Guide

This dissertation is organized in eight chapters, being this the first one. Hereinafter, a small brief about each chapter is presented so as in the beginning of each one right after the title.

- **Chapter 1** - A brief summary and contextualization of the project where this thesis is inserted. Here, goals and achievements are explained and, at the end, there are given some orientations for reading the present document attached with a brief synthesis on the top of every chapter.

- **Chapter 2** - An approach to single point incremental forming and its advantages. Historical contextualization about Stewart-Gough platforms and its divergences regarding serial manipulators. Examples of SPIF machinery used in the literature in presented.
- **Chapter 3** - A perspective about the machine where this work is implemented regarding its parallel platform as well as some of its hardware features such as the hydraulic system, instrumentation, operative system and manufacturing procedure is presented.
- **Chapter 4** - Deduction of the inverse kinematics for the SPIF-A machine as a parallel platform with six degrees-of-freedom. The implementation and further adaptation of an existent model for direct kinematics is described. The machine's workspace regarding its kinematics is computed. Differential kinematics for end-effector speed and actuator forces is presented. A discussion about singularities on parallel platforms is given.
- **Chapter 5** - The development of online and offline software implemented on the machine for motion control and visualization is described. The algorithm and preprocessing apparatus used to describe various types of motions is mentioned, as well as the built operator interface is presented.
- **Chapter 6** - A brief introduction about PID and fuzzy logic controllers is given as well as its design and implementation both with anti-windup system.
- **Chapter 7** - Experiments and its results that were carried out on the machine regarding the chosen type of controllers are illustrated. The SPIF parts produced on the machine and its capability on motion accuracy is also demonstrated. A results discussion is given at the end.
- **Chapter 8** - Final considerations about the developed work on the present dissertation is given. Some future work is presented in order to continue the machine's development. Earned skills and other relevant information, such as the machine's recognition on media, is sighted.

Chapter 2

Literary Review

An approach to single point incremental forming and its advantages. Historical contextualization about Stewart-Gough platforms and its divergences regarding serial manipulators. Examples of SPIF machinery used in the literature in presented.

2.1 Introduction

"A robot is a re-programmable multi-functional manipulator designed to move materials, parts, tools, or specialized devices, through variable programmed motions for the performance of a variety of tasks."

by Robotics Institute of America

Nowadays, there is an increasingly demanding need of development for manufacturing techniques that have changed the way how people produces parts over the time. Since industrial revolution in the 18th century, great advances have been made in the automation of various activities that were primarily made by hand. For sure, the insertion of machinery in every day life has stimulate people for scientific progresses. Today, many authors and research groups uses either serial or parallel robots/manipulators to do their experiments looking for new methods and improvements in the scientific community. As an example of that, SPIF is a recent technology that many people are interested on developing and use its advantages for manufacturing parts. Using either a serial or parallel manipulator, researcher groups adapts this kind of machinery to perform their experiments. Said that, industrial revolution and the expansion of automation systems are responsible for many research that are known today. Huge steps were achieved in the past by sharing daily life with robots that are programmed by humans to perform a variety of tasks, in the name of science.

2.2 Single Point Incremental Forming

Mechanical industry is constantly demanding for new technologies capable of improving the existent and well known methods that are used nowadays. Improving competitiveness means achieving more with less resources and SPIF is being studied and used by some researchers and institutions to find a more cheaper and versatile way of doing incremental sheet forming (ISF). The most used process for sheet forming is Die/Punch which is very expensive and limited by the geometry of the forming part. For every different part, new die and punch are required to complete the process for being possible to form the new part. So, in 1967 Edward Leszak [3] patented an innovative and alternative process to die/punch know as Incremental Dieless Forming. Since then, SPIF is being studied but only during the last decade has been truly used in experiments due to the fast advance is machinery, automation and control.

Many institutions and researchers adopted the idea of adapting a conventional CNC milling machine for SPIF operations but it results in a limited range of applications in terms of materials and geometry. The market dedicated for ISF is yet small and embryonic resulting in costly parts and unattractive for industry. Also, lack of geometrical accuracy and long forming times are contributing for a slow impulse of ISF industry. The current project SPIF-A, where this dissertation is based on, depicts in a development of a new machine capable of overcome some of the limitations from the adapted CNC machines that are currently being used.

2.2.1 SPIF Description

Single Point Incremental Forming is a simple process but innovative that is capable of producing non-asymmetric parts requiring simple tools and a metal sheet. Usually, the tool is a cylindrical metal with flat or spherical hardened tip to prevent wearing which moves along the metal sheet that is restrained on a blank holder with a clamping frame. Dies with the shape of the part are not required for this process, however, there is a need for a backing plate (easy to obtain) that will help to acquire initial formability (see Figure 2.1).

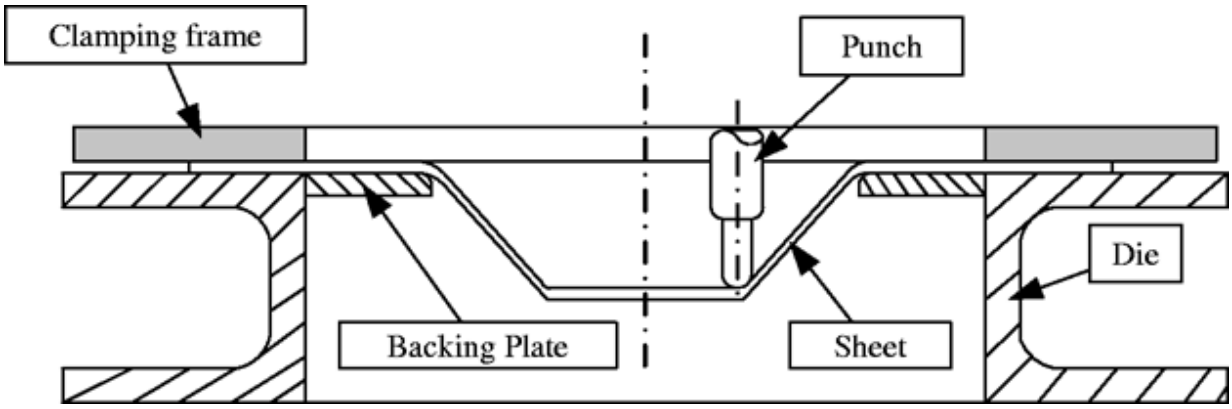

Figure 2.1: Prime components for Single Point Incremental Forming [45].

The deformation is held by applying pressure on the surface of the metal sheet through the metal tool that forces an incremental deformation.

Acording to Jeswiet et al. [20], SPIF presents some advantages and disadvantages as follows:

Advantages:

- SPIF operations are quiet and substantially free of noise adaptable to a conventional lathe or CNC machine.
- High flexibility, forming part and shape is easily changed without the need of new die and tool, once it is a dieless process.
- Directly from CAD, parts can be produced without the need of any specialized tool. Part size is only limited by the machine's available working space.
- Rapid Prototypes can be easily achieved by using SPIF, which is much harder using other process.
- Bending-Stretch and it's incremental nature of the process lead to an increased formability.

Disadvantages:

- Small production batches are achieved in comparison to deep drawing or other counter technologies due to it's long forming time.
- Multi-steps is required to produce 90°angles, it cannot be done in a single step.
- Along the process, springback is always occurring and demanding for correction algorithms that are being developed by Meier et al [21].

2.2.2 SPIF Machinery

As said before, many researchers opt by adapting CNC milling machines for ISF operations. Exception made to Amino Corporation [46] or by Julian Allwood's group at Cambridge University [47] that developed their own SPIF machinery, as illustrated in Figure 2.2 b). Some researchers are also considering serial kinematics robots in order to perform SPIF operations. There are plenty of examples developed by other group of researchers, such as, Duflou et al. [48], as well as Shim & Park [49], Fratini et al. [50], Filice et al. [51], Ceretti et al. [52] and Ambrogio et al. [53].

University of Oporto also has its own adapted machine to perform SPIF operations. Suriyaprakan [72] used that machine to study multi-stage incremental forming on aluminium alloy 1050, as shown in Figure 2.2 a).

Most of adopted CNC milling machines are 3-axis due to it's stiffness and high speed machining for extended production rate. Usually, the tool path is processed by CAD/CAM software that contains all the information about the part geometry. The sheet metal is

(a) University of OPorto ISF machine [72]

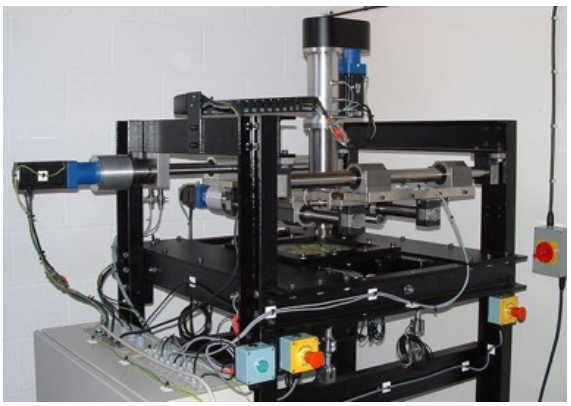

(b) Cambridge ISF machine [47]

Figure 2.2: University of OPorto and Cambridge ISF machine.

normally attached to a adapted forming table (see Figure 2.1) that can have translational motion in the X,Y and Z axis. Depending of the adopted CNC milling machine, this motion can be obtained either by the forming table or tool.

Figure 2.3: Serial manipulator to perform SPIF operations [21].

Serial kinematics manipulators is an alternative to the CNC milling machines considered by some authors that use this kind of machine to perform their SPIF operations (see Figure 2.3). High flexibility and 6 degrees-of-freedom are the main attractive characteristic to use these manipulators for tool positioning. In other hand, it fails by the small capacity of supporting lateral forces and low tool positioning due to its cumulative link position error. The adaptation to ISF process on serial manipulators is very similar to the one performed by CNC milling machines in terms of hardware requirements. Given the CAD model of the forming part, the model is divided in horizontal layers in the CAM software and therefore the tool path is generated. Figure 2.4 shows some of the machinery, CNC milling machines and serial manipulators, used to perform SPIF operations.

Figure 2.4: Machinery for performing ISF. From left to right: Adapted CNC milling machine by Ambrogio et al. [53], Amino's purpose built machine [46] and serial manipulator used by Strano [55].

A clamping frame must be added to the table in order to fix the sheet metal (see Figure 2.5 b)). Continuous springback during the SPIF operation prejudice its final produced geometry. Cutting oriented software has been largely demonstrated by some authors, for instance by Meier et al. [54], large dimensional errors in the final part. Correction algorithms are crucial and demanded to avoid dimensional deviations in the SPIF process. For this reason, continuous sprinback is one of the most important topcis in study on ISF research.

Despite the straightforward adaptation from serial manipulators and CNC machines, due to its limitations of low capacity for lateral forces and cumulative link errors, ISF literature focus on low strength materials such as aluminum, polymers or high strength materials but with very limited sheet thickness. Callegari et al. [73] used a tricep manipulator, as illustrated in Figure 2.5 a), to discover the advantages of robotised cells vs. CNC machines.

(a) Tricep [73] (b) SFB/TR73 [74]

Figure 2.5: Tricep and the SFB/TR73 adapted milling machine for SPIF operations.

2.2.3 SPIF Forces

The forming forces involved on this process are one of the most important aspects of the deformation process. Allwood et al. [22] opted to divide their analyses in two different tool loading situations, as illustrated in Figure 2.6. The author states that the forces involved on SPIF process can be predicted using an approximate calculation by a theoretical model. If the tool moves normally to a flat sheet, it causes a hemispherical indentation of the sheet. In other hand, if the tool moves tangent/horizontally to the deformed area, it creates a one-side groove.

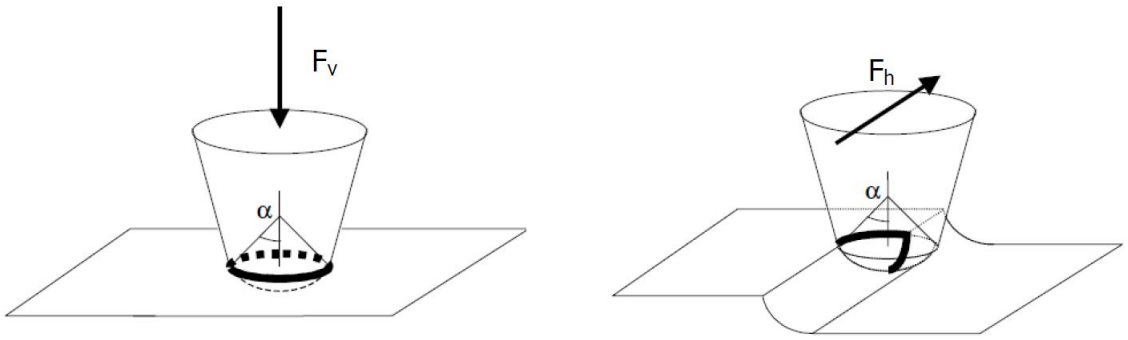

(a) Hemispherical indentation (b) One-sided groove

Figure 2.6: Vertical and horizontal load situations [22].

Many researchers developed experimental and numerical simulations in order to achieve the forces in SPIF process. In Table 2.1 shows some of the forces estimated/measured by different researchers. However, there are different parameters between each experiment or simulation that entirely changes the amount of forces needed on the process. Parameters such as different materials, blank thickness, tool diameter, step size, toolpath, etc. were chosen to best suite each particular case.

Table 2.1: Measured/Estimated SPIF forces by different researchers.

Researchers	SPIF Force [kN]	Method
Allwood et al. [22]	13 (Vertical) and 6.5 (horizontal)	Theoretical
Duflou et al. [23]	1.46	Experimental
Rauch et al. [56]	0.9	Experimental
Jackson et al. [57]	3	Experimental
Durante et al. [58]	2	Experimental
Bouffioux et al. [59]	1.3	Simulation
Decultot et al. [60]	12	Experimental
	14	Simulation

2.2.4 SPIF Applications

There is a vast field of applications for Single Point Incremental Forming. From aerospace, automotive to home appliances or even medical proposes, there are some examples where this technology can be implemented. With help of CAD/CAM software is possible to get complex forms plus the possibility of using several different materials such as aluminum, steel, composite and polymeric material. It is ideal for rapid prototyping combined with reverse engineering to replace incomplete or unique parts. Presented by Allwood et al. [22], some parts obtain by SPIF can be seen in figure 2.7.

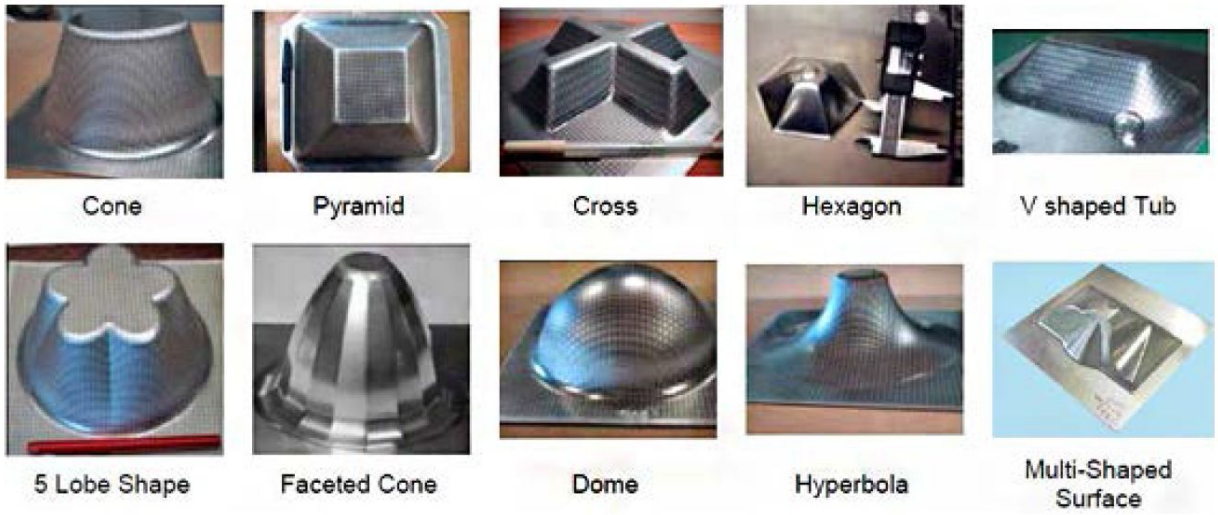

Figure 2.7: Panoply of parts obtained by SPIF Manufacturing [22].

Example of medical purposes, Duflou et al. [23] studied and manufactured a cranial implant using reverse engineering from his patient's skull. Afterwards, his missing skull part was raised from a single aluminum sheet, as shows figure 2.8.

Figure 2.8: Cranial implant produced using SPIF technology [23].

Some other applications, see Figure 2.9, for automotive industry where SPIF was implemented to create an heat/vibration shield and a silencer housing for trucks.

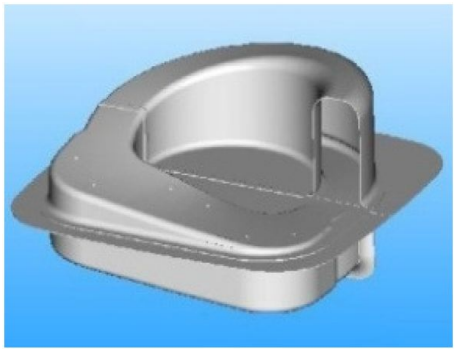

(a) Automotive heat/vibration shield [24]

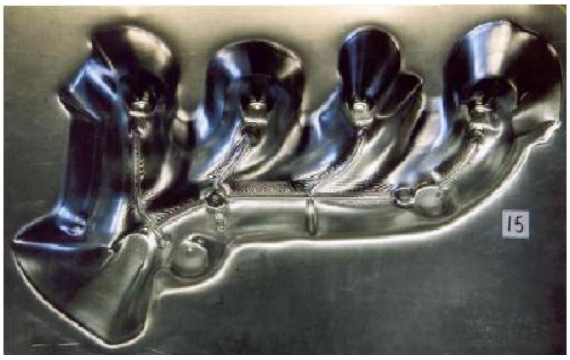

(b) Silencer housing for trucks [25]

Figure 2.9: Other applications for SPIF technology.

2.3 Conception of a parallel structure for SPIF operations

At the University of Aveiro, Marabuto et al. [2] carried a discussion about constructing a parallel platform to perform SPIF operations. Their motivation was based in the literature where other research groups use either serial kinematics manipulators or adapted CNC milling machines to do their experiments. However, this group of researchers wanted to avoid the limitations of such machines and studied the implementation of an parallel structure with 6 degrees-of-freedom. With higher stiffness and lower position errors regarding high loads, the research group concluded that there are many advantages in building a Gough-Stewart platform to do SPIF operations. Therefore, the SPIF-A machine was built in the University of Aveiro which is the machine where this thesis is related. It is currently patented being the first parallel machine to perform SPIF operations in Portugal.

2.3.1 The Gough-Stewart platform

Stewart-Gough parallel platform is well known in scientific community and in the world of Parallel Kinematics Machines(PKM) for its simple, very robust and attractive design whose platforms are connected using UPS (Universal-Prismatic-Spherical) joints.

Despite being aesthetically simple, looking at its mathematical apparatus, designated as Articulated Octahedron [30], it is way more complex. Consists in two rigid parallel platforms, one of them fixed and the other one mobile being capable of gesticulate around its 6 DOF: lateral, longitudinal and vertical linear movement (X,Y,Z) and respective axis rotation usually called as Roll, Pitch and Yaw that together represents the three Euler angles. These two rigid platform are finally connected through six links that can vary its length, it can be either hydraulic, pneumatic or electrical actuators. Augustin Louis Cauchy during the 19th century studied this model and its advantages but the first machine for real applications was built by Eric Gough, a British automotive engineer, around early 1950s

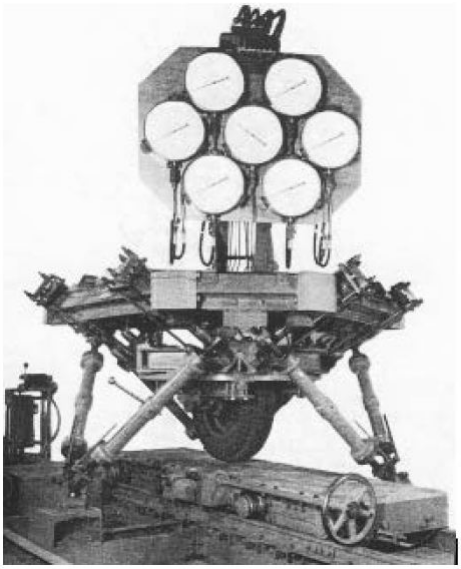

Figure 2.10: Gough Universal Rig [31].

based on Cauchy's model [31]. That machine named as Universal Tire-Testing Machine at Birmingham's Dunlop tire factory, uses six hydraulic jacks as actuators to move the platform known as synergistic motion and it was a successful machine.

D. Stewart later published Gough's design in 1965 to the Institution of Mechanical Engineers, arguing its application as an flight simulator [32]. Later, this innovative technology was adapted for 5 axis milling machines [33] and due to its design and regarding the six legs, the term "Hexapod" was trademarked by Geodetic Technology [34]. Today, is well known as Gough-Stewart platform and is widely used in many applications, some of them are illustrated in the appendix F. This dissertation is based on this parallel platform and its advantages for Single Point Incremental Forming.

2.3.2 Parallel Robots vs Serial Robots

In general, parallel robots can be defined as a closed-chain mechanism whose the end effector is attached to the base by several independent kinematics chains [8]. There are plenty of possible configurations for parallel robots but the most used and studied is the Stewart-Gough platform that is constituted by two platforms (fixed and mobile) generally connected by six linear actuators (Prismatic articulation) that are assembled through universal and/or spherical joints. Therefore, this configuration is usually denominated as 6 DOF-UPS (6 degrees of freedom with universal, prismatic and spherical joints) mechanism.

This kind of configuration for parallel robots has some advantages compared to robots with series kinematics, such as:

- **Load capability** —It is able to manipulate loads that are higher than its own weight. The load in the mobile platform it is distributed by the 6 actuators in a way that each

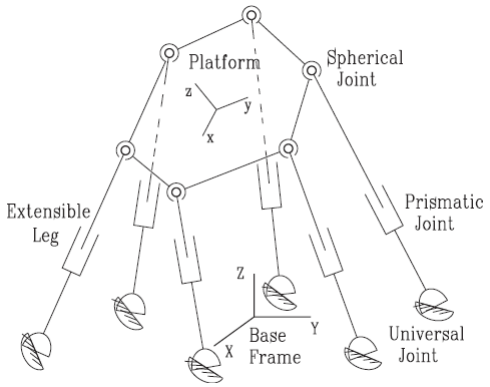

Figure 2.11: The 6-UPS Stewart Platform [9].

one only supports a fraction of the total load, conferring an high efficient machine.

- **Higher Accuracy** —In serial kinematics manipulators (SKM), positioning error increases with the number of joints between the base and the end-effector. Due to the configuration of the 6 actuators in parallel robots, the error accumulation is lower than in conventional series robots.
- **Higher Velocity** —Despising the load in the mobile platform, it is much easier to the actuators to move because the inertia in each link is lower.
- **Degrees of Freedom** —Achieving 6 DOF in series robots implies adding more links to the kinematics chain, this is not required in parallel configuration.
- **Higher Stiffness** —Parallel manipulators are also known to have higher stiffness compared to serial manipulators. Contrary to serial configurations, the higher number of links the higher stiffness on parallel structures.

However, parallel manipulators has some disadvantages:

- **Complex Kinematics** —Parallel mechanism often represents complex kinematics solutions and there are no generalized model in opposition to series mechanism where most of the series kinematics follows through an certain solution pattern.
- **Singularities** —The analysis of singularities in the kinematics chain is much more complicated and it depends of the adopted parallel configuration.
- **Working Space** —Reduced working space and complex to compute.

The main difference between SKM's and PKM's is its kinematics chain. In serial systems, each actuator concerns on its own position and it is nominated only to one axis. Simpler mechanical structures and control technology is achieved by this approach. However, this *stacked* systems tends to add errors and therefore, its accuracy is lower than

parallel systems. Unlike serial configuration, all actuators act on the same platform improving accuracy and generates a low inertia system. Alongside, compact structure can be obtained with less friction but very demanding on control complexity and it requires much more expertise than serial kinematics.

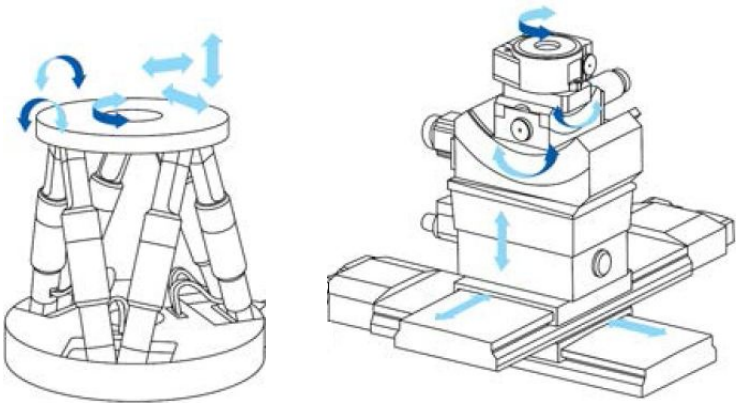

(a) Parallel Position Manipulator

(b) Serial Position Manipulator

Figure 2.12: Parallel and Serial Positioning Manipulators [5].

Chapter 3

SPIF-A Machine

A perspective about the machine where this work is implemented regarding its parallel platform as well as some of its hardware features such as the hydraulic system, instrumentation, operative system and manufacturing procedure is presented.

The SPIF-A research project [2] decided to build a Gough-Stewart platform regarding the requirements for SPIF operations that were demonstrated in Chapter 2. In order to achieve a machine capable of performing all the required SPIF operations in terms of position accuracy and load capability, the initial research conducted by Marabuto [4] concluded that the best option was a six linear parallel platform. This machine, see Figure 3.1, is placed at the welding/stamping laboratory on the department of Mechanical Engineering at the University of Aveiro.

(a) (b)

Figure 3.1: Actual SPIF-A machine.

3.1 Machine Parallel Platform

The SPIF-A machine is enhanced with a Gough-Stewart parallel platform regarding a 6-6 configuration, implemented by Miguel Martins [6] during his dissertation. It consists in two platforms being one of them fixed to the machine's structure (top platform) and the other one is movable (mobile platform). In this kind of PKM's, the top and mobile platforms are connected by the six hydraulic servo-actuators each one of them has one universal joint attached to each end. However, these U-joints are limited to a maximum rotational limit of 45° in either direction. The servo-actuators are responsible for conferring movement to the mobile platform as well as the necessary force to make it happen regarding external disturbances. These servo-actuators are constituted by a magnetostrictive linear transducer, servo-solenoid valve and a hydraulic cylinder with low friction hydrodynamic seals for a precise motion control and feedback. At maximum allowed pressure (210 bar), one hydraulic actuator can perform a maximum force of 65.4 KN while extending length and 32 KN while shortening length. The spindle system, that is composed by a tool holder and a shaft where the tool is connected, are attached to the mobile platform conferring the necessary hardware to perform SPIF operations. This spindle system was studied by Sonia Marabuto [4] and later implemented by Miguel Martins [6].

3.2 Hydraulic System

In order to move the hydraulic actuators, hence, the SPIF-A's Gough-Stewart platform, a hydraulic power system is need to supply enough hydraulic pressure and flow rate that are required for a smooth and well functioning of the entire platform. The maximum allowed pressure for these actuators are 210 bar. Ideally, higher pressure confers best performance and a stiffer system which is easier to control.

Figure 3.2: New hydraulic plant and its components.

Since its first appearance, the SPIF-A machine has passed through many hardware

implementations and essential upgrades for its well functioning. During this thesis, it was discussed and implemented hardware upgrades on the machine's hydraulic power system: An increase in the oil reservoir capacity, a variable displacement pump, an accumulator, a hydraulic fluid distributor, filters and other hardware. Due to the magnitude of flow rate needed on the machine, the oil reservoir was upgraded to 200 liters. Additionally, the hydraulic plant has a secondary independent system for hydraulic fluid cooling, enhanced with a heat exchanger.

The brand new hydraulic pump is a PVQ40 model. It has a maximum displacement of 40 cc/rev and was internally set to supply around 160 bar. Regarding the electrical motor already installed on the machine of 15 KW with 1500 rpm, the hydraulic pump characteristics based on manufacturing data is as follows:

- Flow Rate: Up to 60 liters per minute.
- Overall efficiency: Around 85%.
- Volumetric efficiency: Around 95%.
- Sound level: 68dB at full stroke.

This hydraulic pump is known to use the maximum power from the electrical motor at a constant pressure while at low sound levels. Its variable displacement is great to achieve a better performance from the hydraulic actuators. As known, at different situations these hydraulic actuators may require an increase or decrease in flow rate.

$$P_{req} = \frac{Q_t \cdot \Delta P_t}{600 \cdot \eta_t} \qquad [Kw] \tag{3.1}$$

Looking at the Equation 3.1, for a maximum power of $P_{req} = 15$ Kilowatts, a desired pressure $\Delta P_t = 160$ bar and an overall efficiency of the system $\eta_t = 0.75$, the highest achievable flow rate will be around $Q_t = 42$ liters per minute. Obviously, without an accurate value of η_t and depending of the actual performance of the existent electrical motor, Q_t will substantially vary. The overall efficiency of the hydraulic system η_t regarding the pressure drops between all the existent connections and hoses, mechanical efficiency and based on other components of the system, is predicted to be low and estimated to be around $\eta_t = 0.75$.

Basic math calculations can be done to determine the highest linear velocity of the platform on the worst case scenario. This case happens when all the six actuators are extending length at the very same time, i.e, the entire platform is moving on Z-Axis. However, such case will never happen during SPIF operations, only in manual motions. Let's consider $\dot{m}_{wcs_1}$ as the flow rate of one hydraulic actuator:

$$\begin{aligned} \dot{m}_{wcs_1} = \frac{Q_t}{6} &= v_{max} \cdot A_c \\ &= v_{max} \cdot \frac{\pi}{4} \cdot d_{bore}^2 \end{aligned} \tag{3.2}$$

Given $Q_t = 0.000703\ m^3/s$ and a bore diameter $d_{bore} = 0.063\ m$, the maximum linear velocity on the worst case scenario will be $v_{max} = 0.0375\ m/s$ or $v_{max} = 2250\ mm/min$. This linear velocity is merely for information. During SPIF operations, higher velocities will be certainly obtained.

The hydraulic fluid distributor is a key component to achieve a good performance on the actuators. It is important to make sure that the hydraulic resistance between the pump and each servo-valve is equal to substantially increase the performance of the actuator motion. Once there is no pressure and flow rate sensor at the entrance of each sensor, the actuators will act as if they were all under the same circumstances. There are no dynamic model of the platform, hence, the control is not based on the inlet pressure and flow on each actuator chamber. So, it is crucial to implement a device capable of distributing the flow among all the six actuators under homogeneous hydraulic resistances.

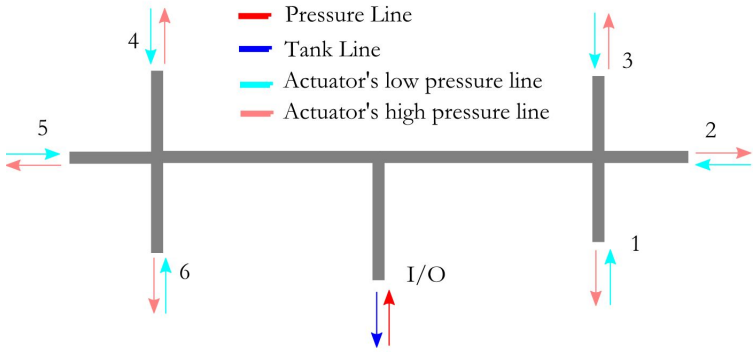

Figure 3.3: SPIF-A's older hydraulic distributor - scheme.

The older distributor on the SPIF-A machine is illustrated on Figure 3.3 and it was entirely made of "L", "T" and straight hydraulic junctions with multi-variable sections. Looking at the same figure, for instance, the output number six and one faces a double ninety degree junction, which will increase their pressure drops compared to the output number five or two. It was clearly visible and no doubt about it that there was a deficit of flow rate on some actuators during their motions. It's assorted flow rate causes instability to the parallel platform leading to uncontrolled movements at high actuator speeds. To overcome this mechanical failure, it was studied and designed a hexagonal shape distributor as show on Figure 3.4.

Its equally spaced six faces allows to have a homogeneous path from the input to the six output channels. More important than reducing the pressure drops on the entire hydraulic system, is to guarantee that each actuator receives the very same conditions as the other ones. With the same parameters, all actuators will act accordingly to each other, increasing their overall performance. The pressure and tank lines, P and T respectively, are connected on the top and bottom of the hexagon. The twelves hoses from the actuators are connected on the sides of the hexagon, accordingly to tank and pressure channels. Most important, the fluid that comes from the pressure line enters on the top of the hexagon and it is equally available to the six secondary channels that leads to the servo-solenoid valves. This way,

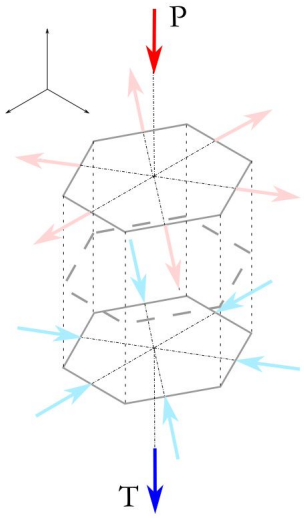

Figure 3.4: SPIF-A's new hydraulic distributor - scheme.

it is guaranteed a homogeneous hydraulic resistance between the main channel to the six secondary ones.

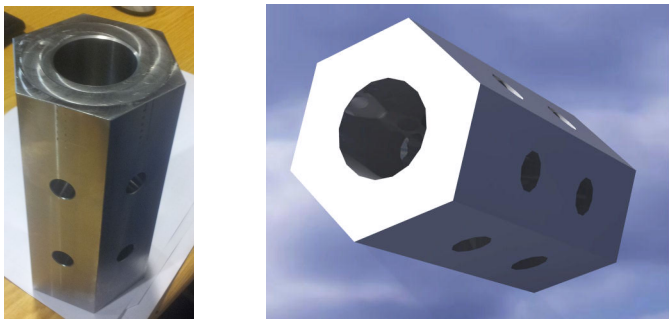

(a) Machined hydraulic distributor.

(b) Hydraulic distributor in CAD.

Figure 3.5: SPIF-A's new hydraulic distributor.

The hexagon distributor was carefully dimensioned to be compacted and it was machined in high strength steel to support the internal pressures on the walls and threads as shown in Figure 3.5. It was placed in the middle on the top platform (see Figure 3.6) as close as possible to the actuators. The original hoses that are connected to the actuators were cut to half of its initial length, hence, the fluid now travels a smaller path.

The machine's hydraulic system is also equipped with a hydropneumatic accumulator set at 120 bar ready to introduce extra flow rate on the pressure channel. Last but not the least, the hydraulic plant is also featured with pressure filters which is important to keep the hydraulic fluid clean so that the servo-solenoid valves are not damaged.

Figure 3.6: Hydraulic distributor placed on the SPIF-A machine.

3.3 Machine Instrumentation

The machine is currently equipped with some instrumentation essential for motion control and data acquisition such as force measuring system (FMS). Each hydraulic actuator is equipped with a magnetostrictive linear transducer (see Figure 3.7), that determines with high resolution (2 μm) the absolute length of the cylinder rod. The digital output signal is then read and converted by I/O modules on the xPC machine for further usage on feedback control.

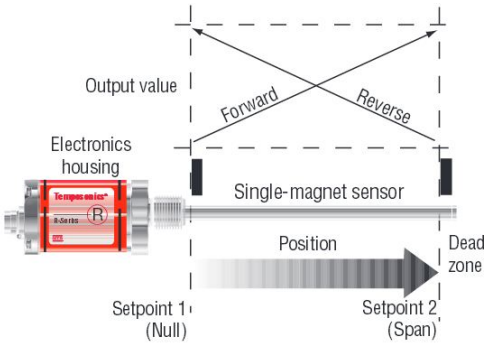

Figure 3.7: The magnetostrictive linear transducer.

For a proper control of the forming operation and for further analysis and studies, the machine is equipped with load cells for force acquisition. It was implemented and projected by Miguel Martins [6] and later Torrão [5] developed a method for force measuring on the tool edge during SPIF operations.

Despite the existent instrumentation available on the machine, during this thesis more instrumentation has been added. A pressure transducer (see Figure 3.6) was acquired and installed on the hydraulic distributor for data acquisition in real time. This pressure feedback helps to understand how the pressure varies while perform SPIF operations.

Every numeric control machine has its own digital or analog console to display or introduce determined data or tasks, such as manual data inputs, manual control, parameteriza-

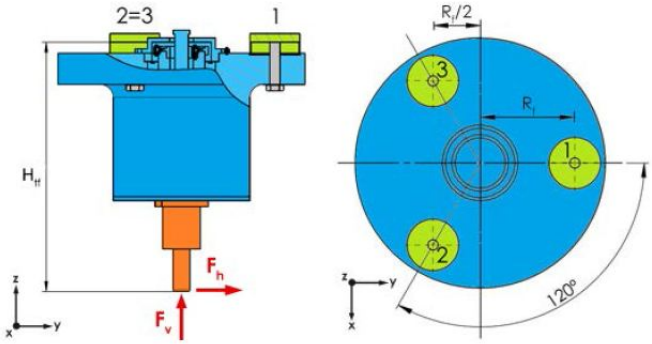

Figure 3.8: Spindle forces and load cell configuration [5].

tion among other options. SPIF-A machine has also its own analog console as illustrated in Figura 3.9. Through this console via analog input and output data is possible to control and specify some tasks on the SPIF-A machine.

Figure 3.9: SPIF-A's control console.

It is a hand made prototype with basic materials and gadgets. It is constituted by a joystick, variable potentiometers, pushbuttons, switch button, emergency button and a small block containing up to 15 individual keys. The joystick was dismantled and adapted from a conventional one. Its main function is to manually control the motion of the platform on all 6 DOFs. The idea behind this prototype is to be able to do manual basic tasks on real time on the machine. Some features of this console are directly connected to the xPC I/0 modules for real time operations and others are connected to the host computer for pre-processing operations. It has a cable of three meters long that allows the operator to move around the SPIF-A machine while performing tasks. One of its key element is the possibility for manual positioning which is great for settling zero part and tool approximation. Now, this console is capable of:

- Manual motion;
- Manual/Automatic mode switching;

- Emergency STOP;
- Speed control on automatic mode;
- Abort experience (If performing any).

There are yet options and buttons not assigned. It was recently made and it will go through optimization and performed to do some other tasks. However, it is a functional and essential device to the SPIF-A machine.

It was noticed that during the acquisition of the analog signal from the load cells, the FMS data was floating a lot even when the machine is stopped. This analog floating may be caused by external electrical disturbances, such as the switching power supply. To avoid or minimized these effects, it was studied and implemented a simple low-pass RC filter on every analog signal from the load cells.

The well-known Nyquist sampling theorem provides a prescription for the nominal sampling interval required to avoid aliasing so that there are minimum losses of information during the analog to digital conversion (ADC). The theorem states:

"The sampling frequency should be at least twice the highest frequency contained in the signal."

Said that, the sampling frequency on the SPIF-A machine is given by the xPC that runs one thousand times the Simulink^{TM} software per second, i.e, the sampling frequency is 1KHz. Hence, according with the Nyquist sampling theorem the signal spectrum should be limited to 500 Hz. In Figure 3.10 is illustrated the scheme of such filter.

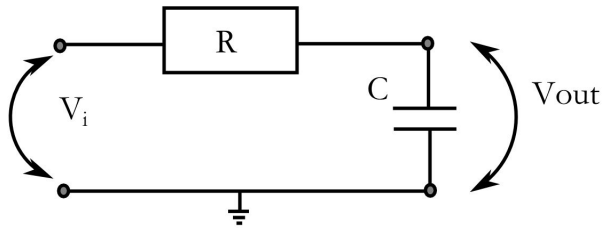

Figure 3.10: Scheme for a low-pass RC filter.

However, it is important to establish a cutting frequency F_c lower than 50Hz, which is the frequency used on surrounding power lines. A resistor of $R_{rc} = 4700\ \Omega$ and a capacitor $C_{rc} = 1\ \mu F$ was the choice to build this low-pass filter.

The cut-off frequency given R_{rc} and C_{rc} is

$$w_c = \frac{1}{RC} = 212.76 \qquad [rad/s] \tag{3.3}$$

or

$$f_c = \frac{1}{2\pi RC} = 33.86 \qquad [Hz] \tag{3.4}$$

The frequency response regarding the first-order low-pass RC filter is presented on the bode diagram shown in Figure 3.11.

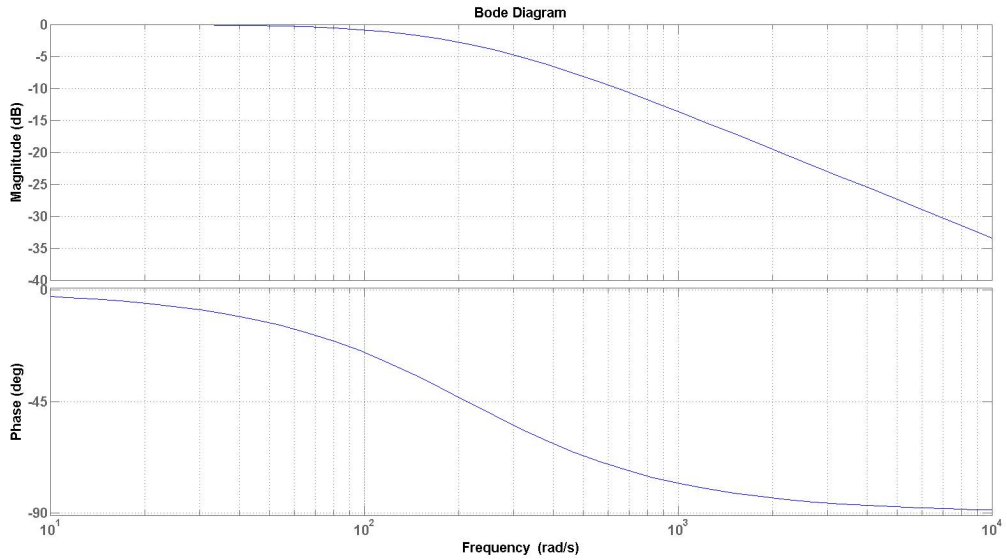

Figure 3.11: Bode diagram for the refereed low-pass RC filter.

3.4 Machine Operative System

Base operative system is held via Simulink™ and Matlab™ that can be managed by the host operator. The real time target machine is a Speedgoat™ SN1584, a brand whose equipment are developed with compatibility with Simulink™ and Matlab™ software. Therefore, it is easy to communicate and execute target tasks via xPC Target™ toolbox. The communication between the host and the real time target machine is carried by TCP/IP whose protocols are automatically implemented by Matlab™'s toolbox. The xPC target controller reads and writes information on the target machine by I/O modules installed on SPIF-A's hardware. These modules are responsible to acquire and transmit data from the cylinder's position transducers, load cells and servo-hydraulic actuators. It is also possible to command external objects such as bottoms, lights or switches through Simulink™ that controls/reads the I/O modules. In Figure 3.12 is illustrated the data flow between the host operator and SPIF-A machine through the Speedgoat™ target controller.

Figure 3.12: Data flow and communication apparatus between the host station and the SPIF-A machine.

3.5 Manufacturing Procedure

Alike any other machine, the SPIF-A machine also has its own manufacturing procedure. From part design to its manufacturing, there are some intermediate steps that need to be accomplished. Initially, the part geometry is idealized in a CAD platform and then sent to a CAM software where the tool path is created. After that, the CAM file is read and pre-processed, on the developed machine's software, by the operator. Consequently, all the data required on the machine is loaded and the part manufacturing takes place. The diagram below exemplifies the manufacturing procedure on the actual SPIF-A machine.

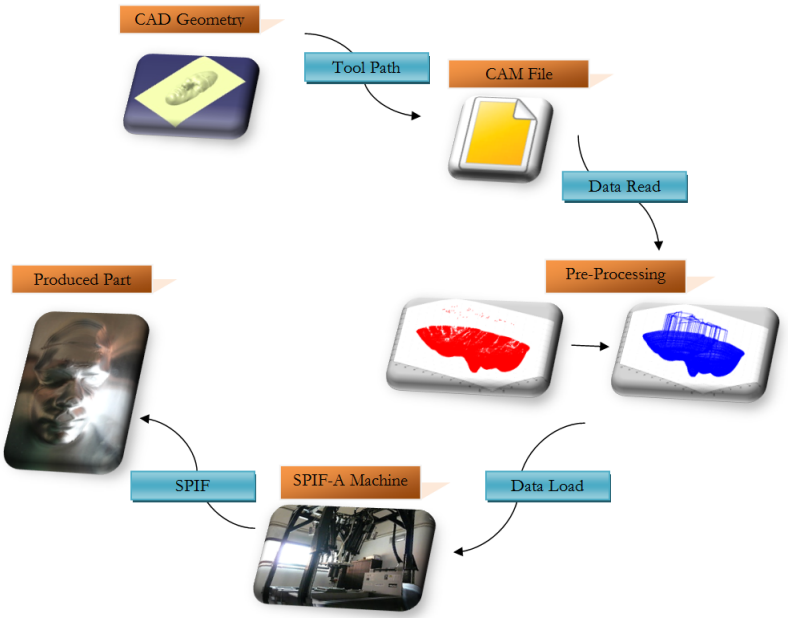

Figure 3.13: SPIF-A's manufacturing diagram.

Chapter 4

SPIF-A Kinematics

Deduction of the inverse kinematics for the SPIF-A machine as a parallel platform with six degrees-of-freedom. The implementation and further adaptation of an existent model for direct kinematics is described. The machine's workspace regarding its kinematics is computed. Differential kinematics for end-effector speed and actuator forces is presented. A discussion about singularities on parallel platforms is given.

During the late 1980s and early 1990s, forward kinematics in Gough-Stewart platforms enjoyed the central status in the research on these parallel manipulators. The forward kinematics of serial manipulators is straightforward while the inverse kinematics is complicated due to non-linear equations. In other hand, the inverse kinematics of such parallel platforms like Gough-Stewart is relatively easier but challenging about its forward kinematics. After the appearance of some solutions for the forward kinematics of Gough-Stewart platforms by some researchers, during 1990s there was a steady increase in research interest in the field of parallel manipulators for various applications and configurations. In 1995 alone, more than fifty papers about the various points of interest on parallel platforms have appeared [70]. Since then, many researchers studied many approaches and solutions for a fast and best computation regarding the forward kinematics for parallel platforms.

4.1 Inverse Kinematics

Inverse kinematics of PKM's are quite more straight forward than SKM's. It's parallel structure allows to deduce the transformation matrices needed between each stage of the Gough-Stewart platform. In the past, SPIF-A kinematics was not well configured and largely failed on position accuracy compared to a caliper rule or metric tape measurements. Also, it was only able to perform 3-axis tasks. Therefore, a complete review to the inverse kinematics was done in order to deduce new transformation matrices using homogeneous coordinates.

In Figure 4.1 are illustrated the top and bottom platform as well as the coordinate system and actuator's coupling points. Let Kr_{top}, θ_{top_i} and Kr_{bot}, θ_{bot_i} be the radius of the

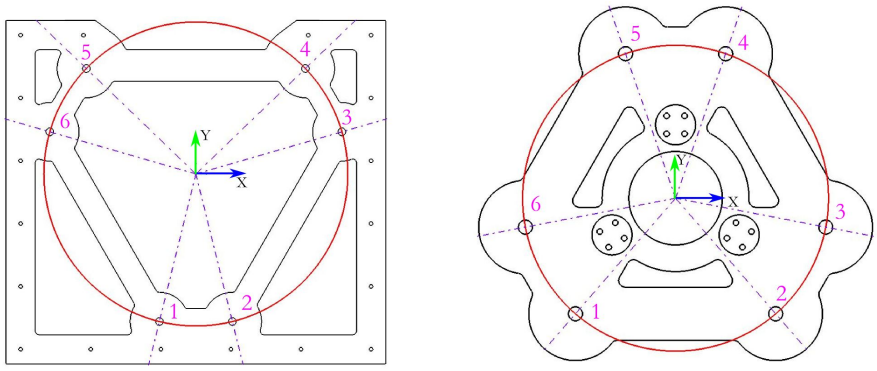

(a) Top platform. (b) Bottom platform.

Figure 4.1: SPIF-A's top and bottom platform.

red circumference and the vertex angles of top and bottom platforms, respectively. The vertex angles of both top and bottom platforms are described in Equation 4.1 and Equation 4.2, respectively. The radius of Kr_{top} and Kr_{bot} are 416.333 and 229.129 millimeters, respectively.

$$\begin{bmatrix} \theta_{top_1} \\ \theta_{top_2} \\ \theta_{top_3} \\ \theta_{top_4} \\ \theta_{top_5} \\ \theta_{top_6} \end{bmatrix} = \begin{bmatrix} 1.8134 \\ 1.3283 \\ -0.2810 \\ -0.7662 \\ 3.9078 \\ 3.4226 \end{bmatrix} \quad [rad] \tag{4.1}$$

$$\begin{bmatrix} \theta_{bot_1} \\ \theta_{bot_2} \\ \theta_{bot_3} \\ \theta_{bot_4} \\ \theta_{bot_5} \\ \theta_{bot_6} \end{bmatrix} = \begin{bmatrix} 2.2846 \\ 0.8571 \\ 0.1901 \\ -1.2373 \\ -1.9043 \\ 2.9515 \end{bmatrix} \quad [rad] \tag{4.2}$$

For the top platform, the vertex points $K_{top}(i) = [x_i, y_i, 0, 1]^T$ with $i \in \{1, 2, 3, 4, 5, 6\}$ regarding the local coordinate system are:

$$
\begin{aligned}
K_{top} &= \begin{bmatrix} x_1 & x_2 & x_3 & x_4 & x_5 & x_6 \\ y_1 & y_2 & y_3 & y_4 & y_5 & y_6 \\ 0 & 0 & & 0 & 0 & 0 \\ 1 & 1 & 1 & 1 & 1 & 1 \end{bmatrix} \\
&= \begin{bmatrix} cos(\theta_{top_1}) & cos(\theta_{top_2}) & cos(\theta_{top_3}) & cos(\theta_{top_4}) & cos(\theta_{top_5}) & cos(\theta_{top_6}) \\ -sin(\theta_{top_1}) & -sin(\theta_{top_2}) & -sin(\theta_{top_3}) & -sin(\theta_{top_4}) & -sin(\theta_{top_5}) & -sin(\theta_{top_6}) \\ 0 & 0 & & 0 & 0 & 0 \\ 1 & 1 & 1 & 1 & 1 & 1 \end{bmatrix} \cdot Kr_{top} \\
&= \begin{bmatrix} -100.0008 & 100.0008 & 400.0000 & 299.9993 & -299.9993 & -400.0000 \\ -404.1448 & -404.1448 & 115.4692 & 288.6756 & 288.6756 & 115.4692 \\ 0 & 0 & & 0 & 0 & 0 \\ 1 & 1 & 1 & 1 & 1 & 1 \end{bmatrix}
\end{aligned} \tag{4.3}
$$

The coordinates of the vertex points K_{top} are given in millimeters. Taking the same reasoning, the vertex points of bottom platform $K_{bot}(i) = [x_i, y_i, 0, 1]^T$ with $i \in \{1, 2, 3, 4, 5, 6\}$ regarding the local coordinate system are:

$$
\begin{aligned}
K_{bot} &= \begin{bmatrix} x_1 & x_2 & x_3 & x_4 & x_5 & x_6 \\ y_1 & y_2 & y_3 & y_4 & y_5 & y_6 \\ 0 & 0 & & 0 & 0 & 0 \\ 1 & 1 & 1 & 1 & 1 & 1 \end{bmatrix} \\
&= \begin{bmatrix} cos(\theta_{bot_1}) & cos(\theta_{bot_2}) & cos(\theta_{bot_3}) & cos(\theta_{bot_4}) & cos(\theta_{bot_5}) & cos(\theta_{bot_6}) \\ -sin(\theta_{bot_1}) & -sin(\theta_{bot_2}) & -sin(\theta_{bot_3}) & -sin(\theta_{bot_4}) & -sin(\theta_{bot_5}) & -sin(\theta_{bot_6}) \\ 0 & 0 & & 0 & 0 & 0 \\ 1 & 1 & 1 & 1 & 1 & 1 \end{bmatrix} \cdot Kr_{bot} \\
&= \begin{bmatrix} -149.99989 & 149.9989 & 225.0005 & 75.0016 & -75.0016 & -225.0005 \\ -173.2063 & -173.2063 & -43.2998 & 216.5060 & 216.5060 & -43.2998 \\ 0 & 0 & & 0 & 0 & 0 \\ 1 & 1 & 1 & 1 & 1 & 1 \end{bmatrix}
\end{aligned} \tag{4.4}
$$

The coordinates of the vertex points K_{bot} are given in millimeters.

Let's consider a global coordinate system (GCS) for the entire kinematic scheme (see Figure 4.3) placed on the same spot as the local coordinate system (LCS) of the top platform and a desired three dimensional coordinate C_{3D} regarding the established zero part ZP. Therefore, the transformation matrix, R_{top}, between the LCS of the top platform and the GCS is the identity matrix.

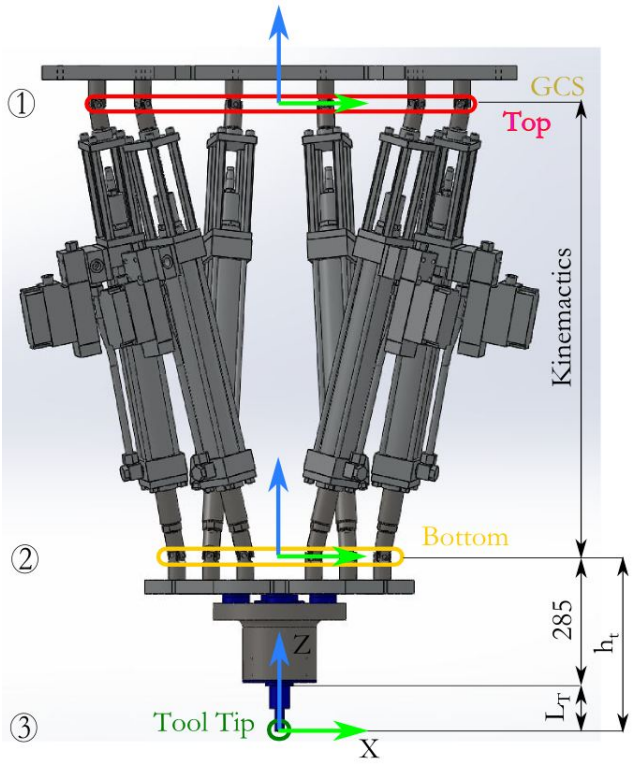

Figure 4.2: SPIF-A kinematic reference points and its coordinate systems.

$$C_{3D} = \begin{bmatrix} X \\ Y \\ Z \\ \alpha \\ \beta \\ \gamma \end{bmatrix} + ZP = \begin{bmatrix} X \\ Y \\ Z \\ \alpha \\ \beta \\ \gamma \end{bmatrix} + \begin{bmatrix} ZP_x \\ ZP_y \\ ZP_z \\ ZP_\alpha \\ ZP_\beta \\ ZP_\gamma \end{bmatrix} \tag{4.5}$$

$$R_{top} = \begin{bmatrix} 1 & 0 & 0 & 0 \\ 0 & 1 & 0 & 0 \\ 0 & 0 & 1 & 0 \\ 0 & 0 & 0 & 1 \end{bmatrix} \tag{4.6}$$

Hence, the coordinates, P_{top}, of the LCS in GCS regarding the top platform are

$$P_{top} = R_{top} \cdot \begin{bmatrix} 0 \\ 0 \\ 0 \\ 1 \end{bmatrix} = \begin{bmatrix} P_{tx} \\ P_{ty} \\ P_{tz} \\ 1 \end{bmatrix} = \begin{bmatrix} 0 \\ 0 \\ 0 \\ 1 \end{bmatrix} \tag{4.7}$$

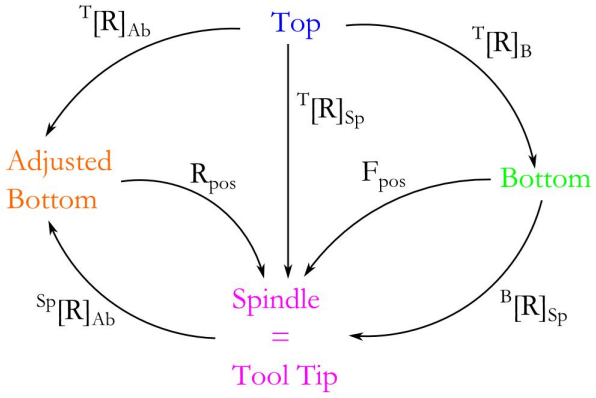

Figure 4.3: Coordinate system transformation diagram.

because both referential systems are coincident.

The rotational matrix R_{RPY} is a configuration, among the other possible Euler configurations, referred as Roll-Pitch-Yaw that consists in a rotation α around the X-axis (Yaw), followed by a rotation β around the Y-axis (Pitch) and finally a rotation γ around the Z-axis (Roll) [61]. To simplify the result, let's consider the cosine (cos) as c and the sine (sin) as s:

$$rot(z,\gamma) = R_{roll} = \begin{bmatrix} cos(\gamma) & -sin(\gamma) & 0 & 0 \\ sin(\gamma) & cos(\gamma) & 0 & 0 \\ 0 & 0 & 1 & 0 \\ 0 & 0 & 0 & 1 \end{bmatrix} \tag{4.8}$$

$$rot(y,\beta) = R_{pitch} = \begin{bmatrix} cos(\beta) & 0 & sin(\beta) & 0 \\ 0 & 1 & 0 & 0 \\ -sin(\beta) & 0 & cos(\beta) & 0 \\ 0 & 0 & 0 & 1 \end{bmatrix} \tag{4.9}$$

$$rot(x,\alpha) = R_{yaw} = \begin{bmatrix} 1 & 0 & 0 & 0 \\ 0 & cos(\alpha) & -sin(\alpha) & 0 \\ 0 & sin(\alpha) & cos(\alpha) & 0 \\ 0 & 0 & 0 & 1 \end{bmatrix} \tag{4.10}$$

$$R_{RPY} = \begin{bmatrix} c(\gamma)c(\beta) & c(\gamma)s(\beta)s(\alpha) - s(\gamma)c(\alpha) & c(\gamma)s(\beta)c(\alpha) + s(\alpha)s(\alpha) & 0 \\ s(\gamma)c(\beta) & s(\gamma)s(\beta)s(\alpha) + c(\gamma)c(\alpha) & s(\gamma)s(\beta)c(\alpha) - c(\gamma)s(\alpha) & 0 \\ -s(\beta) & c(\beta)s(\alpha) & c(\beta)c(\alpha) & 0 \\ 0 & 0 & 0 & 1 \end{bmatrix} \tag{4.11}$$

Euler angles, despite being simple to work with, have some singularities when the rotational axis become aligned. Known as gimbal lock in gyroscopes, this phenomenon occurs around angles of 90 degrees [62]. However, as mentioned before, the SPIF-A's Gough-Stewart platform is mechanically limited to 45 degrees range due to the link's U-joints.

The space between the top and bottom platform, when all actuators are full retracted, is given by the constant h_i. Hence, the transformation matrix that encompasses the translation h_i and the Euler rotations is represented by ${}^{T}[\mathrm{R}]_{B}$ in the Equation 4.13

$$Z_t = \begin{bmatrix} 1 & 0 & 0 & 0 \\ 0 & 1 & 0 & 0 \\ 0 & 0 & 1 & -hi \\ 0 & 0 & 0 & 1 \end{bmatrix} \tag{4.12}$$

$$\begin{aligned} {}^{T}[\mathrm{R}]_{B} &= Z_t \cdot R_{RPY} \\ &= \begin{bmatrix} c(\gamma)c(\beta) & c(\gamma)s(\beta)s(\alpha) - s(\gamma)c(\alpha) & c(\gamma)s(\beta)c(\alpha) + s(\alpha)s(\alpha) & 0 \\ s(\gamma)c(\beta) & s(\gamma)s(\beta)s(\alpha) + c(\gamma)c(\alpha) & s(\gamma)s(\beta)c(\alpha) - c(\gamma)s(\alpha) & 0 \\ -s(\beta) & c(\beta)s(\alpha) & c(\beta)c(\alpha) & -h_i \\ 0 & 0 & 0 & 1 \end{bmatrix} \end{aligned} \tag{4.13}$$

The coordinates P_{bot} regarding the LCS of the bottom platform compared to the GCS are:

$$P_{bot} = R_{top} \cdot {}^{T}[\mathrm{R}]_{B} \cdot \begin{bmatrix} 0 \\ 0 \\ 0 \\ 1 \end{bmatrix} = \begin{bmatrix} P_{bx} \\ P_{by} \\ P_{bz} \\ 1 \end{bmatrix} \tag{4.14}$$

The matrix ${}^{B}[\mathrm{R}]_{Sp}$, a simple translation on the LCS Z-axis, represents the transformation matrix between the bottom platform to the tool tip. The constant h_t, in the Equation 4.15, represents the length of the spindle system plus the length of the tool L_t.

$${}^{B}[\mathrm{R}]_{Sp} = \begin{bmatrix} 1 & 0 & 0 & 0 \\ 0 & 1 & 0 & 0 \\ 0 & 0 & 1 & -ht \\ 0 & 0 & 0 & 1 \end{bmatrix} \tag{4.15}$$

$$h_t = 285 + L_t \tag{4.16}$$

Therefore, the overall transformation matrix between the top platform and the tool tip is given by ${}^{T}[\mathrm{R}]_{Sp}$, as presented in the Equation 4.17. Note that, at this stage, it is already being implemented the 6 DOF motions based on Euler angles.

$$
\begin{aligned}
{}^{T}[\mathrm{R}]_{Sp} &= R_{top} \cdot {}^{T}[\mathrm{R}]_{B} \cdot {}^{B}[\mathrm{R}]_{Sp} \\
&= \begin{bmatrix} c(\alpha)c(\beta) & c(\alpha)s(\beta)s(\gamma) - s(\alpha)c(\gamma) & c(\alpha)s(\beta)c(\gamma) + s(\alpha)s(\gamma) & 0 \\ s(\alpha)c(\beta) & s(\alpha)s(\beta)s(\gamma) + c(\alpha)c(\gamma) & s(\alpha)s(\beta)c(\gamma) - c(\alpha)s(\gamma) & 0 \\ -s(\beta) & c(\beta)s(\gamma) & c(\beta)c(\gamma) & -h_i - h_t \\ 0 & 0 & 0 & 1 \end{bmatrix}
\end{aligned} \tag{4.17}
$$

However, the inverse kinematics of the Gough-Stewart platform does not ends here. Initially given any Euler angle such as $\alpha \neq 0$ and/or $\beta \neq 0$, will cause the bottom platform to rotate around its X-axis and/or Y-axis. The tool and spindle system are attached to it, hence, the tool tip coordinates in the GCS will be altered without directly changing the X,Y or Z desired coordinates. In this particular case, the tool tip has to be on the same three dimensional point as before, regarding the GCS. Only the bottom platform has to twist around X-axis and/or Y-Axis. For that reason, there is a special need for a compensation when working with Euler angles, i.e, working on 6 DOF. Here, the tool tip's "fake" three dimensional coordinates F_{pos} in the GCS are as follows,

$$
F_{pos} = {}^{T}[\mathrm{R}]_{Sp} \cdot \begin{bmatrix} 0 \\ 0 \\ 0 \\ 1 \end{bmatrix} = \begin{bmatrix} P_{fx} \\ P_{fy} \\ P_{fz} \\ 1 \end{bmatrix} \tag{4.18}
$$

Let's consider the transformation matrix ${}^{Sp}[\mathrm{R}]_{Ab}$ the adjustment needed to correct the tool tip spacial coordinates on 6 DOF operations. This adjustment is just a simple three dimensional translation regarding the deviation caused by the Euler angles and the desired spacial coordinates X, Y and Z. In Figure 4.4 this effect is illustrated.

$$
{}^{Sp}[\mathrm{R}]_{Ab} = \begin{bmatrix} 1 & 0 & 0 & -P_{fx} + X \\ 0 & 1 & 0 & -P_{fy} + Y \\ 0 & 0 & 1 & -P_{fz} + Z - h_t - h_i \\ 0 & 0 & 0 & 1 \end{bmatrix} \tag{4.19}
$$

Assuming that ${}^{T}[\mathrm{R}]_{Ab}$ is the same as ${}^{T}[\mathrm{R}]_{Sp}$ but with the refereed adjustments, the new and final transformation for the bottom platform ${}^{T}[\mathrm{R}]_{Ab}$ is given by the Equation 4.20.

$$
\begin{aligned}
{}^{T}[\mathrm{R}]_{Ab} &= {}^{T}[\mathrm{R}]_{B} \cdot {}^{B}[\mathrm{R}]_{Sp} \cdot {}^{Sp}[\mathrm{R}]_{Ab} \\
&= {}^{T}[\mathrm{R}]_{Sp} \cdot {}^{Sp}[\mathrm{R}]_{Ab} \\
&= \begin{bmatrix} c(\beta)c(\alpha) & c(\alpha)s(\beta)S(\gamma) - c(\gamma)s(\alpha) & s(\gamma)s(\alpha) + c(\gamma)c(\alpha)s(\beta) & r_{14} \\ c(\beta)s(\alpha) & c(\gamma)c(\alpha) + s(\beta)s(\gamma)s(\alpha) & c(\gamma)s(\beta)s(\alpha) - c(\alpha)s(\gamma) & r_{24} \\ -s(\beta) & c(\beta)s(\gamma) & c(\beta)C(\gamma) & r_{34} \\ 0 & 0 & 0 & 1 \end{bmatrix}
\end{aligned} \tag{4.20}
$$

where, r_{14}, r_{24} and r_{34} are as follows,

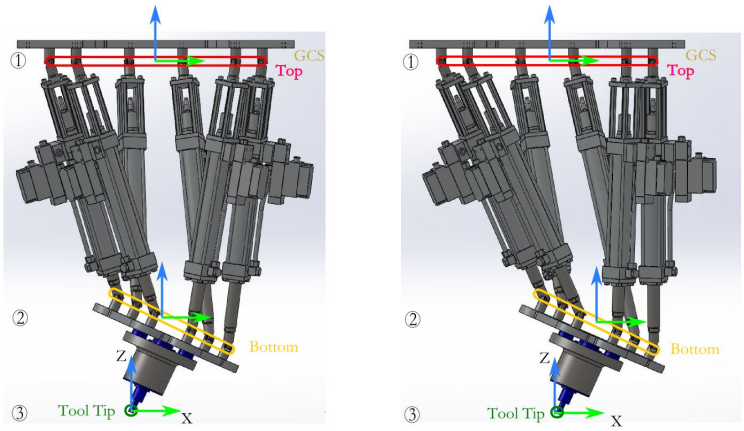

(a) Fake tool tip position F_{pos}.

(b) Real tool tip position R_{pos}.

Figure 4.4: Adjustment effect on the tool tip by the orientation of the bottom platform.

- $r_{14} = (s(\gamma)s(\alpha) + c(\gamma)c(\alpha)s(\beta))\, h_t + X$
- $r_{24} = (s(\gamma)c(\beta)c(\alpha) - c(\alpha)s(\gamma))\, h_t + Y$
- $r_{34} = -160 - h_i + c(\beta)c(\gamma)h_t - h_t + Z + L_t$

The value -160 is a tool compensation factor, i.e, it is directly related to the tool length L_t. It is a sort of window where the tool length can vary without causing negative values of actuators length. For instance, if $L_t = 0$ it is similar to $Z = -160$ on SPIF-A work space. In other hand if $L_t = 160$ is the same has $Z = 0$ (still possible, the link lengths are not yet less than zero). In some cases, if the tool length is above 160 millimeters, it will cause a full retraction of the actuators length plus a negative virtual gap. Although physically limited, there is no danger to the machine structure. In this particular cases, establishing a zero part can solve the problem.

The top platform is fixed at $C_{3D} = [0\ 0\ 0\ 0\ 0\ 0]^T$ in GCS, therefore, the associated transformation to the vertex points K_t is the identity matrix R_{top}, i.e, it will not suffer any translational or rotational transformation.

$$WK_t = R_{top} \cdot K_t \tag{4.21}$$

However, the bottom platform vertex WK_b, initially coincident with the top platform regarding the GCS, will be modified by the final transformation matrix ${}^{T}[\mathrm{R}]_{Ab}$ that already takes into account the above mentioned adjustments.

$$WK_b = {}^{T}[\mathrm{R}]_{Ab} \cdot K_b \tag{4.22}$$

Now, is possible to compute the real three dimensional coordinate of the tool tip R_{pos}. Even with or without any orientation on the bottom platform, i.e, either 3-axis or 6-axis manipulation, the adjustment is already implemented. Hence, the tool tip spacial coordinates in the GCS are as follows:

$$R_{pos} =^{T} [\mathrm{R}]_{Ab} \cdot \begin{bmatrix} 0 \\ 0 \\ 0 \\ 1 \end{bmatrix} = \begin{bmatrix} P_{rx} \\ P_{ry} \\ P_{rz} \\ 1 \end{bmatrix} \tag{4.23}$$

The actuators length is the distance between each correspondent vertex of the bottom and top platform subtracted by the original length of the actuator itself. Here, the distance between both platforms is $\neq 0$. To compute this tree dimensional length on the GCS, the subtraction of the bottom vertexes by the top vertexes will result in six 3D vectors. The length of these vectors is calculated by determining its norm. However, this length has to be subtracted by the original length of the actuators C_i.

$$C_L = norm(WK_b - WK_t) - C_i = \begin{bmatrix} C_{L1} \\ C_{L2} \\ C_{L3} \\ C_{L4} \\ C_{L5} \\ C_{L6} \end{bmatrix} \tag{4.24}$$

Concluding, C_L is the required actuator length to achieve the given desired three dimensional point and its orientation $C_{3D} = [X\ Y\ Z\ \alpha\ \beta\ \gamma]$. These actuators lengths will be further sent to the control stage where all the control apparatus will take place and ensure that the machine reaches the desired C_{3D}.

4.2 Forward Kinematics

Forward kinematics is, for sure, the most dramatic mathematical analysis and solution on Gough-Stewart platforms. SPIF-A is no exception to that. For a given set of actuators length, there are several solutions that can lead up to 64 solutions [64]. There are three different types of Gough-Stewart platforms, 3-3 type, 6-3 type and the most complex and challenging 6-6 type which is the one implemented on the SPIF-A machine. Here, if the link joints are distinctly and arbitrarily placed on the base and moving platform, it makes more complex the mathematical analysis of forward kinematics and it can lead up to 40 different solutions [65]. However, by optimizing the link joints geometry on base and moving platforms, the number of possible solutions may be drastically reduced. The SPIF-A's platform link joints geometry is like a semi regular hexagon, and studies claims that its number of solutions is dropped to 24 [66]. Figure 4.5 shows one of many possible situations which for the same set of link lengths it gives different solutions.

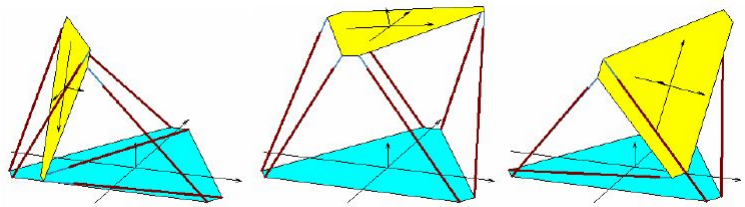

Figure 4.5: Different possibilities given the same actuator length [63].

4.2.1 Adopted Numerical Solution

There are many numerical solutions to solve forward kinematics on parallel manipulators. Contrary to serial kinematics manipulators, there are no exact mathematical model to describe the forward kinematics on Gough-Stewart platforms. Usually, the approach relies on methods such as numerical elimination, iterative numerical method or based on redundant auxiliary variables [67].

Numerical elimination bases on converting the non-linear equations into a univariate polynomial equation. Lee [65] used algebraic elimination method to solve forward kinematics of a 6-6 type Gough-Stewart platform that directly leads to a 40th degree univariate equation.

Neural network solution is another method used by Geng [68] to solve the forwards kinematics of a parallel platform. The author proposes to use a multiple neural network structure called cascaded CMAC (cerebella model arithmetic computer). This structure provides fast learning and the ability to capture details of unknown non-linear mapping.

Despite the effort from many authors, scientific community splits these methods regarding its advantages and disadvantages and also its computational time. A consensus is yet to be reached, but it is a fact that numerical iterative methods requires less computational power compared to the analytic and algebraic counterparts. However, iterative method's perform entirely depends on the initial approximation. If a good approximation is chosen, the model quickly converges and a single solution is achieved.

The most common methods to solve forwards kinematics in parallel platforms are the Newton-Rapshon method [69] and the first order Newton method [63]. António Mendes Lopes [67] studied and compared these two iterative methods and proposed its own algorithm using Newton's method, on his PhD thesis. His model is known to have a faster convergence rate, less iterations and the use of the inverse Euler jacobian matrix J_E^{-1}.

Mendes Lopes structures his algorithm as follows [67] :

1. Selection of the initial candidate vector containing the platform position and orientation $X_k \equiv X_o$ and the admissible error ε;
2. Determine and invert the Euler jacobian matrix $J_E^{-1}(X_k)$;
3. Determine the spacial actuators error vector $[L - K^{-1}(X_k)]$, where L is the measured actuators length and K^{-1} is the inverse kinematics.

4. Do $\Delta X_k = J_E^{-1} \cdot [L - K^{-1}(X_k)]$;

5. Do $X_{k+1} = X_k + \Delta X_k$, that is the new candidate;

6. If maxval($|[L - K^{-1}(X_{k+1})]|$) $> \varepsilon$, meaning that the error of the new candidate is higher than previously assumed, return to step 2.

The correlation between the link speeds on the joint space with the manipulator's end-effector speed on the euclidean space is given by the kinematic jacobian. The inverse Euler jacobian J_E^{-1} used by Mendes Lopes on his algorithm, can be determined via the inverse of the kinematic one [67].

Mendes Lopes's algorithm only takes into account the top and bottom platform, disregarding any tool or spindle system attached to it. His approach to inverse kinematics is somewhat different of the one deduced in section 4.1. On his approach, what comes after the bottom/mobile platform is useless because the point of interest is the mid point or centroid point of the mobile platform for a standard Stewart platform. In other hand, as explained, on the SPIF-A machine, the point of interest is the tool tip. Hence, the link length must satisfy the desired tool tip spacial coordinates.

Better describing Mendes Lope's algorithm, let's first consider the following parameters:

- M_p: Mobile platform vertex points;
- B_p: Base platform vertex points;
- L_i: Actuator length, $i \in \{1, 2, 3, 4, 5, 6\}$;
- P: Spacial position $P = [x\ y\ z]^T$;
- R: Simplified Euler rotational matrix for the orientation (α , β , γ);

The actuator length L_i is also determined by calculating the norm of the three dimensional vector that connects both vertex of the base and mobile platform:

$$L_i = \|Lv_i\|, i \in \{1, 2, 3, 4, 5, 6\} \tag{4.25}$$

$$Lv_i = P + R \cdot Mp_i - Bp_i = [e_{ix}\ e_{iy}\ e_{iz}]^T \tag{4.26}$$

$$\begin{bmatrix} e_{ix} \\ e_{iy} \\ e_{iz} \end{bmatrix} = \begin{bmatrix} x \\ y \\ z \end{bmatrix} + \begin{bmatrix} r_{11} & r_{12} & r_{13} \\ r_{21} & r_{22} & r_{23} \\ r_{31} & r_{32} & r_{33} \end{bmatrix} \cdot \begin{bmatrix} Mp_{ix} \\ Mp_{iy} \\ Mp_{iz} \end{bmatrix} - \begin{bmatrix} Bp_{ix} \\ Bp_{iy} \\ Bp_{iz} \end{bmatrix} \tag{4.27}$$

The required actuator velocity $\dot{L}_i$ for the desired end-effector linear and angular velocity $\dot{P}$ and w, respectively, given by v_e is computed using the inverse kinematic jacobian J_C^{-1}:

$$\dot{L}_i = J_C^{-1} \cdot v_e \tag{4.28}$$

$$v_e = [\dot{P}\ w]^T \tag{4.29}$$

However, the velocity of the mobile/bottom platform's vertex is different from the velocity of the centroid point on the mobile platform. Hence, according to the rotational matrix R, the end effector velocity v_c is:

$$v_c = \dot{P} + w \times (R \cdot Mp_i) \tag{4.30}$$

The 6x6 inverse kinematic jacobian J_C^{-1} is obtained from the inverse kinematic Equation 4.26:

$$J_C^{-1}(i, 1:6) = \left[\frac{(Lv_i)^T}{\|Lv_i\|} \quad \frac{((R \cdot Mp_i) \times Lv_i)^T}{\|Lv_i\|} \right], i \in \{1, 2, 3, 4, 5, 6\} \tag{4.31}$$

The relationship between the angular velocity w and the first temporal derivative of Euler angles $\dot{P_{E\triangleleft}}$ is

$$w = J_A \cdot \dot{P_{E\triangleleft}} \tag{4.32}$$

where

$$J_A = \begin{bmatrix} 0 & -s(\gamma) & c(\beta)c(\gamma) \\ 0 & c(\gamma) & c(\beta)s(\gamma) \\ 1 & 0 & -s(\beta) \end{bmatrix} \tag{4.33}$$

The link length variations to positional and Euler angles variations is correlated by the inverse Euler jacobian J_E^{-1} that is calculated from the inverse kinematic jacobian J_C^{-1}. Hence, Equation 4.28 is rewritten:

$$\dot{L}_i = \begin{bmatrix} J_{C11}^{-1} & J_{C12}^{-1} \\ J_{C21}^{-1} & J_{C22}^{-1} \end{bmatrix} \cdot \begin{bmatrix} \dot{P} \\ w \end{bmatrix} \tag{4.34}$$

in relation to the Equation 4.32

$$\dot{L}_i = \begin{bmatrix} J_{C11}^{-1} & J_{C12}^{-1} \cdot J_A \\ J_{C21}^{-1} & J_{C22}^{-1} \cdot J_A \end{bmatrix} \cdot \begin{bmatrix} \dot{P} \\ \dot{P}_{E\triangleleft} \end{bmatrix} \tag{4.35}$$

Concluding the demonstration of Mendes Lopes's algorithm [67], the inverse Euler jacobian J_E^{-1} is as follows:

$$J_E^{-1} = \begin{bmatrix} J_{C11}^{-1} & J_{C12}^{-1} \cdot J_A \\ J_{C21}^{-1} & J_{C22}^{-1} \cdot J_A \end{bmatrix} \tag{4.36}$$

Not yet finished, the forward kinematics for the SPIF-A machine needs some additional transformation matrices to the tool tip coordinate system. As aforementioned, $X_k = [X_k \ Y_k \ Z_k \ \alpha_k \ \beta_k \ \gamma_k]^T$ is the new candidate for the given link lengths C_L regarding the inverse kinematics in section 4.1.

Let's consider the rotational Euler matrix R_{FE} for the given Euler candidate angles,

$$R_{FE} = \begin{bmatrix} c(\gamma_k)c(\beta_k) & c(\gamma_k)s(\beta_k)s(\alpha_k) - s(\gamma_k)c(\alpha_k) & c(\gamma_k)s(\beta_k)c(\alpha_k) + s(\alpha_k)s(\alpha_k) & 0 \\ s(\gamma_k)c(\beta_k) & s(\gamma_k)s(\beta_k)s(\alpha_k) + c(\gamma_k)c(\alpha_k) & s(\gamma_k)s(\beta_k)c(\alpha_k) - c(\gamma_k)s(\alpha_k) & 0 \\ -s(\beta_k) & c(\beta_k)s(\alpha) & c(\beta_k)c(\alpha_k) & 0 \\ 0 & 0 & 0 & 1 \end{bmatrix} \tag{4.37}$$

and the interim tool tip coordinates P_{ptt} are:

$$P_{ptt} = R_{FE} \cdot \begin{bmatrix} 0 \\ 0 \\ -h_t \\ 1 \end{bmatrix} = \begin{bmatrix} P_{pptx} \\ P_{ppty} \\ P_{pptz} \\ 1 \end{bmatrix} \tag{4.38}$$

where h_t is the spindle system length plus the tool length. The forward kinematics regarding the GCS is defined as follows,

$$FK_{3DG} = \begin{bmatrix} X_k - P_{pptx} & Y_K - P_{ppty} & -Z_k + P_{pptz} & \alpha_k & \beta_k & \gamma_k \end{bmatrix}^T \tag{4.39}$$

and finally, in the tool tip's LCS,

$$FK_{3DL} = \begin{bmatrix} X_k - P_{pptx} & Y_K - P_{ppty} & -Z_k + P_{pptz} + h_t + h_i & \alpha_k & \beta_k & \gamma_k \end{bmatrix}^T \tag{4.40}$$

4.3 Singularities

Unlike serial manipulators, the Gough-Stewart platform has no kinematic singularities in the strict sense (actuators length can not take values such as zero or less than zero) [70]. It's limitations on motion capabilities relies on the joint limits alone. However, there are force singularities on some link configurations. At such link disposal, the parallel manipulator loses some degree(s) of constraint and becomes uncontrollable. Gosselin and Angeles [70] calls this phenomenon as "singularity of the second kind". The singularities of serial manipulators causes a loss in degrees of freedom and partial locking while in parallel manipulators is associated with a gain of degree of freedom and uncontrollability. Depending on the complexity of the limbs, it can be mentioned that may exist singularities. However, in this context, the limbs have to be associated with individual limbs without coupling between them.

Particular geometrical conditions for singularities of the Gough-Stewart platform were enumerated and studied by many researchers [70], such as Hunt, Fichter and Merlet. Ma and Angeles claims that symmetrical architectures in the Stewart platform can result in singularities extending over the entire workspace or in some particular regions, termed has architecture singularities [70]. Conceptually speaking, the Stewart platform may have singularities compared to other parallel manipulators.

4.4 Actuator forces via differential kinematics

Through differential kinematics, the inverse kinematic jacobian is used to correlate the actuator speeds on the joint space with the manipulator end-effector velocity, on the euclidean work space. However, the kinematic jacobian also correlates the forces on the actuators regarding the forces being applied on the end-effector through the expression 4.41, that follows the well-known d'Alembert principle:

$$F_{ef} = \left(J_K^{-1}\right)^T \cdot \sigma_{af} \Leftrightarrow \sigma_{af} = (J_K)^T \cdot F_{ef} \tag{4.41}$$

where the end-effector forces are denoted by

$$F_{ef} = \begin{bmatrix} F_x & F_y & F_z & F_\alpha & F_\beta & F_\gamma \end{bmatrix}^T \tag{4.42}$$

and the actuator forces by

$$\sigma_{af} = \begin{bmatrix} Fl_1 & Fl_2 & Fl_3 & Fl_4 & Fl_5 & Fl_6 \end{bmatrix}^T \tag{4.43}$$

The inverse kinematic jacobian J_K^{-1}, in this particular case, is the inverse euler jacobian J_E^{-1} deduced by Mendes Lopes [67] that is presented in the Equation 4.36.

$$J_K^{-1} = J_E^{-1} \tag{4.44}$$

Hence, the equation 4.41 is then rewritten considering the Equation 4.44:

$$\sigma_{af} = J_K^T \cdot F_{ef} \Leftrightarrow \sigma_{af} = \left[\left(J_E^{-1}\right)^{-1}\right]^T \cdot F_{ef} \tag{4.45}$$

which is the sames as

$$\begin{bmatrix} Fl_1 \\ Fl_2 \\ Fl_3 \\ Fl_4 \\ Fl_5 \\ Fl_6 \end{bmatrix} = (J_E)^T \cdot \begin{bmatrix} F_x \\ F_y \\ F_z \\ F_\alpha \\ F_\beta \\ F_\gamma \end{bmatrix} \tag{4.46}$$

where $F_\alpha = F_\beta = F_\gamma = 0$ because there are no rotational forces being acquired by the FMS on the tool tip during SPIF forming.

The propose of computing the forces on the actuators can be many. However, on this work, it may be interesting to try different control methods regarding control forces strategies. Impedance control is an approach to the control of dynamic interaction between the manipulator and its environment. On this particular case, on the SPIF-A machine, this type of control may be interesting while performing SPIF operations in a sheet plate.

4.5 End-effector velocity via differential kinematics

The actuator speed can be obtained by the Equation 4.36 where the inverse Euler jacobian J_E^{-1}, calculated from the inverse kinematic jacobian J_C^{-1}, is used. Hence, reformulating the Equation 4.35, the bottom platform velocity can be obtained as follows:

$$v_{bp} = J_E \cdot \dot{L}_i \tag{4.47}$$

where

$$v_{bp} = \begin{bmatrix} \dot{P} \\ \dot{P_{E\triangleleft}} \end{bmatrix} \tag{4.48}$$

The term $\dot{P}$ stand for the three dimensional velocity on X, Y and Z axis while the term $\dot{P_{E\triangleleft}}$ stands for the Euler's angular velocity. While performing 3-Axis machining, the

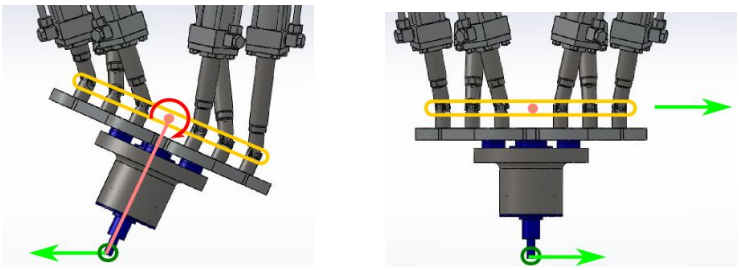

(a) 5-Axis Machining (b) 3-Axis Machining

Figure 4.6: End-effector speed on 3-Axis and 5-Axis motion.

end-effector speed v_{ef} is the same as the bottom platform speed v_{bp}. However, in 5-axis machining, the angular velocity $\dot{P_{E\triangleleft}}$ will induce extra linear speed on the end-effector because the rotation is done on the top of the spindle system, as Figure 4.6 shows.

Concluding, the end-effector linear speed is:

$$v_{ef} = \dot{P} + \dot{P_{E\triangleleft}} \cdot h_t \tag{4.49}$$

4.6 SPIF-A Working Space

The following figure shows the available working space regarding the machine kinematics. It was computed in a way that each actuator length is between its minimum and maximum length. However, to avoid any structural singularities, the X and Y axis were further limited (check Section 5.3.6.2) to a range between -500 and 500 millimeters.

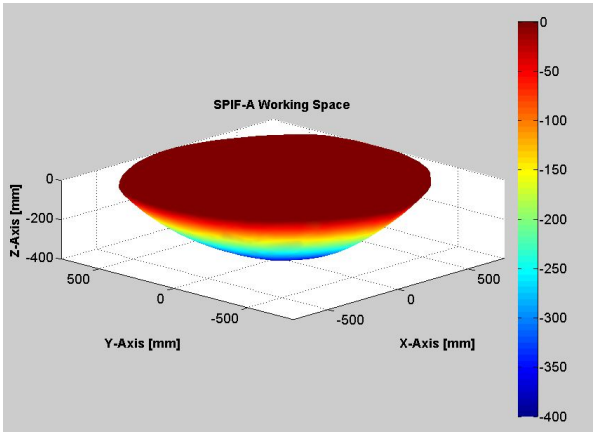

Figure 4.7: SPIF-A working space.

Chapter 5

SPIF-A Software and Motion Control

The development of online and offline software implemented on the machine for motion control and visualization is described. The algorithm and pre-processing apparatus used to describe various types of motions is mentioned, as well as the built operator interface is presented.

"The machine does not isolate man from the great problems of nature but plunges him more deeply into them."

Antoine de Saint-Exupéry
(June 29th 1900 — Jully 31st 1944)

As the quote above says, there is always a lot more to do and research regarding motion control on such parallel platforms like the SPIF-A one.

The majority of the machinery mentioned in the Section 2.2.2 uses the well-known G programming language which is implemented in many industrial machines such as the conventional CNC machines. This type of numeric control basically tells the machine where to move by specifying a target point (X,Y,Z) and its orientation (α,β,γ) preceded by a preparatory function identified by the letter G and followed by a number which corresponds to a particular action. On this programming language there are many more preparatory function that develops certain actions. However, the actual SPIF-A machine only requires the known G01 preparatory function that leads to a linear interpolation between two points in space at a time. To generate the desired trajectory, linear interpolation is done among all the defined points in space by the function G01. An ordinary CAM file is fulfilled with multi preparatory actions which many of them are not used on this machine, for instance, drill cycle. This file also contains the target points and orientations that leads to the desired trajectory. These points and orientations are read, pre-processed and then sent to the machine as a function regarding the time $f(t) = (x, y, z, \alpha, \beta, \gamma)$. For a given instant of time t, there will be an interpolated target point and orientation. All the software was developed using the Matlab^{TM} and Simulink^{TM} applications. Particular algorithms were developed to create the necessary motion, interfaces, simulator and the Simulink^{TM} model.

5.1 Trajectory Management

In every kind of manipulator, either serial kinematic or parallel kinematic, is necessary to proceed to what is called as trajectory management. It is a set of studies and methods that permits to define the velocity of the links in order to make the manipulator to achieve the desired motion on its spacial workspace. These motions can be just as the displacement of the end-effector between two points on the workspace during a determined period of time. Known as continuous trajectory, the path between the initial and final target point is well defined during the desired period of time. In every instant of time t the end-effector coordinates are linearly interpolated.

There are two types of trajectory management studied and implemented on the SPIF-A machine regarding the manual and automatic mode. In manual mode, the continuous trajectory is computed in real time given the desired initial and final target point for a determined end-effector velocity. In automatic mode, there is a pre-processing stage that linearly interpolates all the trajectory points in evenly spaced ones. The result is a set of evenly spaced points defined on the desired experience time.

5.1.1 Manual Mode

Planing a trajectory on the machine's workspace means determining the evolution of the three dimensional coordinates and its orientation over the time where kinematics conditions, such as position, velocity and even acceleration are satisfied. The motion must occur from the initial instant of time t_0 until the final instant of time t_f given the initial and final target point and orientation, $\tau_i = \begin{bmatrix} x_i & y_i & z_i & \alpha_i & \beta_i & \gamma_i \end{bmatrix}$ and $\tau_f = \begin{bmatrix} x_f & y_f & z_f & \alpha_f & \beta_f & \gamma_f \end{bmatrix}$ respectively. Yet, motion may occur with a given initial velocity $\dot{\tau}(t_0) = \dot{\tau_0}$ and a final velocity $\dot{\tau}(t_f) = \dot{\tau_f}$ also with a desired initial acceleration $\ddot{\tau}(t_0) = \ddot{\tau_0}$ and final acceleration $\ddot{\tau}(t_f) = \ddot{\tau_f}$.

5.1.1.1 Function for manual motion

On the simplest case, let's consider a initial and final target point and its orientation τ_i and τ_f, respectively. The initial and final velocity is also considered and equal to zero, $\dot{\tau_0} = \dot{\tau_f} = 0$. It is pretended to have a continuous linear velocity to avoid drastic accelerations that may cause mechanical failure on the machine.

Hence, the function $\dot{\tau}(t) = 0$ has to have two roots for $t = t_0$ and $t = t_f$ and be a continuous function over time. The general function that best fits, in this case, is a third order polynomial defined in t and defined by $\tau(t)$ as follows [61]:

$$\tau(t) = a_0 + a_1 t + a_2 t^2 + a_3 t^3 \tag{5.1}$$

$$\dot{\tau}(t) = a_1 + 2a_2 t + 3a_3 t^2 \tag{5.2}$$

$$\ddot{\tau}(t) = 2a_2 + 6a_3 t \tag{5.3}$$

The equations mentioned above are illustrated in Figure 5.1.

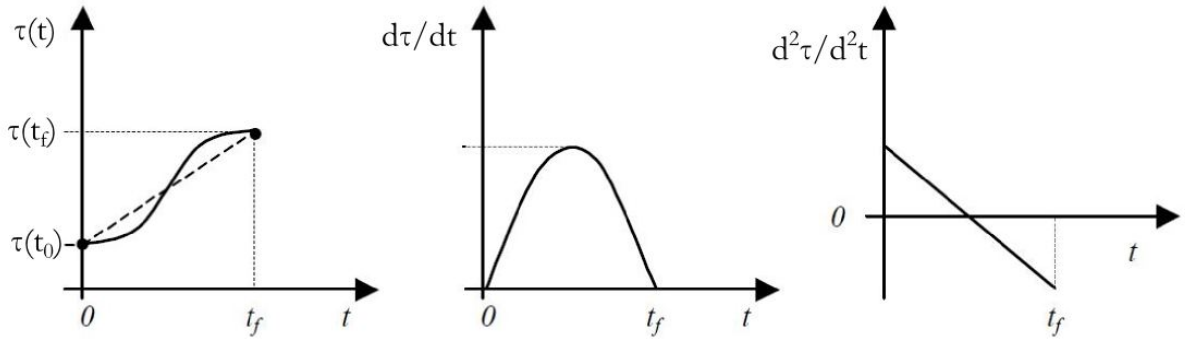

Figure 5.1: Curves of position, velocity and acceleration [61].

The terms a_0, a_1, a_2 and a_3 found in the Equation 5.1 have to be determined. Let's consider the following conditions [61]

$$\tau(0) = 0;\ \tau(t_f) = \tau_f;\ \dot{\tau}(0) = \dot{\tau}_0;\ \dot{\tau}(t_f) = \dot{\tau}_f; \tag{5.4}$$

Combining the Equations 5.1 and 5.2 with the conditions in 5.4, it follows [61]:

$$\begin{array}{rclcrcl} \tau_0 & = & a_0 & & \tau(t_f) & = & a_0 + a_1 t_f + a_2 t_f^2 + a_3 t_f^3 = \tau_f \\ \dot{\tau}_0 & = & a_1 = 0 & and & \dot{\tau}(t_f) & = & a_1 + 2a_2 t_f + 3a_3 t_f^2 \end{array} \tag{5.5}$$

Hence, the Equation 5.1 can be rewritten and obtain the following polynomial for the evolution of the three dimensional coordinates and orientation [61]:

$$\tau(t) = \tau_0 + \frac{3}{t_f^2}(\tau_f - \tau_0)t^2 - \frac{2}{t_f^3}(\tau_f - \tau_0)t^3 \tag{5.6}$$

The Equation 5.6 works for situations where the required initial and final velocity are zero. For initial and final velocities different of zero, the most generalized expression can be derived using the same manner as Equation 5.6 which results [61]:

$$\tau(t) = \tau_0 + \dot{\tau_0}t + \left[\frac{3}{t_f^2}(\tau_f - \tau_0) - \frac{2}{t_f}\dot{\tau_0} - \frac{1}{t_f}\dot{\tau_f}\right]t^2 + \left[-\frac{2}{t_f^3}(\tau_f - \tau_0) + \frac{1}{t_f^2}(\dot{\tau_f} + \dot{\tau_0})\right]t^3 \tag{5.7}$$

For this particular case, on the SPIF-A machine, the Equation 5.6 makes more sense to use because the motion in manual mode is always between the initial and final target point. Hence, the machine starts the motion with $\dot{\tau}_0 = 0$ and ends it with $\dot{\tau}_f = 0$.

5.1.1.2 Implementation of the manual mode on Simulink™

First of all, the Equation 5.6 has to be implemented and tested on Simulink™ environment. If the implementation is plausible, it will fit the Simulink™ model of the machine. Once the SPIF-A machine operates with a real-time machine where the Simulink™ model is being run on every millisecond, the structure of the model has to be built in such way that it has to work either being used or not.

Let's first consider a initial point $P_i = \begin{bmatrix} 0 & 0 & 0 & 0 & 0 & 0 \end{bmatrix}$ and a final desired point $P_f = \begin{bmatrix} -100 & 200 & 300 & 0 & 0 & 0 \end{bmatrix}$ with a desired velocity $v_\tau = 1000$ millimeters per minute. If the model detects that the displacement between P_i and P_f is higher than one micron, it will automatically enable the subsystem (see Figure 5.2). At the end, $P_i = P_f = Coordout$.

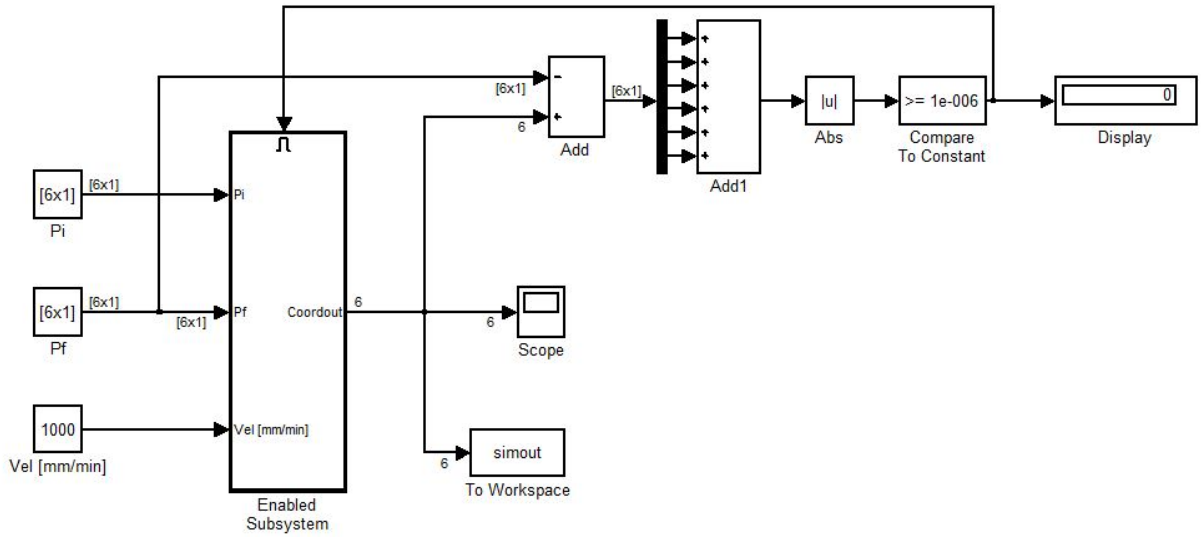

Figure 5.2: Simulink™ for manual mode.

Inside the referred subsystem, all the mathematical apparatus takes place. Regarding the given velocity and the displacement between the initial and final target point, the time that it takes to go from one point to another is as follows:

$$t_f = \frac{\sqrt{(x_f - x_i)^2 + (y_f - y_i)^2 + (z_f - z_i)^2 + (\alpha_f - \alpha_i)^2 + (\beta_f - \beta_i)^2 + (\gamma_f - \gamma_i)^2} \cdot 60}{v_\tau} \quad (5.8)$$

Regarding P_i and P_f the subsystem will be enabled t_f seconds. During this period of time, on every millisecond the model will send new three dimensional coordinates and orientation to the SPIF-A machine, according to the Equation 5.6. Once the machine reaches P_f, the subsystem is disabled until next instruction.

The output of this model is the evolution of the Equation 5.6 over the time. For instance, regarding P_i and P_f and according to the Equation 5.8 will result $t_f = 22.45$ seconds. This means that from $t_0 = 0$ to $t_f = 22.45$ seconds the machine will travel from P_i to P_f according to the behavior of the Equation 5.6, as shown in Figure 5.4.

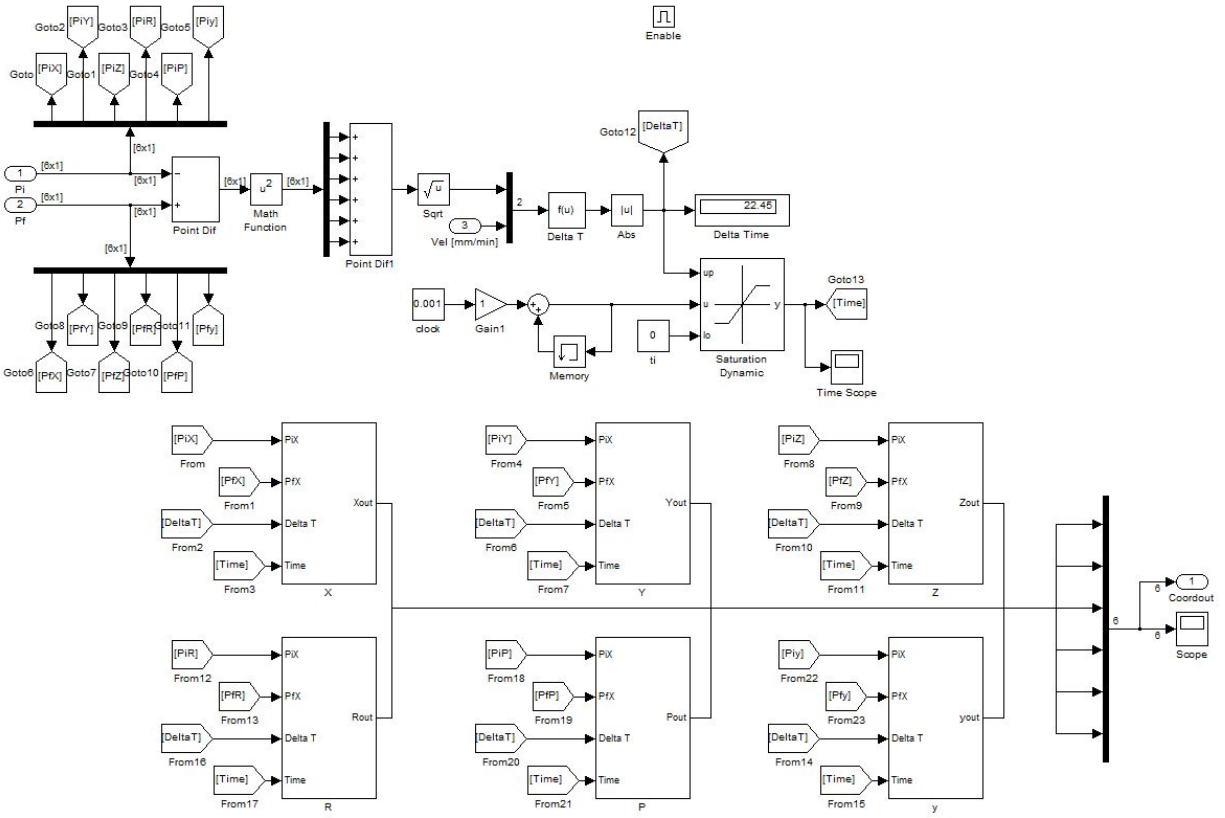

Figure 5.3: Manual's mode Simulink ™ subsystem.

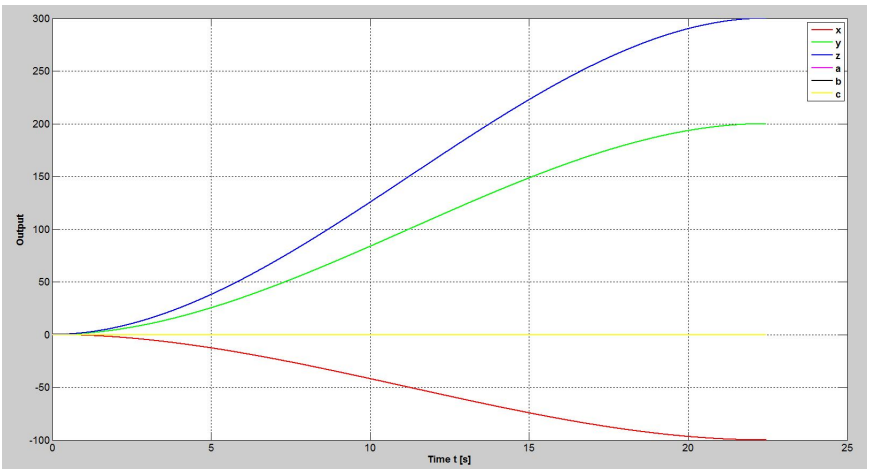

Figure 5.4: Behavior of the Equation 5.6 regarding the given example.

5.1.2 Automatic mode

The automatic mode implemented on the SPIF-A machine allows to run a pre-processed set of points that consist in a certain trajectory over time. These set of data points are initially generated from the CAM software that contains the tool path in order to produce parts. The generated data is most of the times not evenly spaced in the three dimensional space. This data needs to be linearly interpolated so that it will be evenly spaced over the time. An homogeneous behavior of the error over the time will substantially increase the controller performance and there is the possibility to introduce the component of velocity control, that will be further described. Also, a homogeneous behavior of the tool tip will substantially increase the part's surface quality. Uncontrolled moves from the tool tip caused by large quantity of error in the controller often ends up in a premature part failure. So, to optimize all these aspects it was studied and implemented a software module that is capable of converting a set of raw data into a smother one.

5.1.2.1 Linear Interpolation

Given a set of data that results from an experiment, on this particular case, from the CAM software which contains the spacial coordinates and orientations of the tool tip. Let's assume that there is some function $\lambda(t)$ that passes through the data points and perfectly represents the quantity of interest at all non-data points. With interpolation is possible to seek a function that allows to approximate $\lambda(t)$ such that functional values between the original data set values may be estimated. The interpolation here used is the linear interpolation, which is a polynomial of first order that best fits the given set of data points.

Let's consider a set of data points Φ that are not evenly spaced between them over the time t. Let's also consider a linear interpolant λ such as $\Phi_i < \lambda_y < \Phi_{i+1}$ and $t_i < \lambda_x < t_{i+1}$.

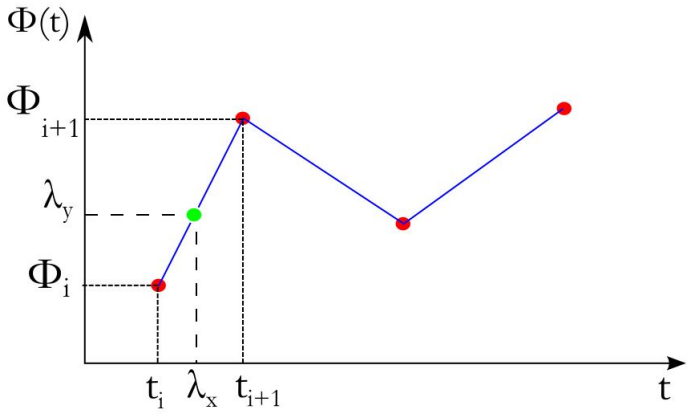

Figure 5.5: Linear interpolation on a data set (red points) and the linear interpolants (blue lines).

The expression to represent the linear interpolant is as follows:

$$\lambda_y = \Phi_i + \frac{\lambda_x - t_i}{t_{i+1} - t_i} \left[\Phi_{i+1} - \Phi_i\right] \tag{5.9}$$

5.1.2.2 Implementation

An interface was created in Matlab™ in order to simply the process on the operator point of view, as shown in Figure 5.7. Initially, the CAM file is selected and then read to generate, by a function **readgcode.m**, all the three dimensional coordinates that defines the tool path and its orientations. The three dimensional displacement between each point is calculated as follows:

$$D_i = \sqrt{(x_{i+1} - x_i)^2 + (y_{i+1} - y_i)^2 + (z_{i+1} - z_i)^2} \tag{5.10}$$

For a tool tip velocity of $v_{tt} = 1000$ millimeters per minute, the required time between each point is computed:

$$t_i = \frac{D_i \cdot 60}{v_{tt}} \tag{5.11}$$

Each increment of time is added to the previous one, so that a continuous function time is established. Then, the raw data that was converted from the CAM file is interpolated on a Simulink™ model (see Figure 5.6) through lookup tables that does the linear interpolation. The lookup table data is constituted by all the tool tip three dimensional coordinates and its orientations followed by the breaking points that are defined by the time function. On every increment of one hundredth of a second, a linear interpolation occurs and the final results is a set of evenly spaced points over time.

Regarding the Figure 5.7, the loaded data (from the CAD/CAM file) is a pyramid represented at red. After computing the three dimensional displacement between each point and given the velocity determining the required time function, the data is interpolated on the Simulink® model through the lookup tables and the final result is a evenly spaced set of points that are shown in blue.

The interpolated data (pyramid at blue) is then saved and sent to the SPIF-A machine and is ready to perform on automatic mode.

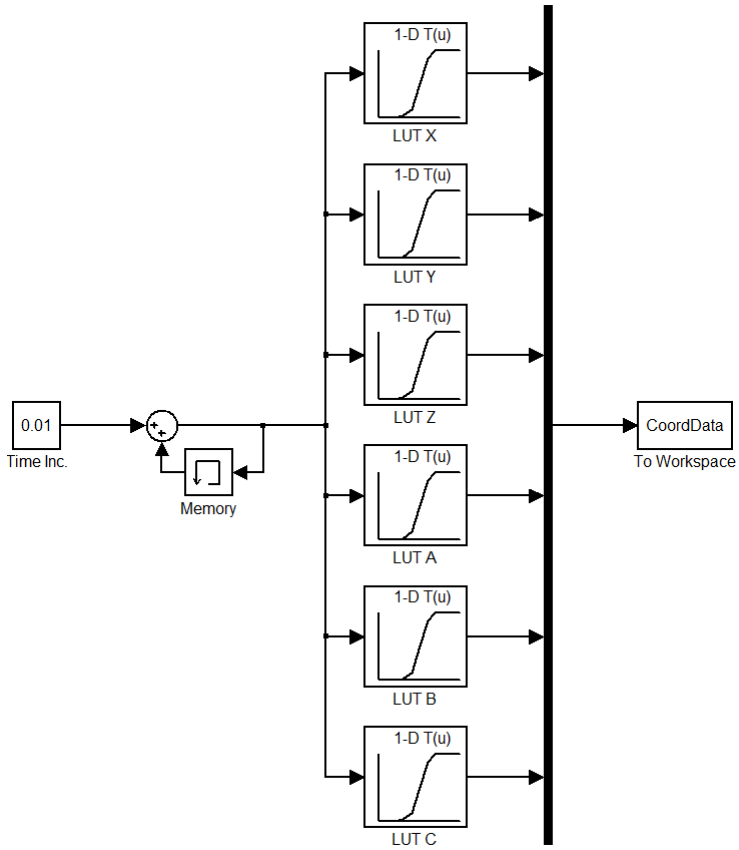

Figure 5.6: Simulink^{TM} model to interpolate raw data.

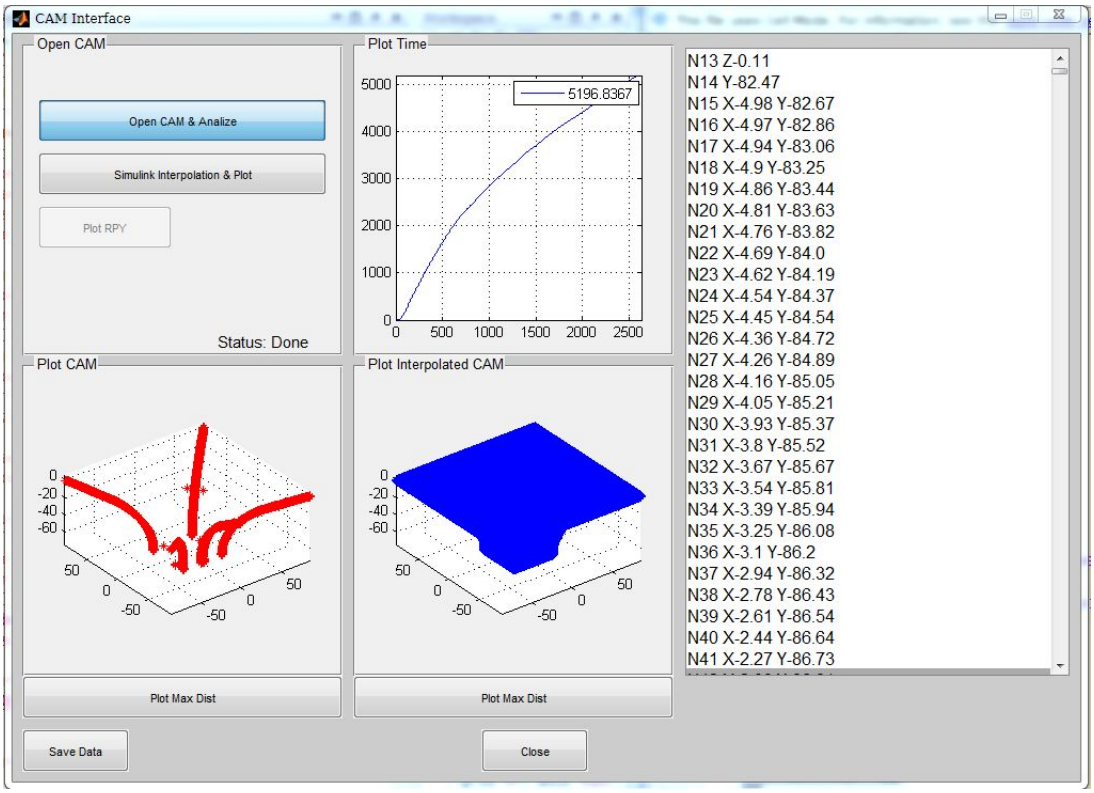

Figure 5.7: Interface created to pre-process the CAD/CAM data.

5.2 Simulator

An interface was developed in Matlab™ to simulate the 6DOF motion of the SPIF-A machine. It serves for off-line analysis where manual motions can be introduced either manually or by an external device such as a joystick. The forward and inverse kinematics is also displayed on the interface which is useful to check if a certain three dimensional coordinate and its orientation is possible to achieve on the SPIF-A machine. This interface is also enhanced with the possibility to read and run CAM files containing the desired tool path. During the simulation of any tool path, is possible to check if it is inside or outside of the SPIF-A working space, i.e, if it is feasible taking into account the machine spacial limitations.

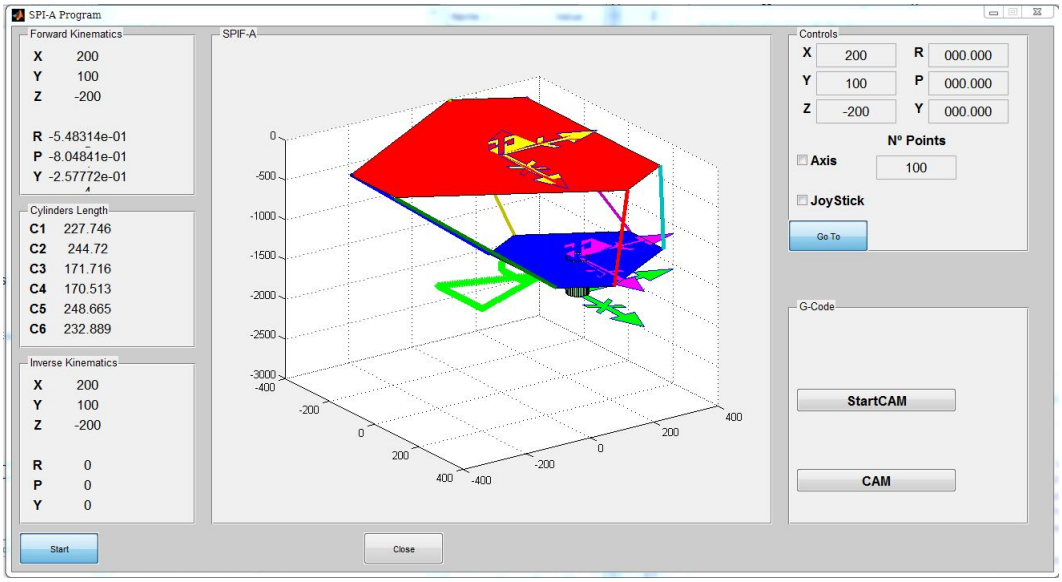

Figure 5.8: Simulator's Interface.

5.3 Target Machine Simulink™ Model

The xPC machine by Speedgoat™ works by running a preloaded Simulink™ model whose variables are read and write by the xPC I/O modules via TCP/IP connection. These variables are read and altered by Matlab™ via command window that it is synchronized to the preloaded Simulink™ model.

The xPC machine communicates with the target machine's hardware via the following two different modules [71]:

- **IO101** —Is a 16-bit analog module with 32 single-ended or 16 differential analog inputs, 8 analog outputs, 8 digital inputs and 8 digital outputs TTL channels. Manufactured by Acromag™.

- **IO401** —It is a digital input module that provides 6 individual channels of 32-bit counters to connect incremental and absolute encoder sensors, it supports both TTL and RS422 differential encoder outputs selectable via DIP switches. Manufactured by TEWS®.

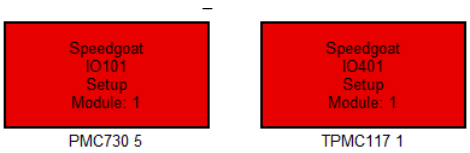

Figure 5.9: xPC target I/O modules configuration.

Speedgoat™ provides a custom library with a range of functions and blocks from analog/digital input/output readers to specialized digital applications, that are usable in Simulink™ environment.

5.3.1 Input Variables

The motion movements that are established either from the interface controls or via manual input from Matlab™ command window are changed on the Simulink™ model in the real-time target machine.

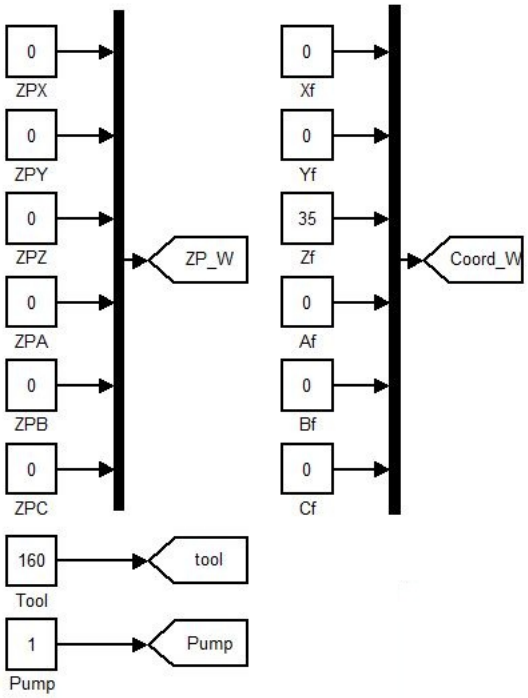

Figure 5.10: Input variables on Simulink™ model.

These variables suits only for manual movements, zero part offset, tool length and pump on/off control. The variables that correspond to ZP_W are related to the zero part offset in terms of tool positioning and orientation. The tool variable is related to the length of the forming tool installed on the spindle system of the SPIF-A machine. The on/off pump control is attributed to the variable pump, where 1 stands for "on" and 0 for "off". The remaining variables that defines $Coord\_W$ are responsible for manual movements on the parallel platform, regarding the tool tip position and orientation. All these variables are being constantly updated while the Simulink™ is running on the target machine.

5.3.2 Actuator encoder reader

The SPIF-A actuators are equipped with absolute linear transducers, that produce RS422 differential output signals. The output signal is read by an absolute encoder block from Speedgoat™ library on the Simulink™ model. The values from the encoder are then analyzed by an embedded Matlab® function.

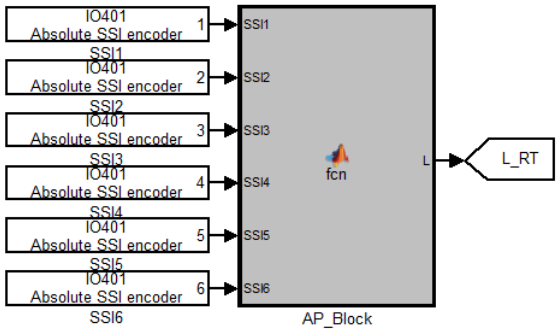

Figure 5.11: Actuator's encoder analyzer block on Simulink™.

The magnetostrictive transducers, that are equipped on the hydraulic actuators, measure the displacement between the sensor on the actuator's rod and the transducer's module. Due to the fact that they are assembled at the rear of the actuator, it measures a position about 52000 micrometers with the rod at its stowed position. The encoder on the Simulink™ model checks if the read position are within the correct range of 0 to about 452000 micrometers and, if not, it returns an error signal output. The embedded function subtracts for each actuator the stowed position offset, hence, the output displacement of all the six rods which are converted from 0 to 400 millimeters which are then used by other blocks on the Simulink™ model.

5.3.3 Analog input reader

All the analog signals used on the SPIF-A machine are connected to the xPC machine via I/O modules that are then read and converted by an encoder block from the Speedgoat™ library on the Simulink™ for further use. Analog signals such has the load

cells responsible for the FMS acquisition and the analog controls from the control console are read here, as well as the pressure transducer installed on the hydraulic distributor (see Section 3.3 to remind machine's instrumentation).

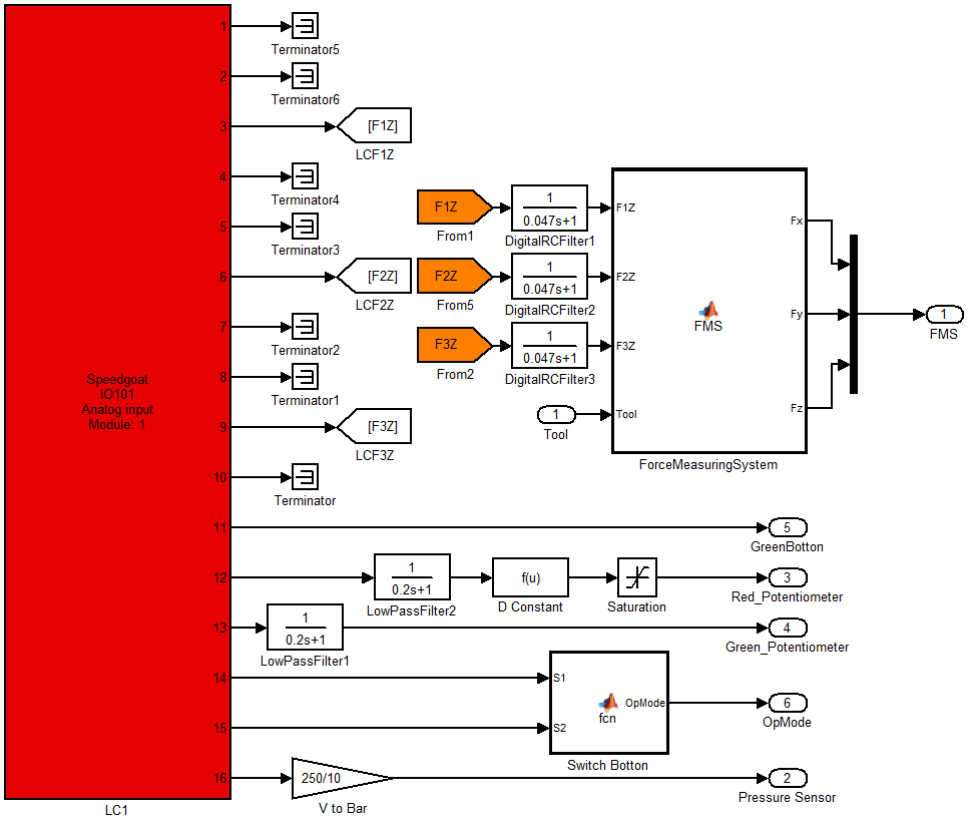

Figure 5.12: Analog input signals reader block on Simulink^{TM}.

The mentioned above load cells (LC) produces nine analog differential signals, that are read from first to the ninth port of the I/0 module. The embedded Matlab^{TM} function is equipped with low pass filters equal to the ones described in the Section 3.3. The LC signals are read, digitally filtered and then processed by the FMS equations deduced by Torrão [5] to produce both horizontal and vertical forces on the tool tip. The port number ten is unused. From eleven to fifteenth, the analog controls from the control console are read. The green bottom produces an output on/off and both red and green potentiometers produces a filtered signal that vary from 0 to 5 volts, for further use. The switch button signal is read and it is responsible to be the selector of the Automatic/Manual mode activation on the SPIF-A machine. Last but not the least, the sixteenth port reads and converts the acquired signal from the pressure transducer to bar.

5.3.4 Inverse Kinematics

The inverse kinematics deduction presented on the Section 4.1 is here implemented on the Simulink™ model. It is responsible to produce an output signal I_K given the desired spacial coordinates and orientation of the tool tip M_Coord, the tool length *tool* and the zero part offset ZP_W that is initially defined on input variables (Section 5.3.1).

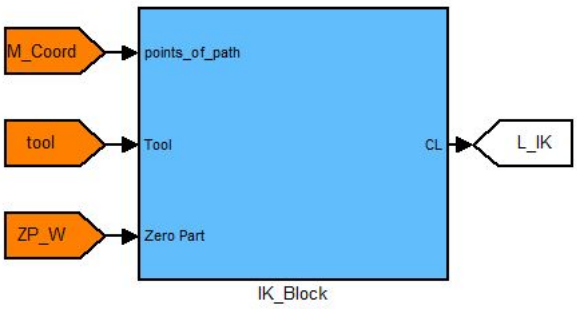

Figure 5.13: Inverse kinematics block on Simulink™.

The output signal is a 6 by 1 matrix containing the required six actuators length. The input signal M_Coord can be either spacial coordinates and tool tip orientation from the manual mode or from the automatic mode. This block is entirely responsible to convert any given spacial coordinate and orientation, no matter where it comes from, into actuators length variables.

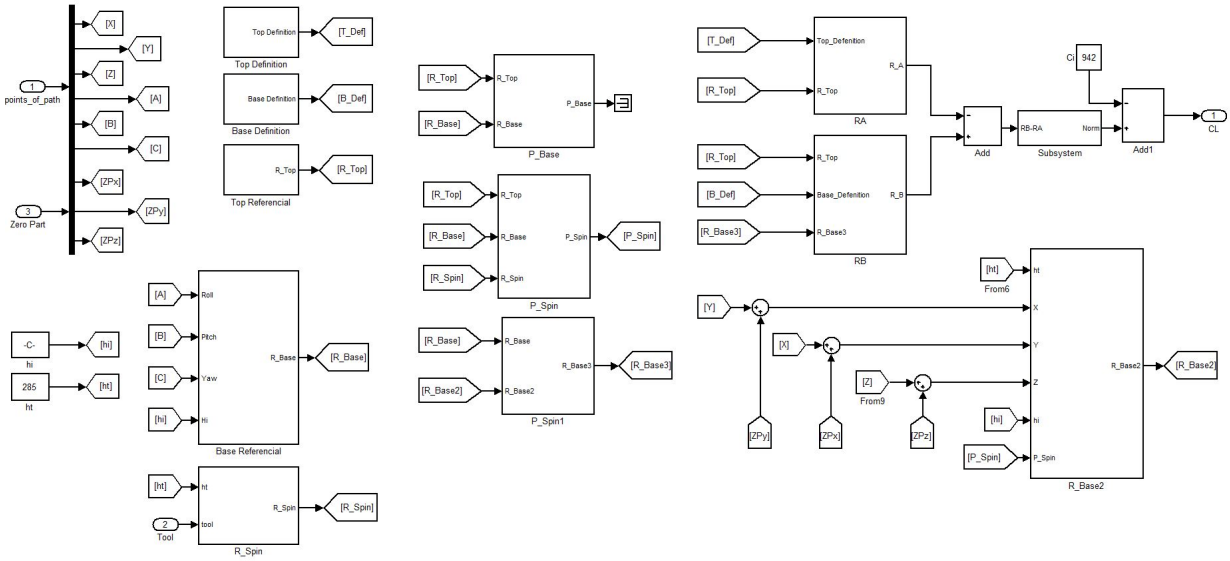

Figure 5.14: Inside of the inverse kinematics block on Simulink™.

5.3.5 Forward Kinematics

The forward kinematics used on the SPIF-A machine was deduced by Mendes Lopes [67] and then adapted to the parallel structure of this machine, as explained in Section 4.2. The iterative method uses the actual actuator length that are read by the Simulink^{TM} in Section 5.3.2 to produce the signal L_RT which is being constantly updated. Given the estimated candidate for the bottom platform by the iterative model, the zero part offset ZP_W and the tool length *tool* signals, the tool tip coordinate and orientation regarding the LCS are computed as described and deduced in Section 4.2.

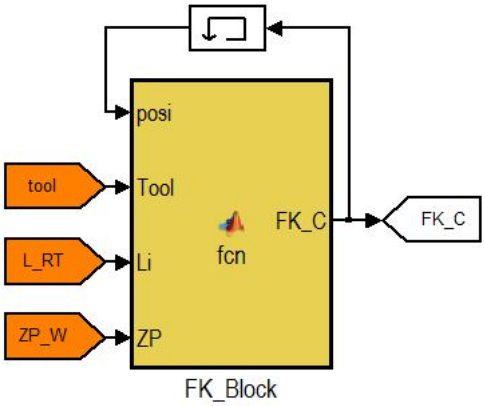

Figure 5.15: Forward kinematics function block on Simulink^{TM}.

Depending of the controller's performance, the forward kinematics accuracy may vary compared to the desired or given initial tool tip coordinate and orientation. To improve the performance of the iterative model and for a fast convergence, the initial value for the beginning of the iteration is last the valid one, memorized in a memory block.

5.3.6 Mode selector and implementation

The SPIF-A machine is equipped with two operations mode, the manual and automatic one as already said. The manual mode develops manual motions that are introduced by the operator on the input variable sections (Section 5.3.1) to create a desired motion as explained in the trajectory management section (Section 5.1) given the desired tool tip target spacial coordinate and orientation $Coor\_W$. The signal responsible to do the commutation between manual and automatic mode is the signal called $OpMode$ that is triggered by the switch button on the control console. If $OpMode$ has value of 1 it stands for automatic mode, otherwise, it stands in manual mode.

The automatic block is preloaded, to the six lookup tables, with the tool path coordinates and orientations. It is also equipped with a real time clock that performs linear interpolation on every fix step of the Simulink^{TM} model. It injects new coordinates and orientations on the machine at a rate specified by the signal C_S, denominated as clock speed.

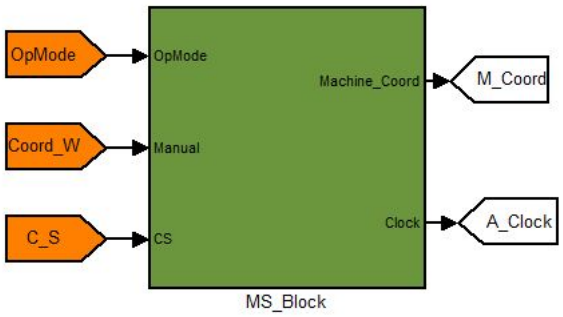

Figure 5.16: Mode selector block on Simulink^{TM}.

This mode selector block is also enhanced with a special block called security check, that either in manual of automatic modes checks if the injected coordinates and orientations are within the SPIF-A working space.

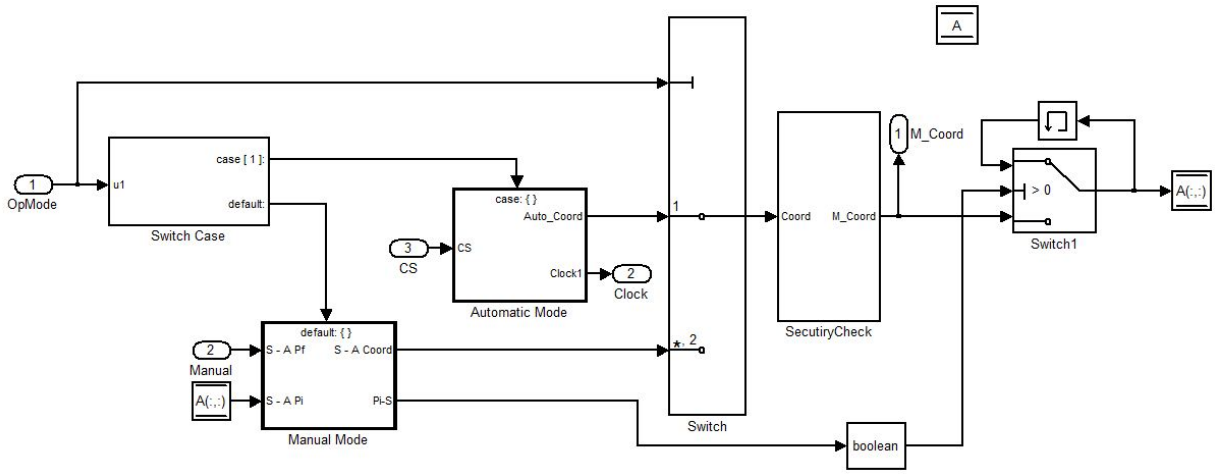

Figure 5.17: Mode selector block on Simulink^{TM}.

5.3.6.1 Velocity control on Automatic mode

Once the lookup tables are preloaded with the tool path containing the tool tip coordinates and orientations, if the automatic mode is activated the real time clock will start to tick on every fixed step of the Simulink^{TM} model. Here, the velocity control is given by the multiplicative factor C_S that will increase or decrease the speed of the real time clock. Therefore, the linear interpolation becomes faster or slower. Initially, has mentioned in the section 5.1.2, the tool path is pre-processed for a machining speed of one thousand millimeters per minute. The factor C_S is programmed to be in range of 0 to 15 and it is varied according to the red potentiomenter on the controle console. A signal of $C_S = 0$ stands for a machining speed of zero millimeters per second, i.e, the machine is stopped and a signal of $C_S = 15$ stands for a maximum theoretical (estimated) speed of fifteen

thousand millimeters per minute. Obviously, depending of the controller and the tool path trajectory, such speeds may be achieved or not. However, this method is suitable to speed up or temporally stop the machine during automatic operations.

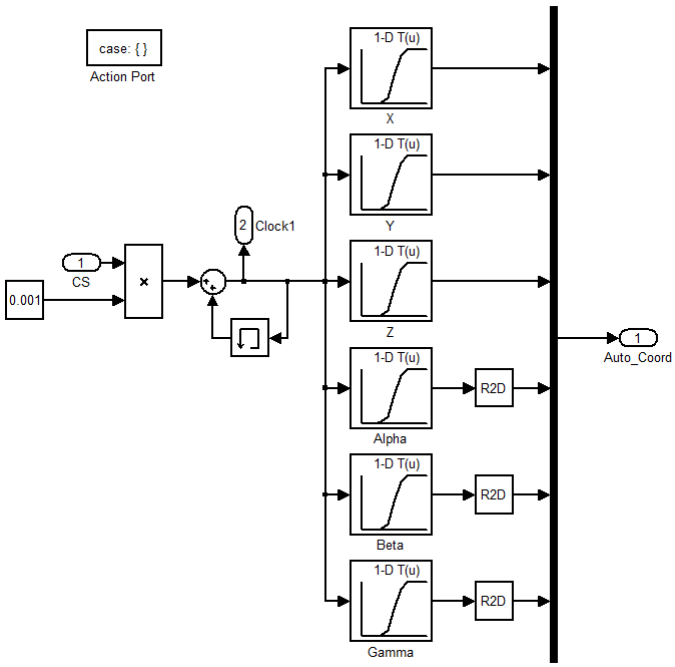

Figure 5.18: Velocity control on automatic mode.

5.3.6.2 Security check

Either in manual or automatic mode, each coordinate and orientation that is being sent to the machine is scanned to check if it is within the machine's workspace. For safety reasons, the values of X and Y cannot stand out of the range between -500 to 500 millimeters. Also, the maximum allowed travel in the Z axis is between 100 and -400 millimeters. Most importantly, and to avoid singularities and any mechanical failure, the Euler angles α, β and γ were chosen to stand in an interval of -25° to 25°. This limitation is also caused by the physical limitations of the U-joints that connects the actuators to the bottom platform. So, during an experiment the collision between the bottom platform with the working table are less likely to occur.

If the desired coordinate or orientation does not meet the security parameters, it will stop the machine and keep it on the last safety coordinate or orientation memorized on the memory blocks, waiting for new instructions.

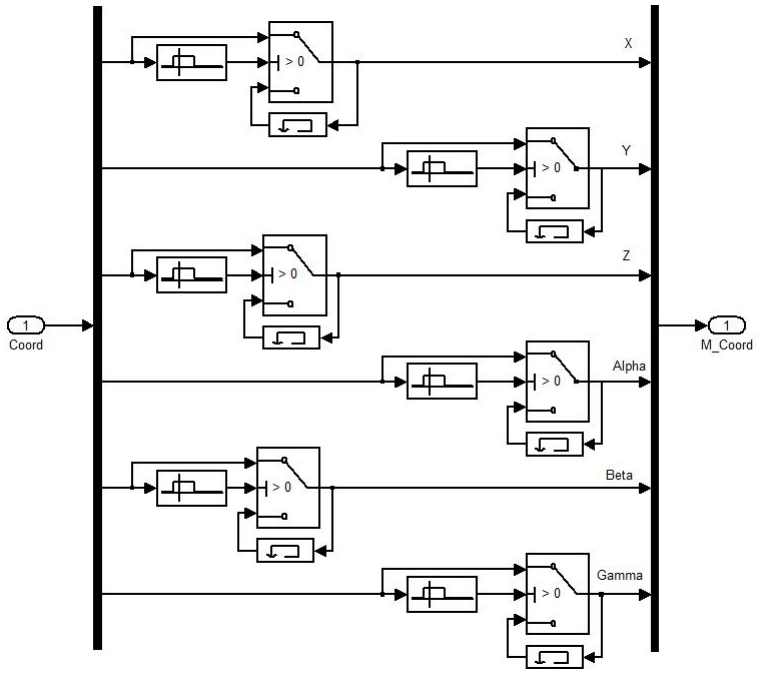

Figure 5.19: Inside Mode's selector block on Simulink^{TM}.

5.3.7 Error and controller blocks

As known, position controllers works based on the actual error between the desired position L_IK and the actual position L_RT of the parallel platform. On the SPIF-A machine, the error is based on the actuators length. It was chosen not to do it with the inverse and forward kinematics for safety and performance reasons. For instance, if the iterative model on the forward kinematics for any reason does not converge, it will cause virtual errors and leading to instability. Once the actuators length are read in real time, the error is the displacement between the read actuator's length L_RT and the inverse kinematics desired actuator length L_IK.

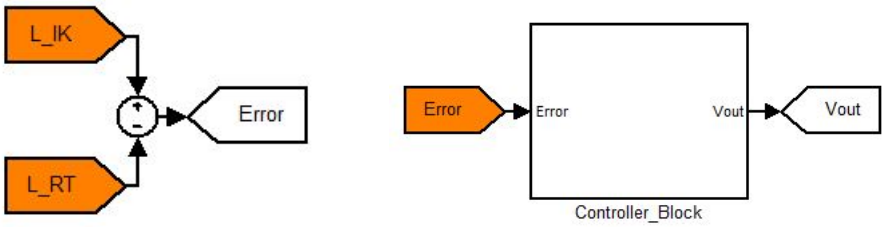

(a) Error block (b) Controller block

Figure 5.20: Error and controller's block on Simulink^{TM}.

5.3.8 Output Signals

The xPC machine is responsible to generate some output analog signals to control the pump and the servo-solenoid valves. After the controller's block, the signal needs to be converted in volts so that it is possible to feed the servo-solenoid valves to perform their motion. Also, the pump signal control on/off is controlled by the xPC machine through an variable that is commanded by the operator.

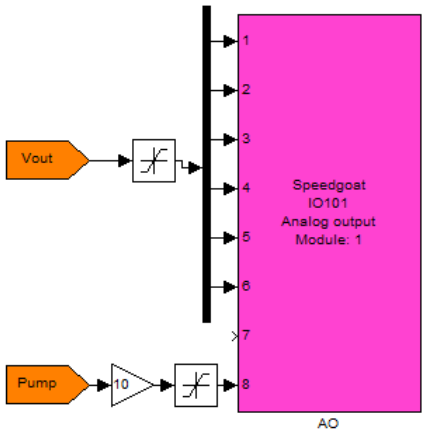

Figure 5.21: Output signals block on Simulink^{TM}.

5.3.9 Scopes for xPC interface

Just for visualizing purposes, it may be interesting to see what is happening, in real time, in the machine. Variables such as the vertical and horizontal forces on the tool tip that are being acquired by the FMS, the actuators errors, the pressure on the hydraulic system, etc. may be observed by plotting these parameters on the xPC interface through the scopes available on the Speedgoat^{TM} library.

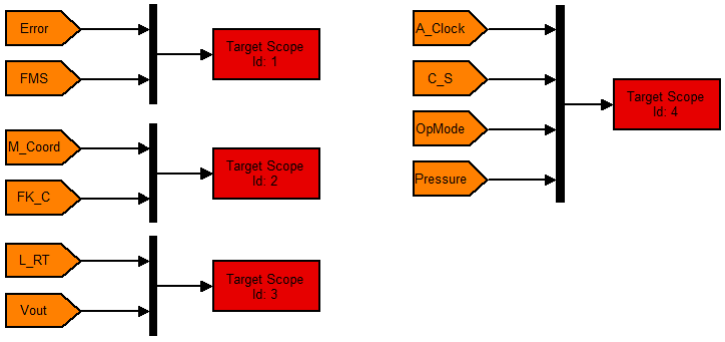

Figure 5.22: Scopes for data visualization on xPC interface.

5.4 Overall look on the Simulink™ model

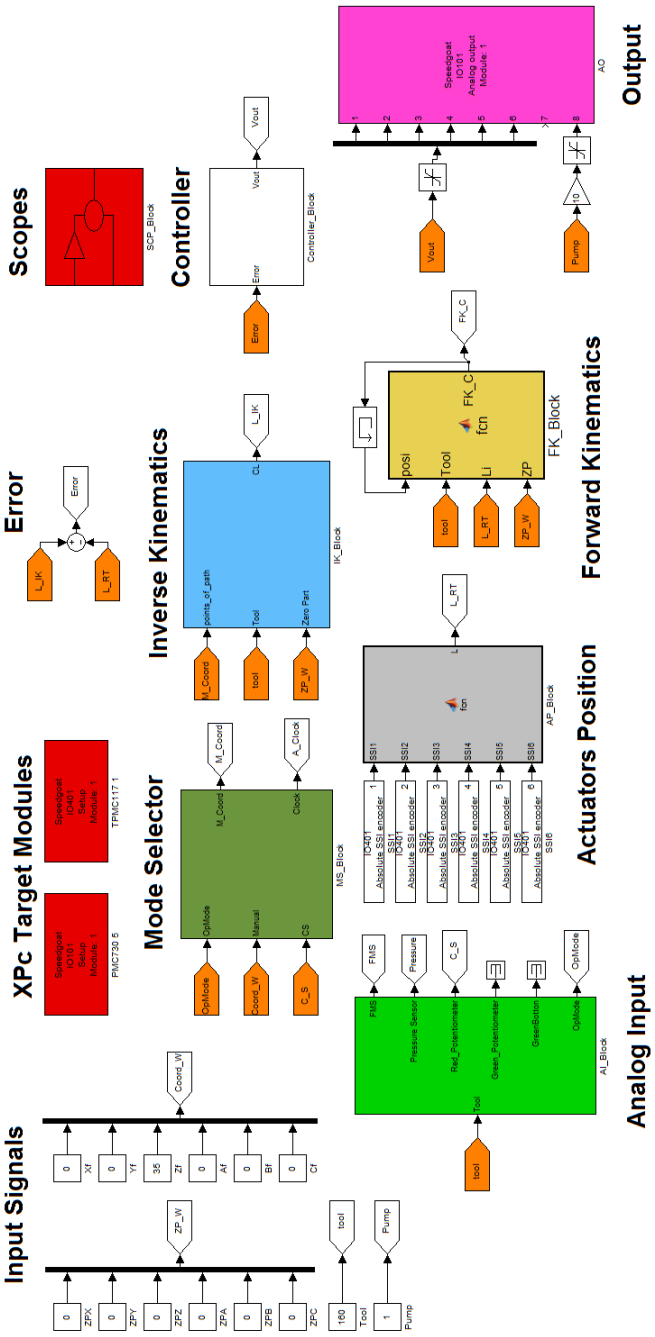

Figure 5.23: Overall visualization of the entire Simulink™ model.

5.5 Operator Interface

A custom made GUI interface was created in Matlab^{TM} in order to simplify the operator's job to handle with the machine's parameters. It has several roles and it is mainly divided into three sections: Automatic, Manual and Simulation modes. The simulation mode is the one already described in the Section 5.2. The manual mode's window is the one where the operator can manually change the machine's variables to perform manual motions. Last but not the least, the automatic mode's windows serves to setup an automatic experiment as well as visualize the FMS's graphic and other relevant information.

This interface is in constant development regarding the most useful operator's needs.

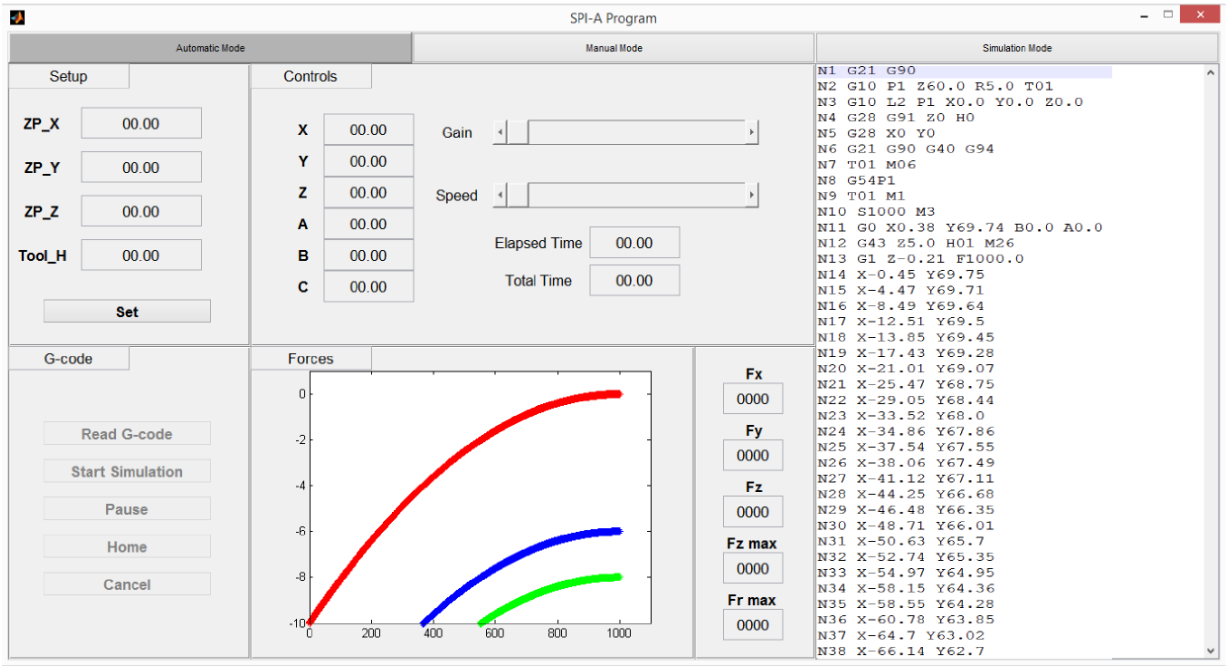

Figure 5.24: SPIF-A's developed interface.

Chapter 6

Position Controller Design and Implementation

A brief introduction about PID and fuzzy logic controllers is given as well as its design and implementation both with anti-windup system.

6.1 Introduction

In many systems, such as parallel manipulators, which have unique physical characteristics, a mathematical model is hard to address. The natural dynamics of the parallel manipulator is often coupled with non-linear equations subject to damping effects. A mathematical model of the SPIF-A machine is not available and it yet to be discovered.

Primarily, linear control methods are designed, such as a conventional PID controller with anti-windup system. Afterwards, more complex control methods such as fuzzy logic controllers (FLC) are designed and implemented proving its capability to deal with non-linear effects also complemented with an anti-windup system.

However, FLC on-line computation is heavy. This problem is solved by representing the FLC model in matrix form. To execute the FLC model in real-time on the xPC target machine, look up tables (LUT) 1D or 2D are created by using specific functions in the Matlab^{TM}'s Fuzzy Logic Toolbox. Hence, for each value of position error and/or position error derivative, an actuation value in the LUT is associated. These LUT are then transferred and used on the Simulink^{TM} model in the xPC target machine.

All the following designed controllers were optimized to decrease the steady state error and to increase the performance of trajectory response, which are the two main aspects of the machine.

6.2 Proportional-Integral-Derivative Control (PID)

"Based on a survey of over eleven thousand controllers in the refining, chemicals and pulp and paper industries, 97 % of regulatory controllers utilize PID feedback."

Desborough Honeywell, 2000.

PID controllers is undoubtedly the most common way of solving practical control problem. This algorithm is often used worldwide by engineers to control any kind of machine that needs positioning and velocity control. PID control can be either approached analytically or by some empirical rules. There are plenty of possible configurations, some of them do not use derivative action. When a actuator is saturated, reset windup is a process that avoids the collapse of the integral action of the controller.

The first controller tested on the machine was the well-known conventional PID, as shown in Figure 6.1 and defined by the equation D.1. This linear control approach serves as an comparison regarding more complex control methods that will be further described, such as the FLC.

In a controller with integral action, the error will always be integrated and so the integral term may become very large or it "Winds Up". So, it is required an opposite sign of the error for a long period of time before the system gets back to normal functioning. An anti-windup method is implemented which will reset the integral term every time the servo-valve gets saturated. More information about integrator windup is presented in the Appendix D.4.

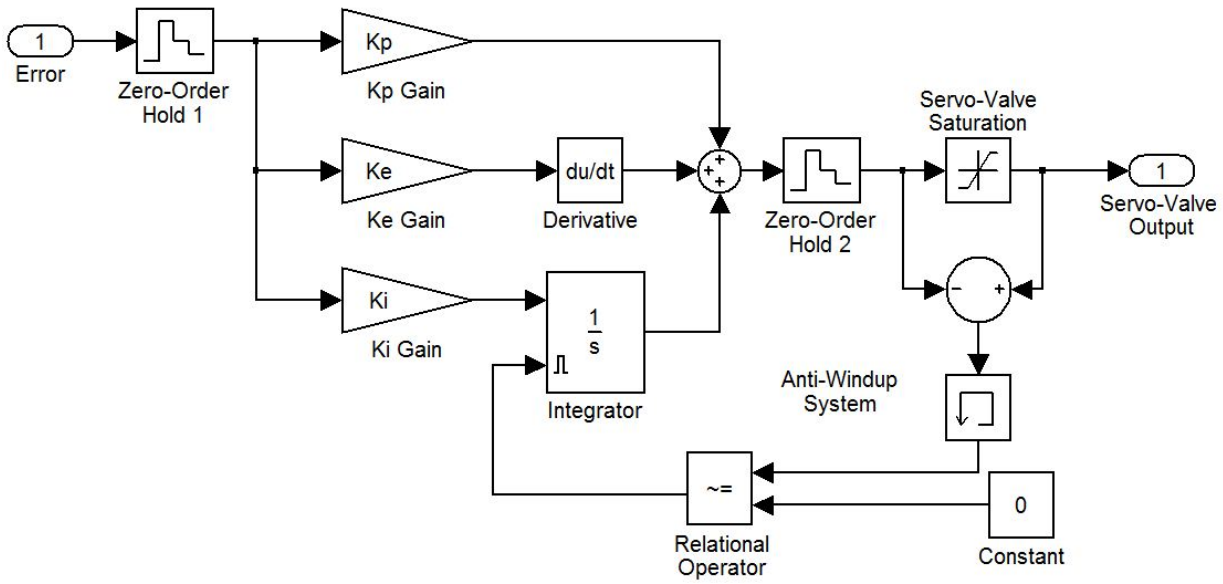

Figure 6.1: Diagram block of a linear PID controller.

$$u(t) = K_p e(t) + K_i \int_0^t e(\tau)d\tau + K_d \frac{de(t)}{dt} \tag{6.1}$$

The following optimized parameters were found: $K_p = 20$, $K_i = 0.01$ and $K_d = 8$.

6.3 Fuzzy Logic Control (FLC)

In opposite to conventional control techniques, FLC is best utilized in complex ill-defined processes that can be controlled by a skilled human operator without much knowledge of their underlying dynamics. The FLC incorporates the "expert skills" of a human operator into the design of the controller. In this kind of non-linear controllers, a process whose input-output relationship is described by a collection of fuzzy rules (If - Then rules) that involves linguistic variables rather than complicated dynamic model of the system. The utilization of linguistic variables, fuzzy control rules, and approximate reasoning provides means to implant human experience into the design of the controller.

A typical architecture of a FLC is shown in Figure 6.2 and comprises four principle steps: fuzzification, fuzzy rule base, inference engine and defuzzification.

A detailed explanation about FLC theory is presented in Appendix E.

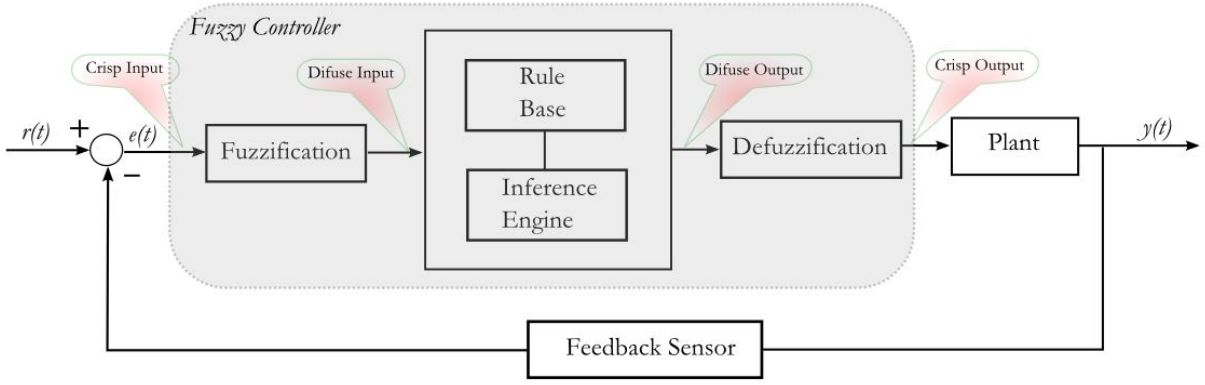

Figure 6.2: Fuzzy logic controller with feedback - Structure

Regarding the inference engine, there are mainly two types: Mamdani and Sugeno fuzzy inference engines.

6.3.1 Hybrid FLC PID Controller

This controller uses the non-linearly contributions of the error regarding the present, past and future. It consists in a development of a fuzzy gain scheduling scheme of PID control. This controller is based on Zhao's developed controller [75] and utilizes fuzzy rules and reasoning to determine the controller parameters, and the PID controller generates the control signal. A better control performance is expected than using a conventional PID controller with fixed parameters. The fuzzy logic controller is responsible to tune the KF_p,KF_i and KF_d parameters in a non-linear way that are then used in the tuned PID, as shown in Figure 6.3.

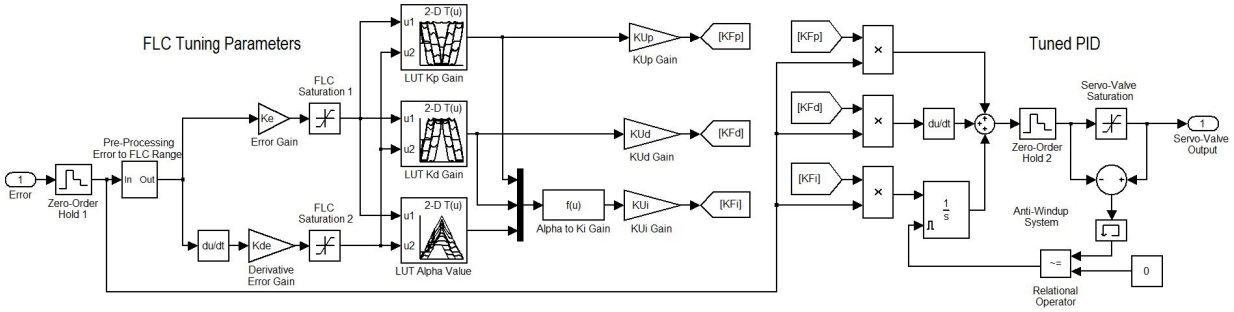

Figure 6.3: The implemented hybrid FLC PID controler's architecture.

To better understand this model, let's assume the following considerations:

- $K_{Fuzzy-P}(e(t), \Delta e(t))$ is the output value for computing the proportional turning term by fuzzy logic rules implemented in the LUT.
- $K_{Fuzzy-D}(e(t), \Delta e(t))$ is the output value for computing the derivative tuning term by fuzzy logic rules implemented in the LUT.
- $K_{Fuzzy-\alpha}(e(t), \Delta e(t))$ is the output value for computing the α_p term by fuzzy logic rules implemented in the LUT.

In this model, three fuzzy logic systems were characterized. All of them are 2D and their inputs are the error $e(t)$ and its derivative component $\Delta e(t)$. The membership functions for both inputs $e(t)$ and $\Delta e(t)$ are illustrated in Figure 6.4.

The tuning parameters to the proportional term $K_{Fuzzy-P}(e(t), \Delta e(t))$ and derivative term $K_{Fuzzy-D}(e(t), \Delta e(t))$ are computed by using the membership functions Big and Small, as presented in Figure 6.5, whose Big and Small functions are defined by the Equations 6.3 and 6.2, respectively.

The $K_{Fuzzy-\alpha}(e(t), \Delta e(t))$ value is governed by four singleton membership functions as shown in Figure 6.6 which were extensive studied and determined by Zhao et al. [75]. He did various simulations regarding step responses to find the best range of $K_{Fuzzy-\alpha}(e(t), \Delta e(t))$ values that best fits many circumstances faced while dealing with position controllers.

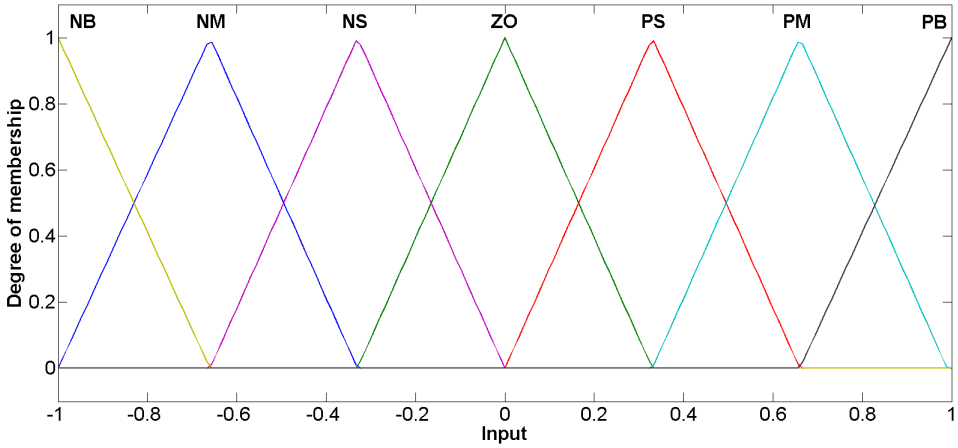

Figure 6.4: Membership functions for both $e(t)$ and $\Delta e(t)$ input.

The adopted fuzzy rules to the gains $K_{Fuzzy-P}(e(t), \Delta e(t))$, $K_{Fuzzy-D}(e(t), \Delta e(t))$ and $K_{Fuzzy-\alpha}(e(t), \Delta e(t))$ are described in Table 6.1, 6.2 and 6.3 respectively. Also, the respective fuzzy surfaces are illustrated in Figures 6.7, 6.8 and 6.9.

$$\mu_{Small}(x) = -\frac{1}{4}\, ln(x) \tag{6.2}$$

$$\mu_{Big}(x) = -\frac{1}{4}\, ln(1-x) \tag{6.3}$$

Table 6.1: Fuzzy tuning rules for $K_{Fuzzy-P}(e(t), \Delta e(t))$.

		$\Delta e(t)$						
		NB	NM	NS	ZO	PS	PM	PB
$e(t)$	NB	B	B	B	B	B	B	B
	NM	S	B	B	B	B	B	S
	NS	S	S	B	B	B	S	S
	ZO	S	S	S	B	S	S	S
	PS	S	S	S	B	B	S	S
	PM	S	S	B	B	B	B	S
	PB	B	B	B	B	B	B	B

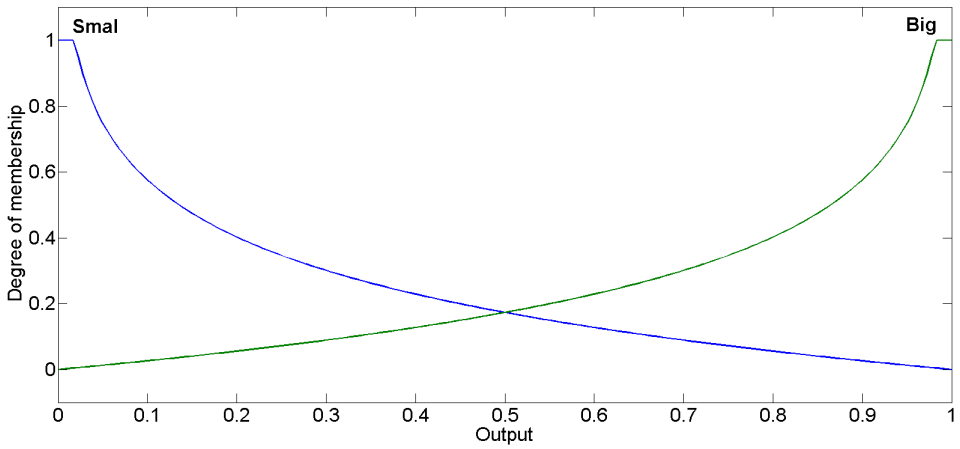

Figure 6.5: Membership functions for $K_{Fuzzy-P}(e(t), \Delta e(t))$ and $K_{Fuzzy-D}(e(t), \Delta e(t))$ tuning parameters.

The integral term is determined by using both output gains $K_{Fuzzy-P}(e(t), \Delta e(t))$ and $K_{Fuzzy-D}(e(t), \Delta e(t))$ with $K_{Fuzzy-\alpha}(e(t), \Delta e(t))$, that together and following the Equation 6.4 the integral gain K_i is computed.

$$K_i = \frac{K_{Fuzzy-P}(e(t), \Delta e(t))^2}{\alpha \cdot Td} = \frac{K_{Fuzzy-P}(e(t), \Delta e(t))^2}{\alpha \cdot K_{Fuzzy-D}(e(t), \Delta e(t))} \tag{6.4}$$

Regarding the Figure 6.3, the controllers is governed by the by the Equation 6.5:

$$u(t) = KF_p e(t) + KF_i \int_0^t e(\tau)d\tau + KF_d \frac{de}{dt} \tag{6.5}$$

where KF_p, KF_i and KF_d are followed by the Equations 6.6, 6.7 and 6.8 respectively.

$$KF_p = K_{Fuzzy-P}(e(t), \Delta e(t)) \cdot KU_p \tag{6.6}$$

$$KF_i = K_i \cdot KU_i \tag{6.7}$$

$$KF_d = K_{Fuzzy-D}(e(t), \Delta e(t)) \cdot KU_d \tag{6.8}$$

The following optimized parameters implemented in the controller, in Figure 6.3, were found : $Ke = 10$, $Kde = 10$, $KU_p = 50$, $KU_i = 1$ and $KU_d = 10$.

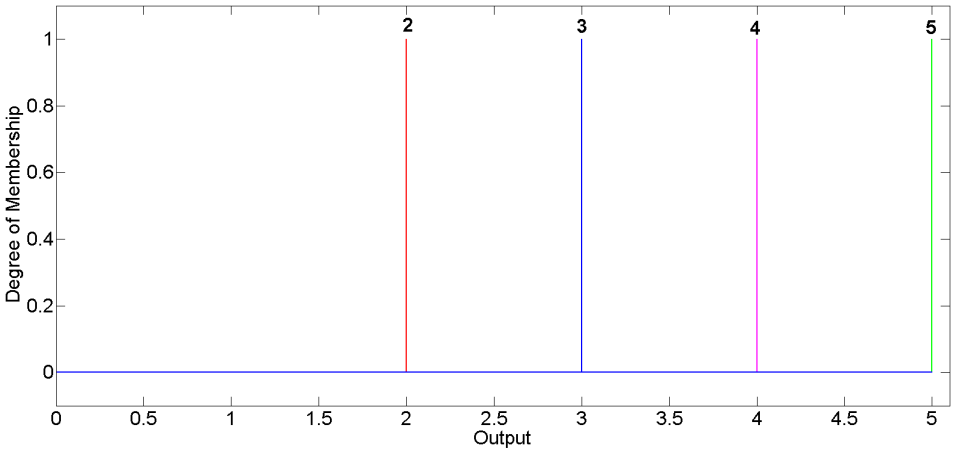

Figure 6.6: Membership functions for $K_{Fuzzy-\alpha}(e(t), \Delta e(t))$ value.

Table 6.2: Fuzzy tuning rules for $K_{Fuzzy-D}(e(t), \Delta e(t))$.

		$\Delta e(t)$						
		NB	NM	NS	ZO	PS	PM	PB
$e(t)$	NB	S	S	S	S	S	S	S
	NM	B	S	S	S	S	S	B
	NS	B	B	S	S	S	B	B
	ZO	B	B	B	S	B	B	B
	PS	B	S	S	S	S	B	B
	PM	B	S	S	S	S	S	B
	PB	S	S	S	S	S	S	S

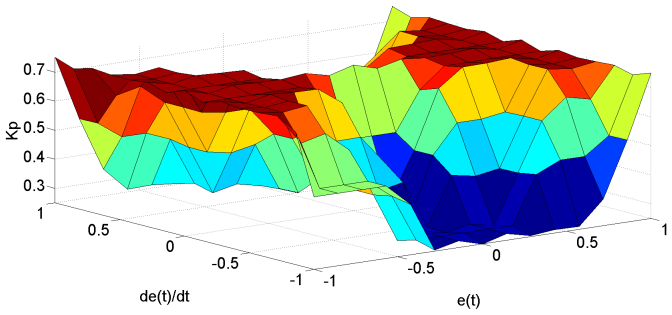

Figure 6.7: Fuzzy surface for $K_{Fuzzy-P}(e(t), \Delta e(t))$ tuning term.

Table 6.3: Fuzzy tuning rules for $K_{Fuzzy-\alpha}(e(t), \Delta e(t))$.

		$\Delta e(t)$						
		NB	NM	NS	ZO	PS	PM	PB
$e(t)$	NB	2	2	2	2	2	2	2
	NM	3	3	2	2	2	3	3
	NS	4	3	3	2	3	3	4
	ZO	5	4	3	3	3	4	5
	PS	4	3	3	2	3	3	4
	PM	3	3	2	2	2	3	3
	PB	2	2	2	2	2	2	2

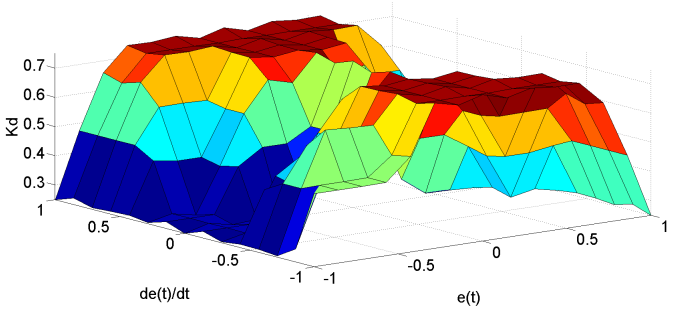

Figure 6.8: Fuzzy surface for $K_{Fuzzy-D}(e(t), \Delta e(t))$ tuning term.

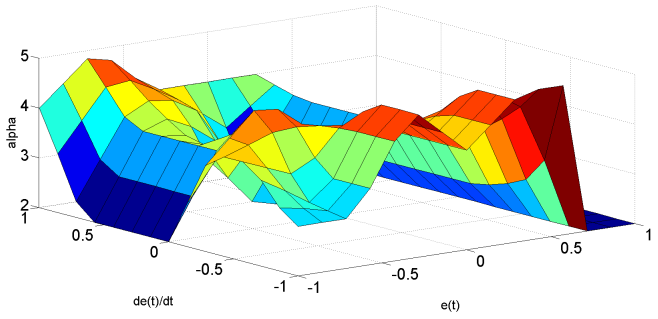

Figure 6.9: Fuzzy surface for $K_{Fuzzy-\alpha}(e(t), \Delta e(t))$ value.

6.3.2 Hybrid FLC P + I Controller

This controller was based in Marco [37] thesis to control a pneumatic system. It non-linearly uses the contribution of the present and future error and linearly the past. The behavior of the error and its derivative is further analyzed by set of fuzzy rules which controls the error's proportional action. For that, one 2D FLC was parameterised. The controller architecture with anti-windup system is illustrated in Figure 6.10.

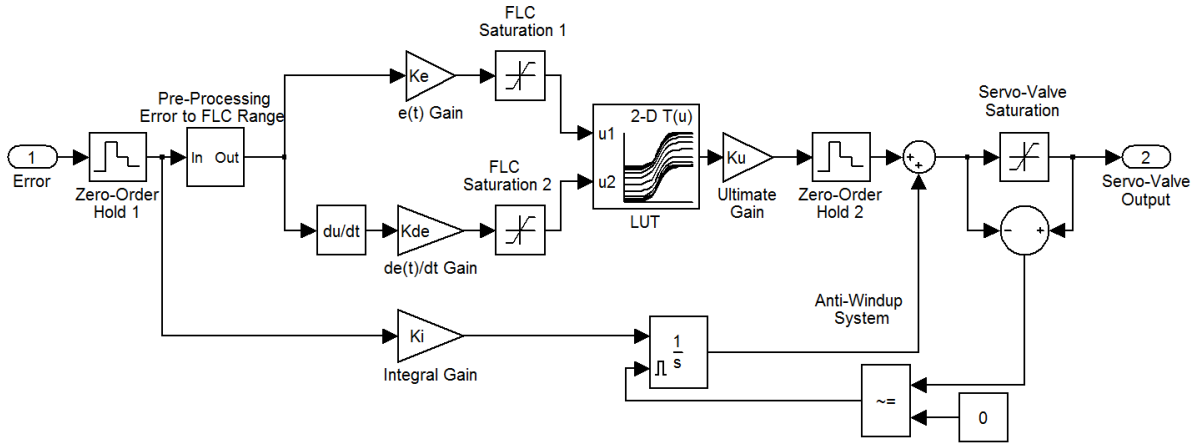

Figure 6.10: Diagram block of a hybrid FLC P + I controller.

The FLC is defined with two inputs: error $e(t)$ and its derivative $de(t)/dt$ and one output K_{Fuzzy}. There are two Gaussian membership functions called as "Negative" and "Positive" associated to both inputs $e(t)$ and $de(t)/dt$, as illustrated in Figure 6.11. Three singleton membership functions, see Figure 6.12, designed as NB (Negative Big), ZO (Zero) and PB (Positive Big) were chosen to associate to the output K_{Fuzzy}. Only four rules were used and are described in Table 6.4.

Table 6.4: Fuzzy tuning rules for $K_{Fuzzy}(e(t), \Delta e(t))$.

		$\Delta e(t)$	
		Negative	Positive
$e(t)$	Negative	NB	ZO
	Positive	ZO	PB

The applied fuzzy inference engine was Takagi-Sugeno type and the fuzzy surface regarding the fuzzy controller is illustrated in Figure 6.13.

Hence, the Equation 6.9 governs the controller shown in Figure 6.10.

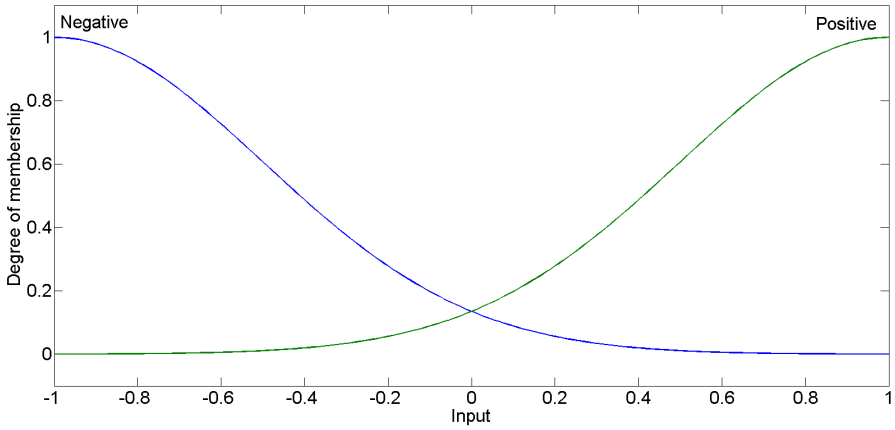

Figure 6.11: Membership functions to both inputs $e(t)$ and $de(t)/dt$.

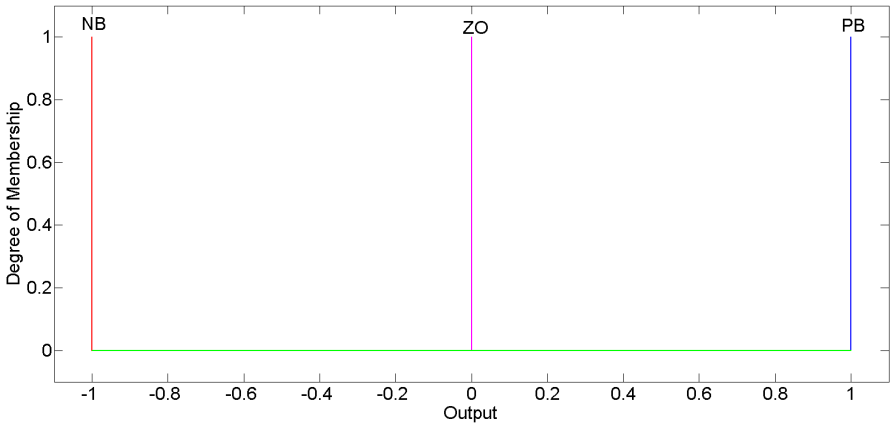

Figure 6.12: Membership functions to the output K_{Fuzzy}.

$$u(t) = K_{Fuzzy}(e(t), \Delta e(t)) \cdot Ku + K_i \int_0^t e(t)dt \tag{6.9}$$

The following optimized parameters were found: $Ke = 200$, $Kde = 200$, $Ki = 0.2$ and $Ku = 500$.

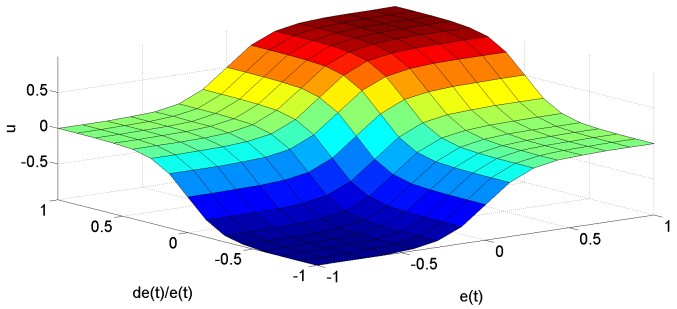

Figure 6.13: Fuzzy surface regarding the K_{Fuzzy} gain.

6.3.3 Hybrid FLC P + ID Controller

This controller is similar to the previous one described above. However, it differs in some aspects mainly on how the error derivative term is used. This controller non-linearly uses the contribution of the present error and linearly the past and future errors. The error's proportional gain is computed by using a set of fuzzy rules that analyses the dynamics of $e(t)$. For that, one 1D FLC was parameterised. The controller architecture with anti-windup system is illustrated in Figure 6.10.

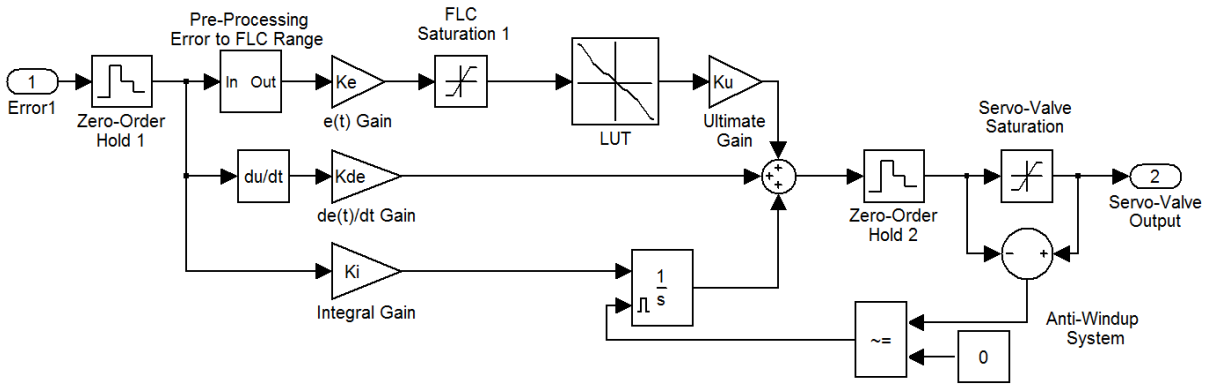

Figure 6.14: Diagram block of a hybrid FLC P + ID controller.

The FLC is defined with one input: error $e(t)$ and one output K_{Fuzzy}. There are seven Gaussian membership functions associated to the input $e(t)$, as illustrated in Figure 6.15. Also seven triangular membership functions, see Figure 6.16, designed as NB (Negative Big), NM (Negative Medium), NS (Negative Small), ZO (Zero), PS (Positive Small), PM (Positive Medium) and, finally, PB (Positive Big) were chosen to associate to the output K_{Fuzzy}. Seven rules were used and are described in Table 6.5.

The applied fuzzy inference engine was Mamdani type which implication, aggregation and defuzzification methods are minimum, maximum and centroid, respectively. The fuzzy surface regarding the fuzzy controller is illustrated in Figure 6.17.

Hence, the Equation 6.10 governs the controller shown in Figure 6.14.

Table 6.5: Fuzzy tuning rules for $K_{Fuzzy}(e(t)$.

e(t)	Output
NB	NB
NM	NM
NS	NS
ZO	ZO
PS	PS
PM	PM
PB	PB

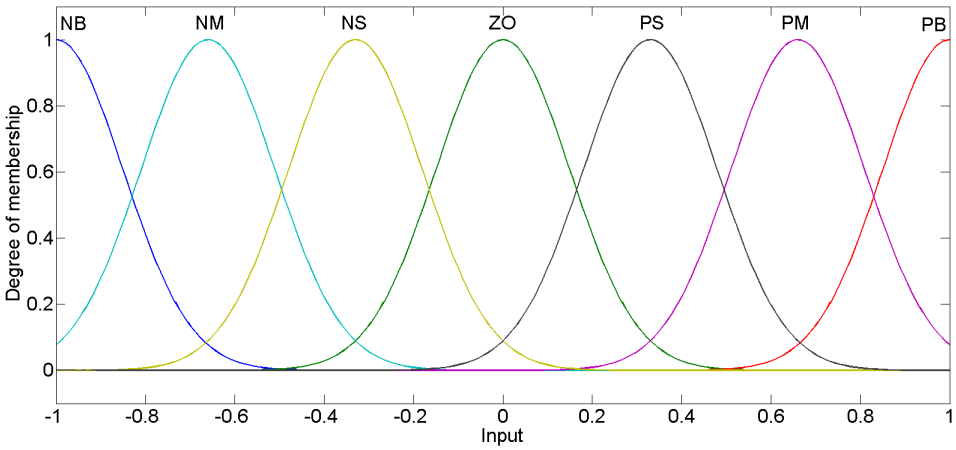

Figure 6.15: Membership functions to the input $e(t)$.

$$u(t) = K_{Fuzzy}(e(t)) \cdot Ku + K_i \int_0^t e(t)dt + K_d \frac{de}{dt} \tag{6.10}$$

The following optimized parameters were found: $Ke = 400$, $Kd = 1$, $Ki = 0.5$ and $Ku = 100$.

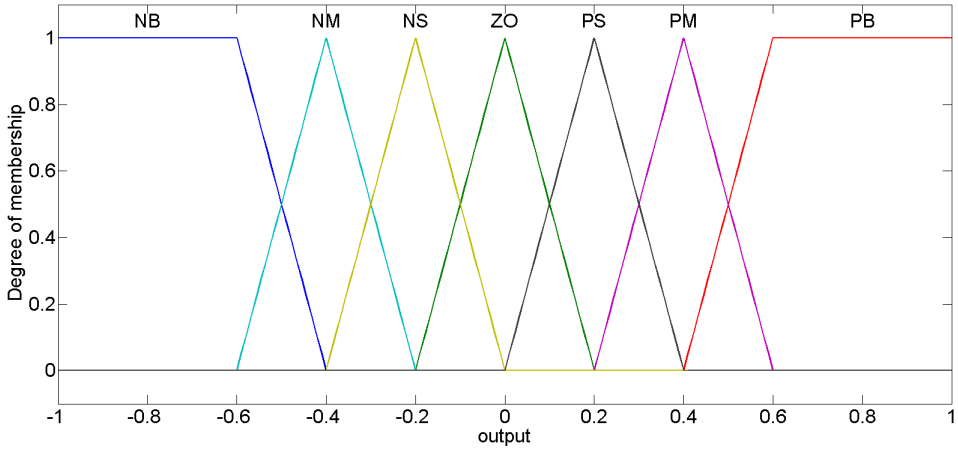

Figure 6.16: Membership functions to the output K_{Fuzzy}.

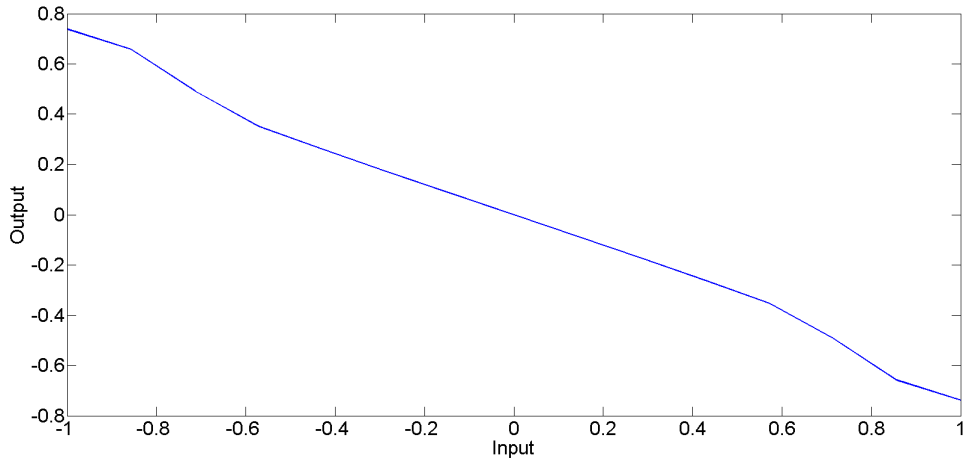

Figure 6.17: Fuzzy surface regarding the K_{Fuzzy} gain.

Chapter 7

Results and Experiments

Experiments and its results that were carried out on the machine regarding the chosen type of controllers are illustrated. The SPIF parts produced on the machine and its capability on motion accuracy is also demonstrated. A results discussion is given at the end.

In order to prove the machine's capability in producing accurate SPIF parts, many experiments were carried. Its novel design with extra DOF's over adapted milling machines (remind SPIF Machinery in Section 2.2.2) with higher stiffness will allow to perform 3-Axis and 5-Axis strategies within a specified machining speed while performing high forming loads. The implemented forward and inverse kinematics presented in Section 4.2 and 4.1, respectively, will be used to compute the desired motions and obtain its feedback. Also, the current instrumentation on the SPIF-A machine (see Section 3.3) will be used whenever it is need.

7.1 Evaluation of the Manual Mode Trajectory

The manual mode trajectory currently implemented in the SPIF-A machine is described in Section 5.1.1 and it is followed by a third order equation (see Equation 5.6) which is enhanced with null initial and final velocity. It makes easier to create manual motions and these are smother rather than to implement a huge step response which could lead to uncontrolled behavior. Here, the intermediate points between the initial and final points are linearly interpolated which makes the motion a lot more pleasant. No vibrations or uncontrolled moves were noticed during this experiment.

The Figure 7.1 shows a trajectory response implemented by the manual mode while moving from $C_{3D_i} = [0\ 0\ 0\ 0\ 0\ 0]^T$ to $C_{3D_f} = [75\ 50\ -75\ -5\ -10\ 15]^T$. The data was acquired via forward kinematics.

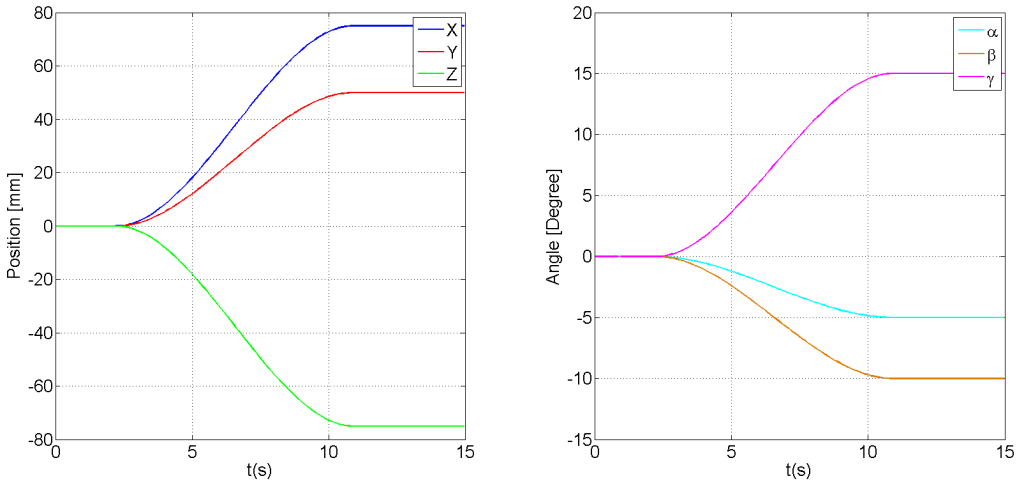

Figure 7.1: Manual mode motion acquired via forward kinematics.

7.2 Evaluation of the Velocity Control in Automatic Mode

Establishing determined machining speed is a key feature in producing SPIF parts. The material's performance in incremental forming highly depends on the adopted speed. So, the developed model described in Section 5.1.2 to establish a velocity control in automatic experiments will be tested. To prove its efficiency, it will be compared to the end-effector speed that can be mathematically obtained by using the Jacobian matrix J_E as deduced in Section 4.5 via differential kinematics.

Two tests were carried out, one regarding 3-Axis machining and another one regarding 5-Axis machining as illustrated in Figure 7.2 and 7.3, respectively.

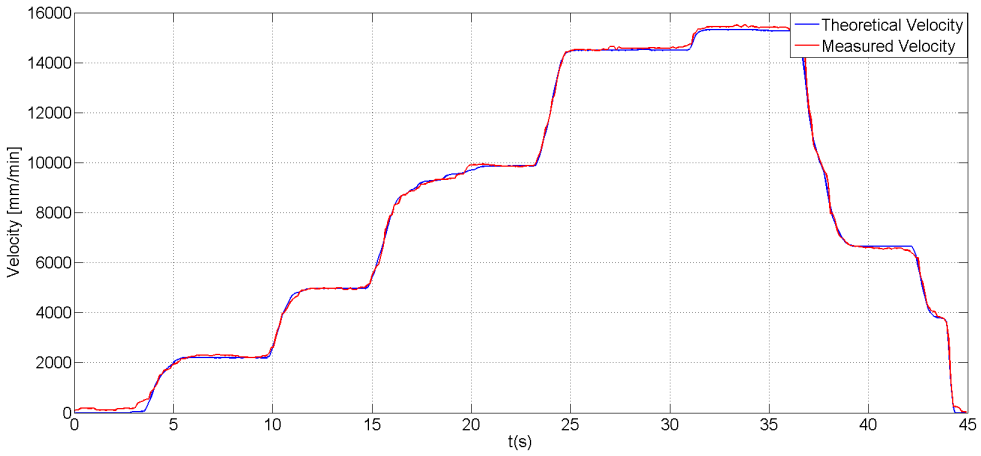

Figure 7.2: Velocity control in automatic mode - 3 Axis experiment.

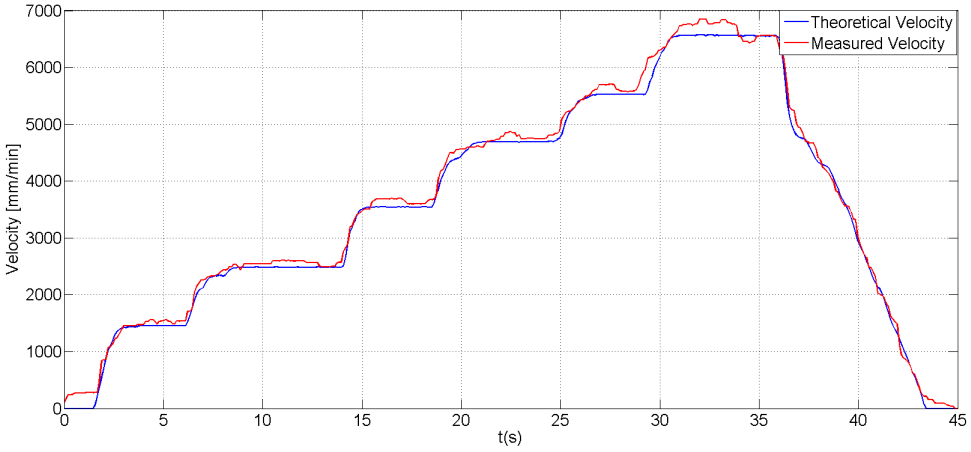

Figure 7.3: Velocity control in automatic mode - 5 Axis experiment

7.3 Controllers Performance Evaluation

In order to evaluate the designed controller's performance, experimental tests were carried on the machine in 5-Axis strategy which is more demanding. These experiments consisted in performing circular motions while forming a hard metal sheet of 3 millimeters thick. Initially, the controller and trajectory data is loaded into the xPC target machine. Primarily, manual motions were done to select the best controller's parameters, by trial and error method. The chosen parameters were the ones to decrease the steady state error and increase the performance in trajectory response. After the tuning of the controller's parameters, the machine is set in automatic mode to do circular motions while in the presence of forming forces. During the data acquisition, the experiment was sliced into three parts: Initially, the machine is stopped at a certain position for steady state data acquisition, then, the automatic mode velocity is gradually increased up to 4000 mm/min to acquire data regarding trajectory response. At the end, the velocity is gradually decreased to zero for a while to evaluate once again the steady state error. All the acquired experiments last around thirty seconds and were acquired via Matlab^{TM} software.

It is pretended to evaluate and compare the fuzzy logic controllers developed in Section 6.3 with the conventional PID controller in Section 6.2 regarding the steady state error and trajectory response while under forming forces.

7.3.1 Experimental Results

Figure 7.4 and 7.5 illustrates the imposed trajectory on the XYZ space and Euler angles $\alpha\beta\gamma$, respectively, to do the controller's performance test. It comprehends a 5-Axis trajectory with a maximum tool's tip angle of fifteen degrees.

Figure 7.6 and 7.7 shows the error in steady state and trajectory response for each tested controllers. The error is computed by the difference of forward and inverse kinematics. In terms of numbers, the Table 7.1 shows the maximum and average error either in steady state and trajectory response for each controller. The data the norm of the space (i.e. $e = \sqrt{e_1^2 + e_2^2 + e_3^2}$).

The controllers outputs which fed the servo-solenoid valves are illustrated in Figure 7.8 and also shows the valve effort imposed on the actuators.

Regarding the differential kinematics to compute the actuators forces (see Section 4.4) are shown in Figure 7.9 and were acquired during one of the experiments.

The pressure transducer installed on the hydraulic distributor (remind Section 3.3) serves to measure the pressure changes and was also acquired during one of the experiments and it is illustrated in Figure 7.1

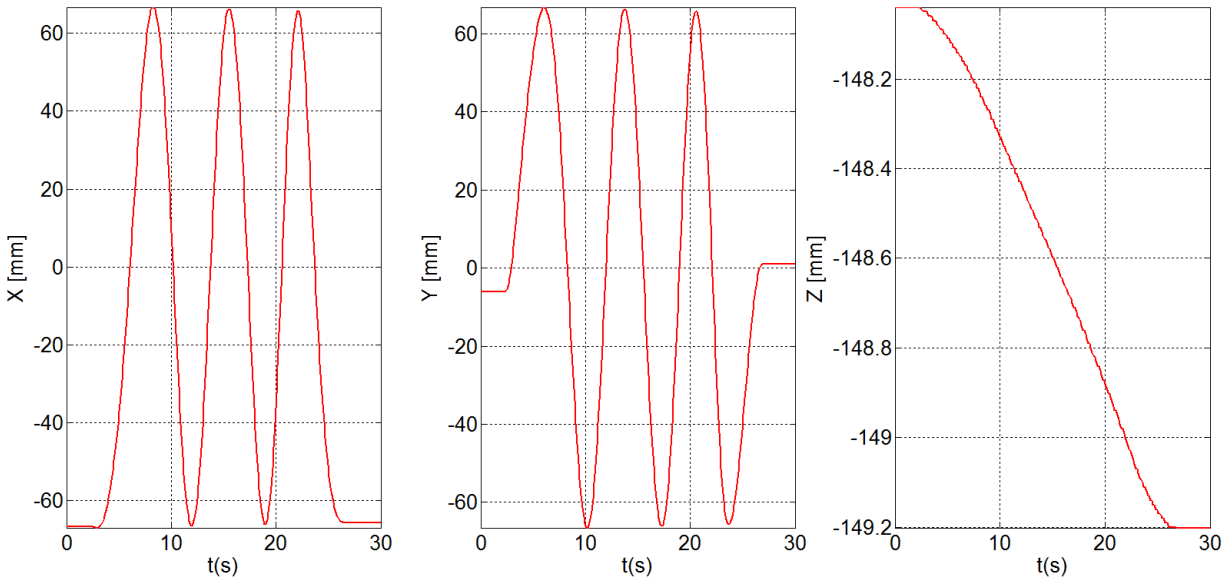

Figure 7.4: Imposed trajectory regarding ZYX.

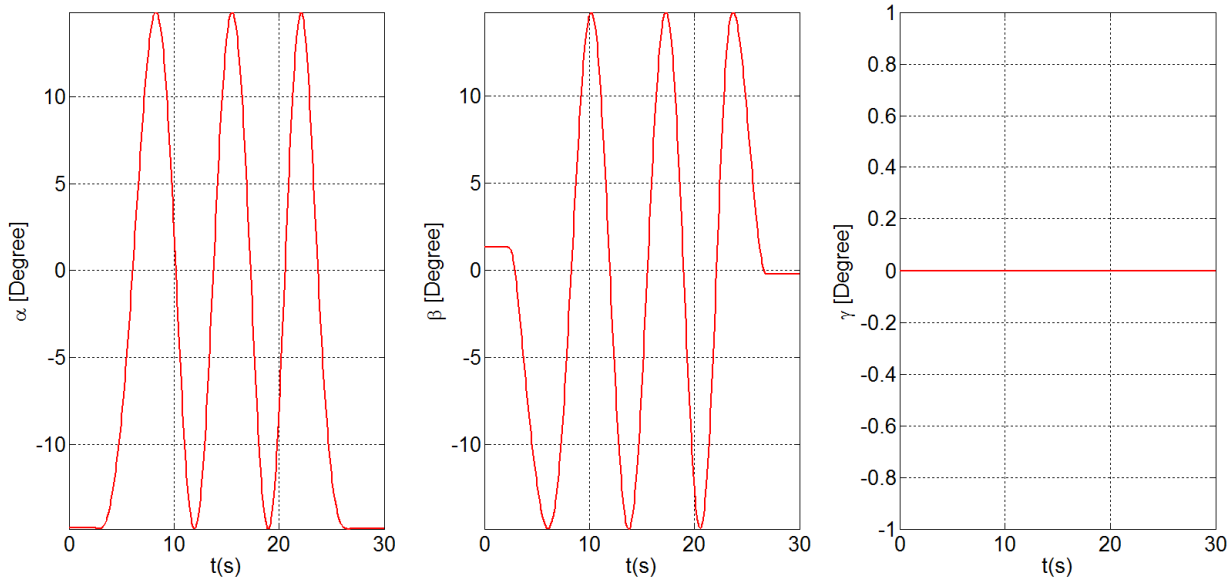

Figure 7.5: Imposed trajectory regarding α,β,γ.

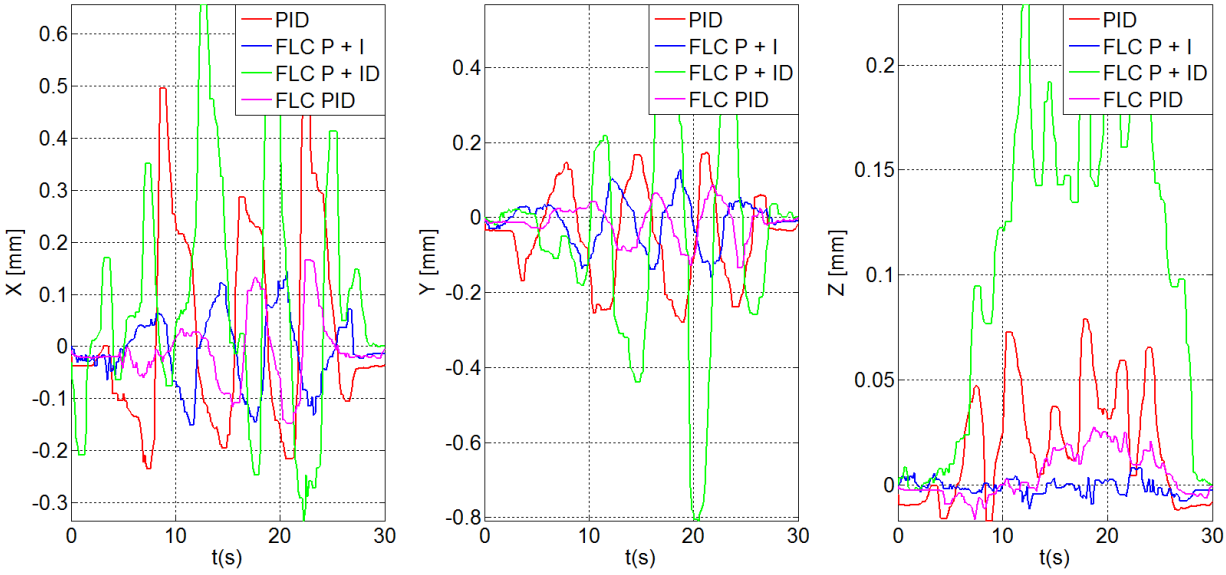

Figure 7.6: Controller's error during the experiment regarding the XYZ space.

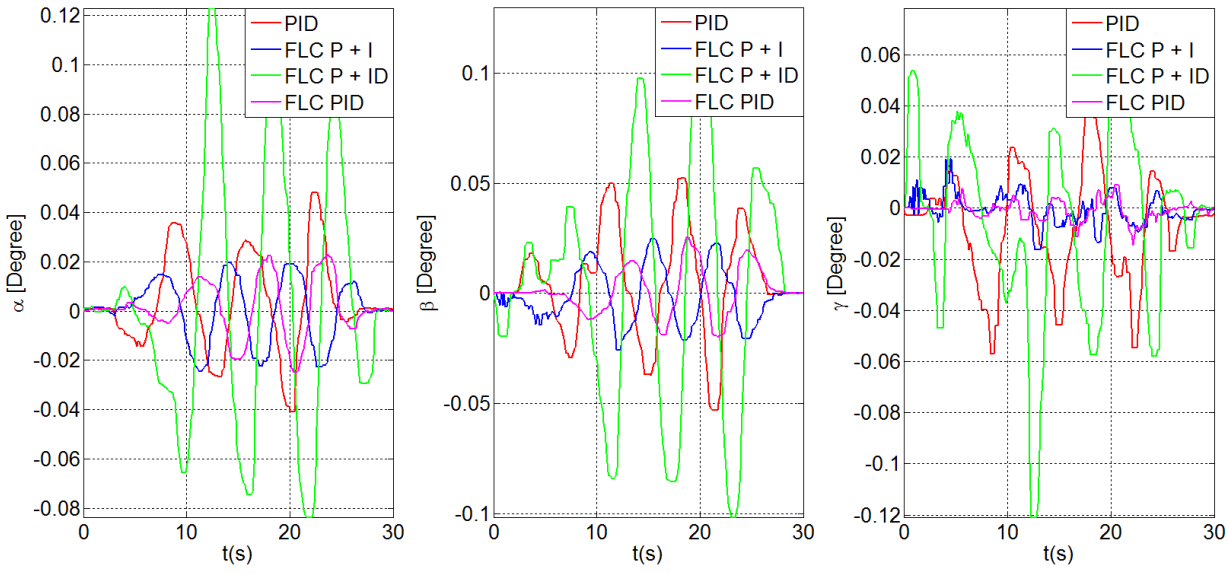

Figure 7.7: Controller's error during the experiment regarding the Euler angles α,β and γ.

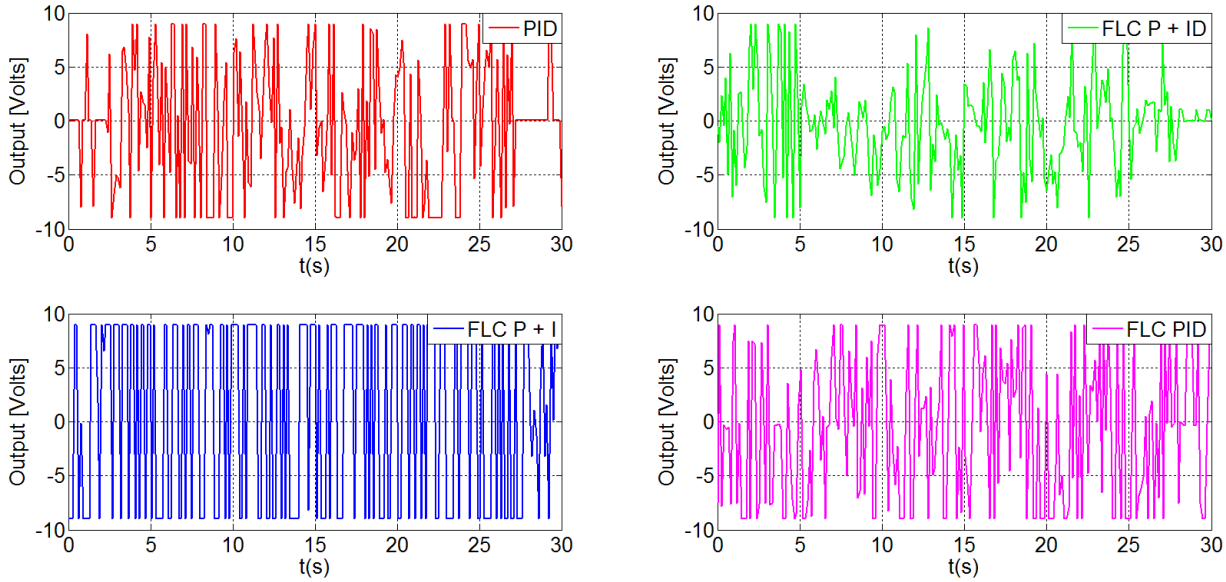

Figure 7.8: Controller's output to the servo-solenoid valves - Valve effort.

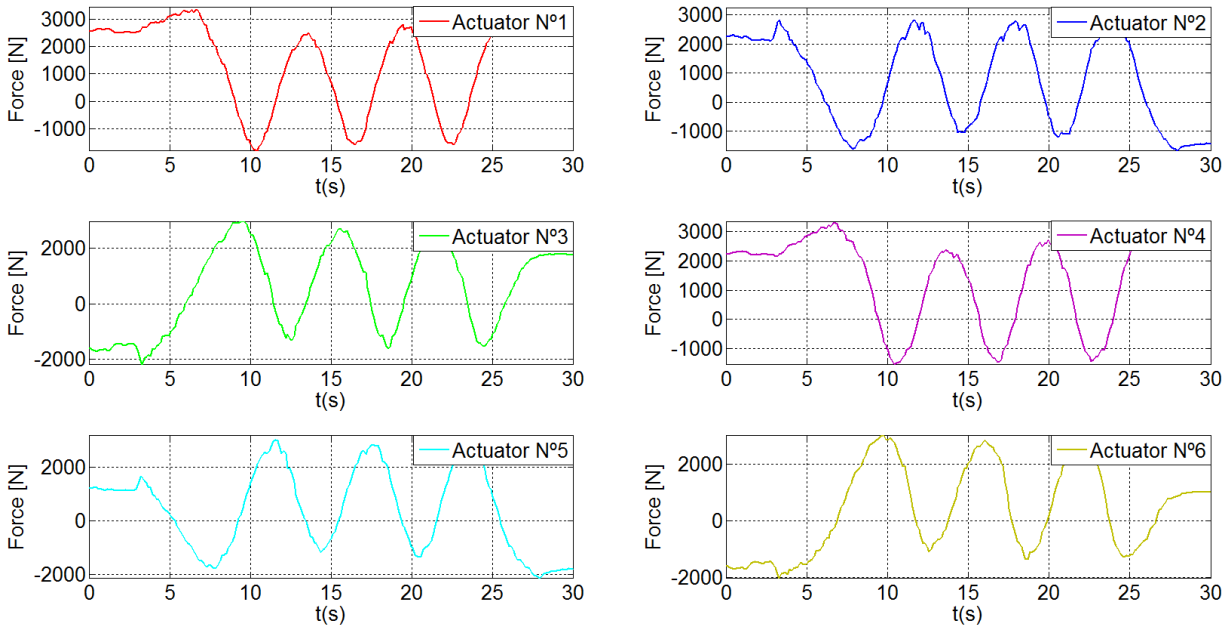

Figure 7.9: Forces being applied on the actuators during one of the experiments via differential kinematics.

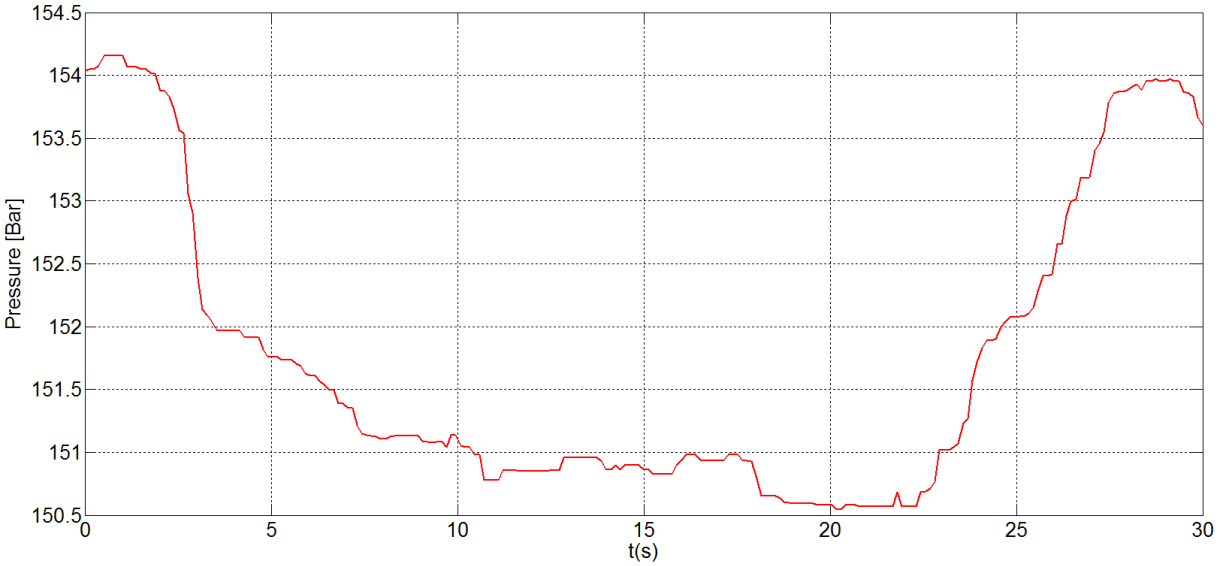

Figure 7.10: Pressure changes on the hydraulic distributor during one of the experiments.

Table 7.1: Steady state error and trajectory response data regarding the tested controllers.

Controller Type	Steady State Error				Trajectory Response			
	Max.		Avg.		Max.		Avg.	
	xyz [mm]	$\alpha\beta\gamma$ [°]	xyz [mm]	$\alpha\beta\gamma$ [°]	xyz [mm]	$\alpha\beta\gamma$ [°]	xyz [mm]	$\alpha\beta\gamma$ [°]
PID	0.1222	0.0180	0.0644	0.0045	0.5750	0.0915	0.2589	0.0403
FLC PID	0.0348	0.0127	0.0216	0.0026	0.2153	0.0381	0.0776	0.0165
FLC P + I	0.2930	0.0587	0.0881	0.0217	1.0667	0.2157	0.4129	0.0884
FLC P + ID	0.0763	0.0143	0.0273	0.0033	0.2195	0.0391	0.0973	0.0200

7.4 Other acquired data

With the available instrumentation presented in Section 3.3 is possible to extract some interesting data for research purposes. For instance, the Figure 7.11 and 7.11 shows the acquired vertical force F_z in function of the part depth while performing frustums experiments using aluminium and high strength steel, respectively. In this particular case, it serves to analyze the formability of material until an occurrence of a rupture. Figure 7.13 illustrates a typical frustum used on this kind of experiments.

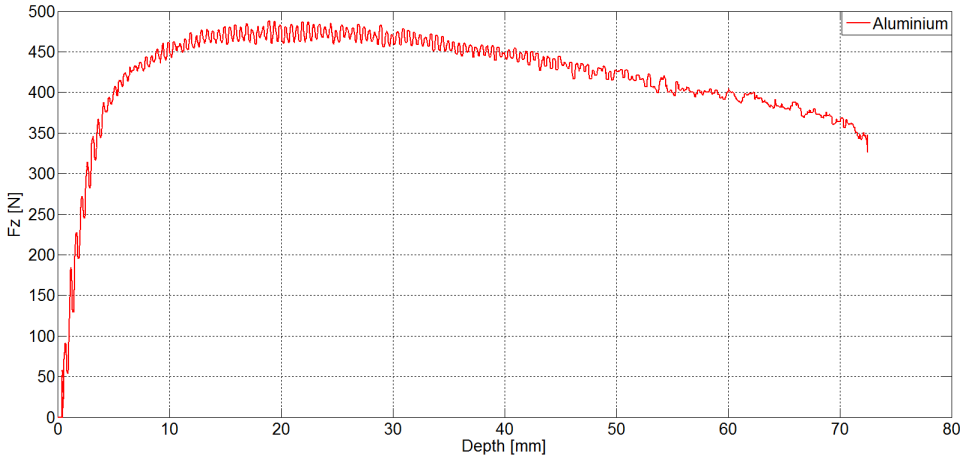

Figure 7.11: Vertical force F_z vs Part depth for aluminium sheet.

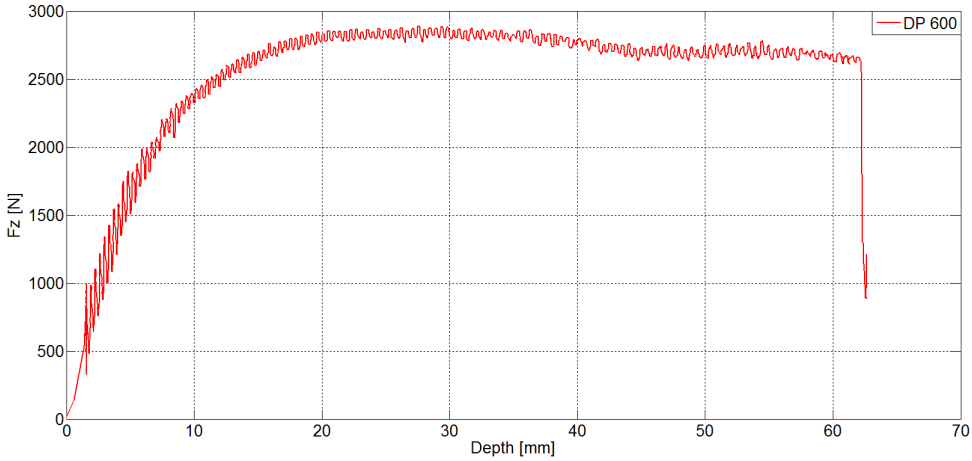

Figure 7.12: Vertical force F_z vs Part depth for high strength steel DP600.

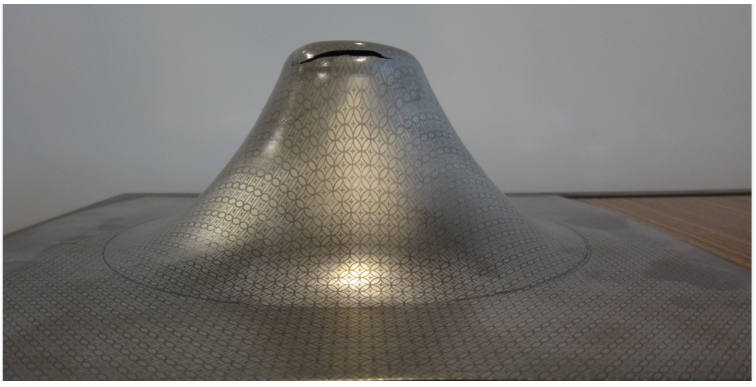

Figure 7.13: Frustum in 1 millimeter thick high strength steel DP600 for rupture analysis.

7.5 Produced SPIF Parts

Proven the SPIF-A's capability in producing SPIF parts with a certain accuracy, parts where being formed since then. Some are just for demonstration and other for specific proposes. More produced parts can be found in Appendix G.

Figure 7.14: Example of one complex geometry in aluminium sheet.

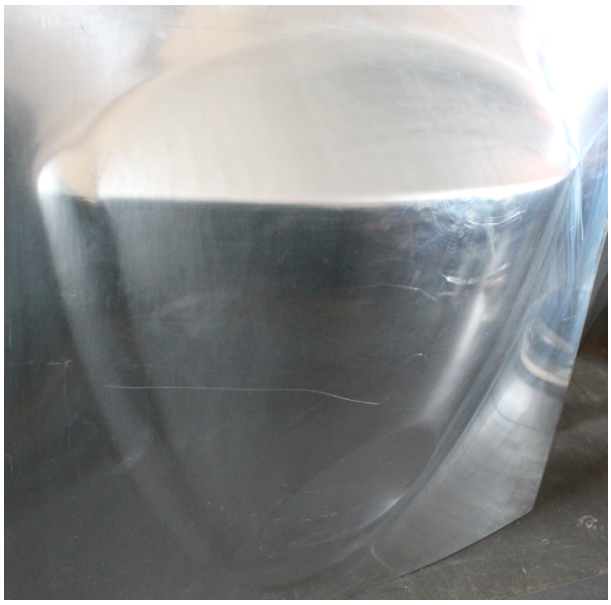

Figure 7.15: Volkswagen Beetle's bonnet.

Figure 7.16: Seatback prototype.

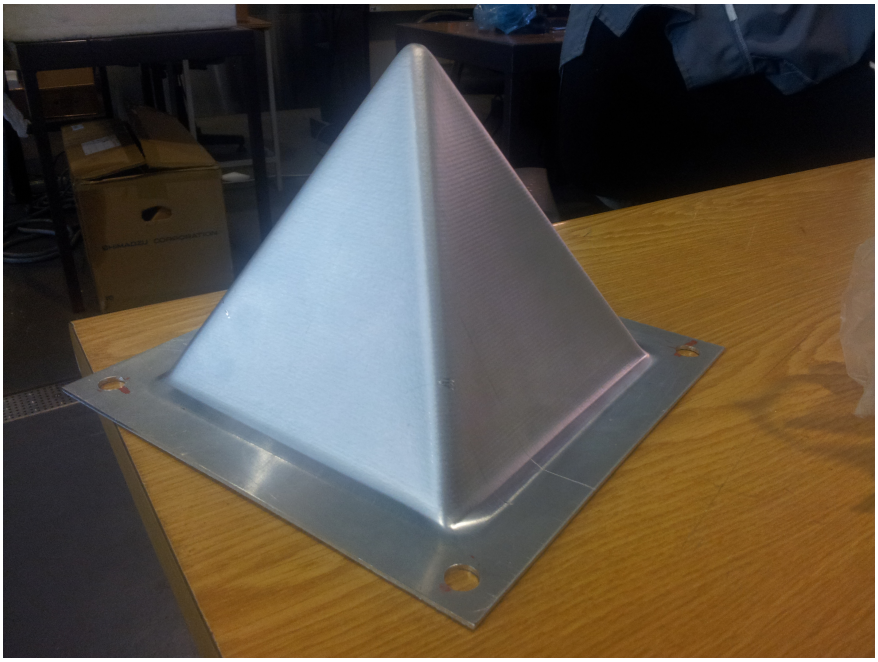

Figure 7.17: Pyramid in 2 millimeter thick aluminium sheet with 150 millimiter depth.

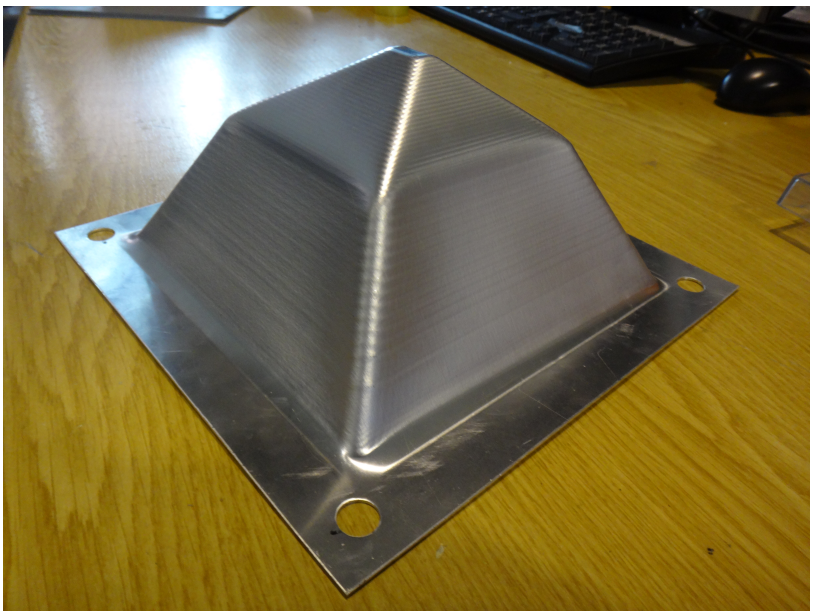

Figure 7.18: Pyramid in 1 millimeter thick aluminium sheet with 90 millimiter depth in which wall angle is varying.

7.5.1 Part's Surface Finish

In this section are represented some examples of the surface finish in SPIF parts done in the SPIF-A machine.

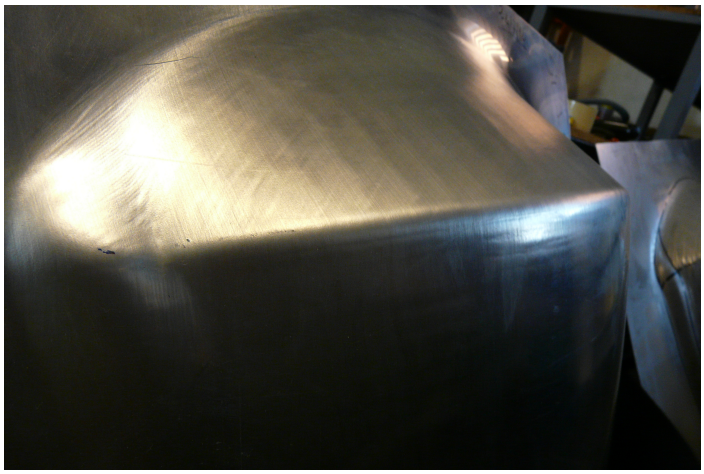

Figure 7.19: Part's surface finish - Volkswagen Beetle's bonnet.

Figure 7.20: Part's surface finish - example 1

Figure 7.21: Part's surface finish - example 2

7.6 Results Discussion

The developed system to perform manual motions on the SPIF-A machine's workspace has proven to be effective as its motions are smooth. The machine memorizes its current standing point and, if given any desired point (different of the current standing point), the subsystem is enable and the machine starts to move slowly, reaching its maximum speed (Implemented by the operator through a parameter) and then gradually decreases until it stops. It is suitable to perform any motion given any point in the XYZ and Euler angles $\alpha\beta\gamma$ space.

Regarding the developed system for automatic experiment, the pre-processing tools (ex. linear interpolation) has revealed to be effective in how it handles the raw data from the CAM file and converting it into evenly spaced points. Also, the velocity control method implemented in automatic experiments, which consist in speeding up or down the real-time clock in the LUT, seems to be incisive and efficient proved by the end-effector velocity via differential kinematics where the kinematic jacobian J_E is used. In 3-Axis strategy, the SPIF-A machine reached an impressive 15 000 mm/min machining speed while in 5-Axis strategy the machine speed goes up to 6500 mm/min. Obviously, in 5-Axis strategy the hydraulic power requirements are higher and so the maximum achievable speed is lower. However it was comproved via differential kinematics.

About the designed and implemented controllers, it was expected a low performance from the conventional PID controller in handling with non-linear system behaviors. Its overall performance was not bad and achieved a maximum steady state error of 0.1222 millimeters in the XYZ space and 0.0180 degrees in Euler angles space. However, in trajectory response performance, the PID controller revealed to be less effective and the error raised up to 0.5750 millimeters in the XYZ space and 0.0915 degrees regarding the Euler angles. Its fixed proportional, derivative and integral terms does not help handling non-linear behaviors. Being that said, fuzzy logic controllers were also designed and implemented. There are many possible configurations of FLC controllers, regarding its number

of inputs, outputs, the adopted membership functions and fuzzy rules. There were three FLC tested on the SPIF-A machine and the best one of them is the FLC PID. This FLC controller stands to be the most complex among the three, where the proportional, derivative and integral terms are non-linear. However, it was expected a good performance from a non-linear PID controller in which its parameters are tuned by a set of fuzzy rules. This controller has achieved the best overall performance comprising an average steady state error of 0.0216 millimeters in the XYZ space and 0.0026 degrees regarding the Euler angles. While performing automatic experiments, the PID tuned by fuzzy logic rules handled very well and the average error in trajectory response was around 0.0776 millimeters in the XYZ space and 0.0026 degrees in Euler angles space. The other remaining two FLC controllers, FLC P + ID and FLC + P, were less complex and governed with less fuzzy rules and so the overall performance was lower compared to the FLC PID. However, the FLC P + I controller performance was worst compared to the linear PID in which the terms are fixed. It is not valid to directly state that the FLC P + I controller is less effective than the conventional PID controller. The parameters chosen for these controllers relied on trial and error attempt and for sure, the chosen parameters to the FLC P + I controller were not the best ones. However, it is valid to state that the FLC P + I and FLC PID controller, regarding its tuned parameters by trial and error, did perform better than the linear PID. Hence, most importantly, extra knowledge was acquired while studying FLC and its capability to handle with non-linear effects. A thinner tune of the FLC parameters would, for sure, result in a better perform. Missing the dynamic model of the SPIF-A machine, it is very complicated to find the best controller, for that reason, this topic will be added to the future work. Concluding about the implemented controllers, the valve effort on the servo-solenoid valves was higher on the FLC P + I controller and lower on the FLC P + ID, perhaps, is the reason why this controller achieved the worse overall performance regarding the chosen parameters by trial and error. Ideally, the best effort rate would be a smooth signal. However, due to the nature of these kind of controllers, the servo-solenoid valves are constantly opening and closing many times per second.

Another aspect developed and implemented via differential kinematics is the actuators forces, which are deduced using the kinematic jacobian J_E and the FMS, which are the forces being applied on the end-effector. This implementation is more important for future uses where different types of controllers can be studied, such as impedance control. However, for now, it serves for merely information about the quantity of forces the actuators had to hold while performing these experiments.

The pressure transducer installed on the hydraulic distributor gives us some information about how the pressure on the system. Depending on the velocity and strategy used (3-Axis or 5-Axis), there are pressure floats on the system. However, it is not a major problem because there pressure still stands on high values assuring the stiffness of the parallel platform.

To conclude the present discussion, regarding the motion control and instrumentation implemented in the SPIF-A machine and the produced SPIF parts shown above, let's compare the produced Volkswagen Beetle's bonnet finish in 2013 and now in 2014 under the same circumstances (i.e, CAM file was the same) as Figure 7.22 shows. Clearly, there

is an huge improvement in motion control that is reflected on the part's surface finish and in the produced parts regarding complex geometries. For that reason, the SPIF-A team is researching about the roughness on SPIF parts compared to traditional methods of sheet forming.

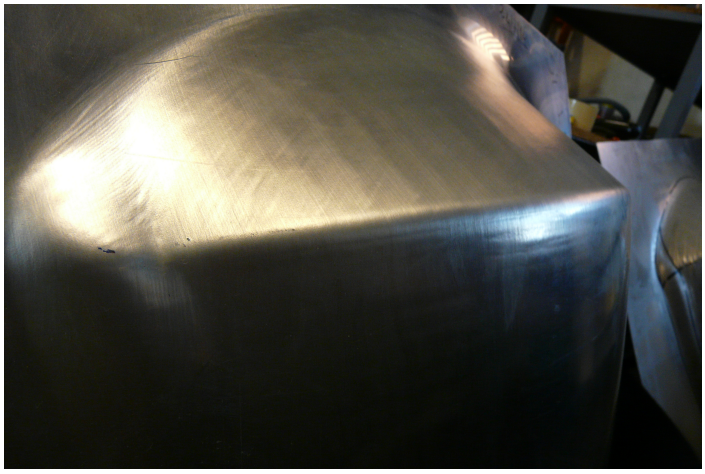

(a) Newer - 2014

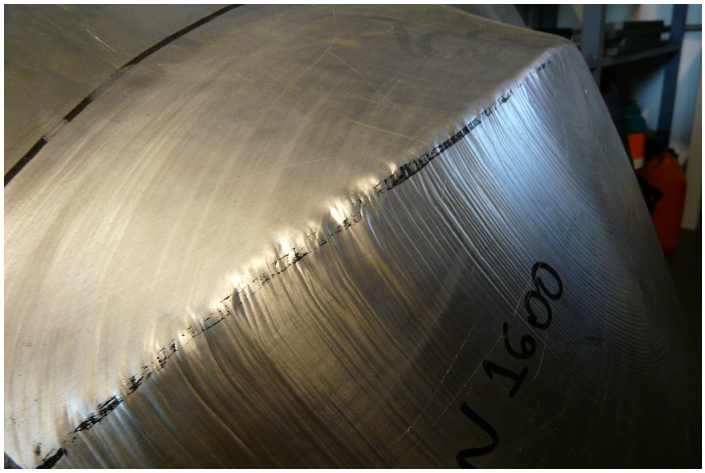

(b) Older - 2013

Figure 7.22: Volkswagen Beetle's bonnet finish comparison.

Chapter 8

Conclusions

Final considerations about the developed work on the present dissertation is given. Some future work is presented in order to continue the machine's development. Earned skills and other relevant information, such as the machine's recognition on media, is sighted.

"It's hard to guess how smart the machines are, but a good rule of thumb is that they're always smarter than you think."

Daniel H. Wilson, *Robogenesis*

As the co-adviser of this dissertation Prof. Ricardo Sousa says, eyebrows were raised about the SPIF-A machine in the University of Aveiro after the developed work presented on this document. An effort now being done by the SPIF-A team in order to develop the potential of SPIF technology and research is taking place. The overall main goal of this dissertation was to get the SPIF-A machine running either in 3-Axis or 5-Axis strategy within a certain accuracy and velocity control. The actual machine's performance was achieved thanks to the various system developed, tested and implemented that allowed a smooth motion control under high forming loads.

During this dissertation, around 80 SPIF parts were produced to various researchers and students to make experimental results in the fields of stereo artificial vision, CAD/CAM strategies for SPIF, SPIF lubricants, incremental forming versus forming speed among others.

The output is a Gough-Stewart parallel platform now equipped with hardware enough to fulfill the machine's power requisites in which the implemented instrumentation and motion control/accuracy allows to perform research on SPIF technology or in its produced parts.

However, there were some setbacks that delayed the conclusion of this dissertation. Primarily, the hardware upgrades to the hydraulic system took immense time to arrive and be implemented, meaning that there were less time to develop more software and instrumentation upgrades and so that will be addressed in the future work.

Figure 8.1: SPIF-A project work station in the University of Aveiro.

8.1 Future Work

In order to keep the machine's development, more work is yet to be done. To achieve top performance, either software or hardware modules have upgraded and, perhaps, new methods and implementations can take place. The actual machine is now on its emergence in SPIF technology and it is starting to take the market's attention. To take advantage of that, more research and human resources need to be used.

8.1.1 Machine Hardware

About the mechanic state of the machine, there are some improvements that can be done. The implemented U-Joints revealed to be responsible for some of the existent backlash on the bottom platform. While performing heavy duty forming, the platform shakes and vibrates on the XOY workspace limiting its overall accuracy. A replacement with spherical joints, which are a lot more robust, can solve the problem.

Regarding the actual implemented instrumentation of the machine (see Section 3.3), the built controle console can be upgraded with many more functionalities to simply and help the operator's tasks. Also, the load cells in use are three dimensional and their measurement is a bit coarse. Its replacement by three brand new one dimensional load cells would substantially increase the quality of the acquired signal.

Currently, the tool's lubricant method used on the machine while performing SPIF

operations to avoid tool's wear, is yield manually using a small spoon. A more robust either manual or even automatic system for tool lubricant can be researched and implemented. The system implemented on some CNC milling machines is unsuitable for this machine, otherwise, the amount of lubricant that is debited would spread across the entire machine. As a suggestion, a sort of system that uses compressed air with a small quantity of lubricant can be developed and implemented.

8.1.2 Machine Software

Regarding the machine's software, the developed interface (Section 5.5) can be upgraded and enhanced with another features to help the operator handling with the machine. Also, it is necessary to develop more functions in other to increase the compatibility with G-code functionality which could additionally comprise the "G02" and "G03" functions, for instance. Working alone with "G01" may not be suitable for some geometry and most of the times the CAM file comprehends many more function rather than "G01" alone.

The prepossessing tools used to compute the required data for performing SPIF operations can be upgraded. For instance, a new algorithm can be developed in order to increase or decrease the machine's speed in automatic experiments regarding some of the part's geometry features. If the geometry has, for example, right or almost right corners in XOY plane, the machine's speed can be managed in order to slow down as it is reaching that same corner to improve the part's surface quality especially in high forming speeds.

In terms of control, the actual positions controllers can be further developed in order to achieve a better performance regarding the steady state error and the machine's capability in trajectory response. Also, another type of control can be implemented, such as force control or impedance control. Impedance control differs from the more conventional approaches to manipulator control by the fact that the controller attempts to implement a dynamic relation between manipulator variables such as end-effector position and force rather than just control these variables alone [76]. This control approach implemented on the SPIF-A machine would be valuable while performing SPIF operations. Every material has its own characteristics and some are harder than others as well as its capacity of incremental formability. New SPIF manufacturing procedures can be studied using impedance control for the purpose of trying to increase the material formability near its rupture point.

Yet, developing the entire machine's dynamic system mathematically would be interesting despite its huge complexity and non-linearity. In this case, different control approaches could be implemented such as model based controllers.

There are yet many opportunities of research regarding SPIF technology. The development of an algorithm attempting to predict and correct springback throughout the forming process would substantially increase the quality of the produced parts in terms of geometrical/dimensional accuracy. However, many research groups, such as Allwood et al. [22] and Meier et al. [21], are currently working on such algorithm and studying how different forming parameters affect the part's geometrical/dimensional accuracy.

Studying the advantages of SPIF parts for prototyping is another interesting research that can be carried along with the SPIF-A's industrial partners. SPIF technology is great

to produce low batches and can be an asset to small industrial enterprises to develop their own products by primarily prototyping them using SPIF.

8.2 Earned Skills

It was extremely beneficial working on the SPIF-A project, during this work. It allowed to improve the research skills needed to solve the most various problems either about theoretical or practical issues. The development of hardware and software in real physical systems has proved to interesting and the connection with industrial world issues has come closer. It required some dexterity and responsibility while being the only person with the required knowledge and know-how in order to be able of performing operations in the machine.

Mutual learning and the capability of interacting with other research groups interested in SPIF parts has proved. Communication skills were increased by representing the SPIF-A machine under potential partners and other research groups.

Team work was essential during the dissertation, the ability of leading with problems and debating future solutions was successful. Team effort has raised in order to take this project to another level and establish a closer connection with interested partners.

Also during this dissertation, hard skills were achieved in terms of software manipulation, such as MatLab™, Simulink™, Maple™ and CATIA V5® for drafting and part design. Writing the present document allowed to extend the knowledge on English language, as well as getting the know-how in elaborating documents using technical vocabulary which is widely used in modern industrial world.

Technical knowledge in hydraulic, electrical and instrumentation systems has become valuable to understand how modern machinery is implemented on manufacturing processes. Also, while developing machine's kinematics and its components, extra dexterity on dealing with mathematical equations has been achieved. Learning a new method for position controller, fuzzy logic controller has proved to be effective how it is easier to handle with non-linear effects compared to the well-known conventional types of position control.

Concluding, it was exciting and compensatory to accept the challenge to be part of the SPIF-A project and contribute to the success of the machine which is comprised in various fields of engineering. It yielded good results both to the SPIF-A project and for personal development to prepare a future engineer to the real industrial world.

8.3 Other Relevant Information

During the course of this dissertation and after the machine's capability in producing SPIF parts have been proved, the SPIF-A project has acquired some media impact and external interest. The head of the project Prof. Ricardo Sousa has given interviews to some magazines, newspapers and websites, as follows in Table 8.1.

Table 8.1: Media news about SPIF-A project.

Title	Source	Date	Page/Hour
"Máquina faz peças de aço com 2 mil Kg"	Revista Sábado	24/07/14	14
"Escultor de aço inédito desenvolvido na universidade"	As Beiras	21/07/14	16
"Escultor de aço desenvolvido na Universidade de Aveiro"	Notícias de Aveiro Online	20/07/14	23:57
"Máquina produz peças únicas em aço"	Diário de Aveiro	18/07/14	7
"Um "osso" para a cabeça? Uma porta para o carro? Uma peça para uma aeronave? É para já!"	Ciênciahoje.pt	17/07/14	19:01
"Estampagem de chapa ganha metodologia na Universidade de Aveiro"	Diário Digital	17/07/14	12:08
"Aveiro cria dispositivo de alta precisão	Diário Notícias	17/07/14	23
"Escultor de aço desenvolvido na Universidade de Aveiro"	Terranova.pt	17/07/14	18:40
"Máquina de estampagem em aço reduz custo de protótipos"	Correio Manhã	16/07/17	17:34
"Máquina de estampagem em aço reduz custo de protótipos"	Porto Canal Online	16/07/17	17:48

Contacts with external enterprises were established in order to promote the SPIF technology on real industrial world. Currently, the SPIF-A project is cooperating with a local enterprise to produce some prototypes regarding the enterprise's need. Figure 7.16 shows a large scale (up to 800x1000 mm) prototype, requested by this enterprise, made on the SPIF-A machine. Also, cooperation is going on with a multinational enterprise and sooner SPIF prototypes will be also made. However, it is known, that there are already enterprises looking forward to commercialize the SPIF-A machine in order to fully establish the connection of SPIF technology with industrial market needs.

Concluding, the figure below illustrates the very first recognition of the SPIF-A machine on the University of Aveiro online newspaper.

Investigação

Estampagem de chapa ganha metodologia inédita no Departamento de Engenharia Mecânica

Escultor do aço desenvolvido na Universidade de Aveiro

16.7.2014

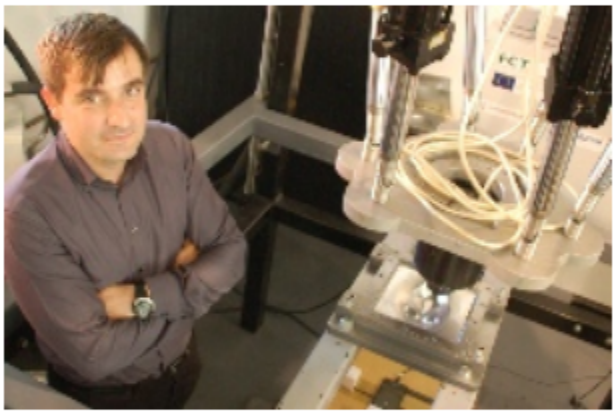

Um implante craniano para substituir um osso da cabeça? Feito em quatro horas. Uma porta para um protótipo de um novo automóvel? Feita em seis horas e meia. Uma peça para a fuselagem de uma nave aeroespacial? Feita em cinco horas. O escultor dá pelo nome de "máquina para estampagem incremental de chapa" e a julgar pelo tempo que demora a fabricar as peças não parece assim tão eficaz. Mas se pensarmos que se tratam de peças exclusivas, feitas por uma máquina capaz de estampar em placas de aço de alta resistência qualquer coisa que se imagine, então a máquina inventada na Universidade de Aveiro (UA) assume um caráter único no mundo.

Figure 8.2: SPIF-A's machine first recognition on the University of Aveiro online newspaper.

Bibliography

[1] Asimov I., "Understanding Physics", New York, New York, USA: Barnes & Noble, p. 88, ISBN 0-88029-251-2, 1988.

[2] Marabuto S. R., Afonso D., Ferreira J. A. F., Melo F. Q. M., Martins M. A. B. E., Sousa R. J. A., "Finding the best machine for SPIF operations", Key Engineering Materials, Volume 473, pp. 861-868, 2011.

[3] Leszak E., "Apparatus and Process for Incremental Dieless Forming", E. Patent US3342051A1, 1967.

[4] Marabuto S. R., "Desenvolvimento de uma mquina para operaes de estampagem incremental", Master Thesis - Universidade de Aveiro, 2010.

[5] Torrão J. N. D., "Control and execution of incremental forming using parallel kinematics", Master Thesis - Universidade de Aveiro, 2013.

[6] Martins M. A. B. E., "Projecto e Contruo de uma Mquina para Estampagem Incremental", Master Thesis - Universidade de Aveiro, 2011.

[7] Sena J. I. V., "Estampagem Incremental: Um novo Conceito de Produo", Master Thesis - Universidade de Aveiro, 2010.

[8] Merlet J. P., "Parallel Robots" Kluwer academic publishers, Dordrecht, The Netherlands, 1st edition, 2000.

[9] Parthajit M., Bhaskar D., Mallik A.K., "Dynamic stability index and vibration analysis of a flexible Stewart platform", Journal of Sound and Vibration, Volume 307, pp. 495-512, 2007.

[10] Astrom K. J., Murray R. M., "Feedback Systems", Princeton University, 2010.

[11] http://www.parallemic.org/, last access at 5th of May 2014.

[12] http://www.fanucrobotics.com/, last access at 5th of May 2014.

[13] http://www.aviationsystemsdivision.arc.nasa.gov/, last access at 5th May 2014.

[14] Koch M. P. et al., "The AMiBA Hexapod Telescope Mount", The Astrophysical Journal, pp. 694:1670 - 1684, April 2009.

[15] Melo A. P., "Teoria dos sistemas de controlo lineares", departamento de electrónica telecomunicações e informática, Universidade de Aveiro, 2010.

[16] MATLAB Fuzzy Logic Toolbox - "What is Fuzzy Logic?", last access at 10th of May 2014.

[17] http://www.lr.tudelft.nl/en/, last access at 25th May 2014.

[18] http://mfgnewsweb.com/, last access at 25th May 2014.

[19] http://sade.disam.etsii.upm.es/, last access at 25th May 2014.

[20] Jeswiet J., Micari F., Hirt G., Bramley A., Duflou J., Allwood J., "Asymmetric Single Point Incremental Forming of Sheet Metal, CIRP Manufacturing Technology", Volume 54, pp. 88-114, 2005.

[21] Meier H., Buff B., Laurischkat R., Smukala V., "Increasing the part accuracy in dieless robot-based incremental sheet metal forming", CIRP Manufacturing Technology, Volume 58, pp. 233-238, 2008.

[22] Allwood J. M., King G., Duflou J. R., "Structured Search for Applications of the Incremental Sheet Forming Process by Product Segmentation", IMECH E, Proceedings Part B, Journal of Manufacture, Volume 219, pp. 239-244, 2004.

[23] Duflou J. R., Lauwers B., Verbert J., "Medical application of single point incremental forming: cranial plate manufacturing", Proceedings of the 2005VRAP Conference, Leiria, pp. 161-164, 2005.

[24] Skjoedt M., Bay N., Endelt B., Ingarrao G., "Multi-stage strategies for single point incremental forming of a cup", 11th ESAFORM conference on metal forming ESAFORM2008, 2008.

[25] Jeswiet J., "Recent results for SPIF", Seminar on Incremental Forming, Cambridge University, CDRom, 2004.

[26] Astrom K. J., "Control System Design", Department of Mechanical and Environmental Engineering, University of California, Santa Barbara, pp. 218-220, 2002.

[27] Carneiro J., "Modelação e Controlo de Actuadores Pneumáticos Utilizando Redes Neuronais Artificiais", Tese de Douturamento em Engenharia Mecânica, Faculdade de Engenharia da Universidade do Porto, Portugal, 2007.

[28] Carvalho J., "Sistemas de controle Automático" LTC Editora, Rio de Janeiro, ISBN 85-216-1210-9, 2000.

[29] Faccin F., "Abordagem Inovadora no Projecto de Controladores PID, Tese de Mestrado em Engenharia Qímica, Universidade Federal do Rio Grande Sul, Brasil, 2004.

[30] Cauchy A. L., "Deuxiéme Mémoire sur les polygones et les polyédres", Journal de l'Ecole Impériale Polytechnique, XVI Cahier, pp. 87-99, 1813.

[31] Gough V. E., "Contribution to discussion of papers on research in Automobile Stability, Control and Tyre performance", Proc. Auto Div. Inst. Mech. Eng., pp. 1956-1957.

[32] Stewart D., "A platform with Six Degrees of Freedom", Proc. Inst. Mech. Eng., Volume 180, pp. 1956-1966.

[33] Rehsteinera F., Neugebauerb R., Spiewack S., Wielandb F., "Putting Parallel Kinematics Machines (PKM) to Productive Work", CIRP Annals - Manufacturing Technology, Volume 48, Issue 1, pp. 345-350, 1999.

[34] Merlet J. C., "Six-axis deformity analysis and correction", Principles of Deformity Correction, Springer, Berlin Heidelber New York, pp. 411-436, 2002.

[35] www.hexapods.net/, last access at 8th July 2014.

[36] Zadeh L. A., "Fuzzy sets", Information and control 8.3, pp. 338-353, 1965.

[37] Santos M. P. S., "Controlo de um sistema servopneumático para ensaios de fadiga", Master Thesis - Universidade de Aveiro, 2009.

[38] Passino K., Yurkovich S., "Fuzzy Control", Addison Wesley Longman, Menlo Park, CA, 1998.

[39] Heske T., Heske J., "Fuzzy logic for real world design", Annabooks, San Diego, USA, 1996.

[40] Chung H. Y., Chiang C. K., "A self-learning and tuning fuzzy logic controller based on genetic algorithms and reinforcements", International Journal of Intelligent Systems Volume 12, pp. 673-694, September, 1997.

[41] Zadeh L. A., "Outline of a New Approach to the Analysis of Complex Systems and Decision Process", IEEE Transaction on Systems, Man and Cybernetics, Vol SMC-3, NO.1, January, 1973.

[42] Mamdani E.H., Assilian S., "An experiment in linguistic synthesis with a fuzzy logic controller," International Journal of Man-Machine Studies Volume 7, pp. 1-13, 1975.

[43] Sugeno M., "Industrial applications of fuzzy control", Elsevier Science Pub. Co., 1985.

[44] Wang Y. M., Yang J. B., Xu D. L., Chin K. S., "On the centroids of fuzzy numbers", Fuzzy Sets and Systems 157, pp. 919-926, 2006.

[45] Sena J.I.V., Alves de Sousa R.J., Valente R.A.F., "On the use of an EAS solid-shell element to simulate incremental formally processes", Engineering Computations Volume 28, pp. 287-313, 2011.

[46] Amino H., Lu Y., Maki T., Osawa S., Fukuda K., "Dieless NC Forming, Prototype of Automotive Service Parts", Proceedings of the 2nd International Conference on Rapid Prototyping and Manufacturing (ICRPM), Beijing, 2002.

[47] Allwood J. M., Houghton N. E., Jackson K. P., "The design of an Incremental Forming machine", 11th Conference on Sheet Metal, pp. 471-478, Erlangen, 2005.

[48] Duflou J.R., Szekeres A., VanHerck A., "Force Measurements for Single Point Incremental Forming and experimental study", Journal of Advanced Materials Research, Vols. 6-8, pp. 441-448, 2005.

[49] Shim M., Park J., "The formability of aluminum sheet in incremental forming", Journal of Materials Processing Technology, Volume 113, pp. 654-658, 2011.

[50] Fratini L., Ambrogio G., Di Lorenzo R., Filice L., Micari F., "Influence of mechanical properties of the sheet material on formability in single point incremental forming", Journal of Materials Processing Technology, Vols. 153-154, pp. 501-507, 2004.

[51] Filice L., Fratini L., Micari F., "Analysis of Material Formability in Incremental Forming", Annals of the CIRP, Vol. 51, pp. 199-202, 2002.

[52] Ceretti E., Giardini C., Attanasio A., "Experimental and simulative results in sheet incremental forming on CNC machines", Journal of Materials Processing Technology, Vol. 152, pp. 176-184, 2004.

[53] Ambrogio G., De Napoli L., Filice L., Gagliardi F., Muzzupappa M., "Application of Incremental Forming Process for High Customized Medical Product Manufacturing", Journal of Materials Processing Technology, Vol. 162, pp. 156-162, 2005.

[54] Meier H., Dewald O., Zhang J., "Development of a Robot-Based Sheet Metal Forming Process", Steel Research, Issue 2005, Dusseldorf.

[55] Strano M., "Technological Representation of Forming Limits for Negative Incremental Forming of Thin Aluminum Sheets", Journal of Manufacturing Processes, Volume 7, pp. 122-129, 2007.

[56] Rauch M., Hascoet J. Y., Hamann J. C., Plennel Y., "Tool path programming optimization for incremental sheet forming applications", Computer-Aided Design, Volume 41, pp. 877-885, 2009.

[57] Jackson K.P., Allwood J.M., Landert M., "Incremental forming of sandwich panels", Journal of Materials Processing Technology, Volume 204, pp 290-303, 2008.

[58] Durante M., Formisano A., Langella A., Minutolo F., "The influence of tool rotation on an incremental forming process", Journal of Materials Processing Technology, Volume 209, pp. 4621-4626, 2009.

[59] Bouffioux C., Eyckens P., Henrard C., Aerens R., Van Bael A., Sol H., Duflou J. R., Habraken A. M., "Identification of material parameters to predict Single Point Incremental Forming forces", Proceedings of IDDRG Conference, Gyor, 2007.

[60] Decultot N., Velay V., Robert L., Bernhart G., Massoni E., "Behaviour modeling of aluminium alloy sheet for Single Point Incremental Forming", International Journal of Material Forming, Volume 1 - Supplement, pp. 1151-1154, 2008.

[61] Santos V., "Robótica Industrial - Apontamentos teóricas", Departamento de Engenharia Mecânica, Universidade de Aveiro, 2003.

[62] Schwab A. L., Meijaard J. P.,"How to draw Euler angles and utilize Euler parameters", ASME International Design Engineering Technical Conferences and Computers and Information in Engineering Conference, Philadelphia, Pennsylvania, USA, 10-13 September, 2006.

[63] Wang S., Wan Y., "A Mixed Real-time Algorithm for the Forward Kinematics of Stewart Parallel Manipulator", Journal of Electronic Science and Technology of China, Volume 4, pp. 173-180, 2006.

[64] Dasgupta B., Mruthyunjaya T.S., "A Canonical Formulation of a Direct Position Kinematics Problem for a General 6-6 Stewart Platform", Mechanism and Machine Theory 31, Volume 6, pp. 819-826, 1994.

[65] Lee T. Y., Shim J. K., "Forward kinematics of the general 6-6 Stewart platform using algebraic elimination", Mechanism and Machine Theory, Volume 36, pp. 1073-1085, 2001.

[66] Huang X., Liao Q, Wei S, "Closed-form forward kinematics for a symmetrical 6-6 Stewart platform using algebraic elimination", Mechanism and Machine Theory, Volume 45 ,pp 327-334, 2010.

[67] Lopes A. M. F. M., "Um dispositivo robótico para controlo de fora-impedância de manipuladores industriais", Doctoral Thesis, FEUP, Universidade do Porto, 1999.

[68] Geng, Zheng, Haynes L., "Neural network solution for the forward kinematics problem of a Stewart platform", Robotics and Automation, IEEE International Conference, 1991.

[69] Song S.K., Kwon D.S., "New Closed-Form Direct Kinematic Solution of the 3-6 Stewart-Gough Platform Using the Tetrahedron Approach", Proceedings of the International Conference on Control, Automation and Systems, October 17-21, Cheju National Univ. Jeju, Korea, pp. 484-487, 2001.

[70] Dasgupta B., Bhaskar, Mruthyunjaya T. S., "A Newton-Euler formulation for the inverse dynamics of the Stewart platform manipulator", Mechanism and Machine Theory 33.8, pp. 1135-1152, 1998.

[71] SN1548 User's Manual, Speedgoat GmbH.

[72] Suriyaprakan P., "Single Point Incremental Forming and Multi-Stage Incremental Forming on Aluminium Alloy 1050", Master Thesis - Faculdade de Engenharia da Universidade do Porto, 2013.

[73] Callegari M., Amodio D., Ceretti E., Giardini C., "Sheet incremental forming: advantages of robotised cells vs. CNC machines", Industrial Robotics: Programming, Simulation and Applications, Low Kin Huat Edition , ARS Publications, pp. 493-514, 2007.

[74] Sieczkarek P., Kwiatkowski L., Khalifa N., Tekkaya1 A, "Novel five-axis forming press for the incremental sheet-bulk metal forming", Proceedings Esaform Conference, Aveiro, Portugal, 2013.

[75] Zhao, Zhen-Yu, Tomizuka, Masayoshi, ISAKA, Satoru., "Fuzzy gain scheduling of PID controllers", Control Applications: First IEEE Conference, pp. 698-703, 1992.

[76] Hogan, Neville, "Impedance control: An approach to manipulation: Part II-Implementation", Journal of dynamic systems, measurement, and control, Volume 107.1, pp. 8-16, 1985.

Appendices

Appendix A

Hydraulic Distributor Drawing

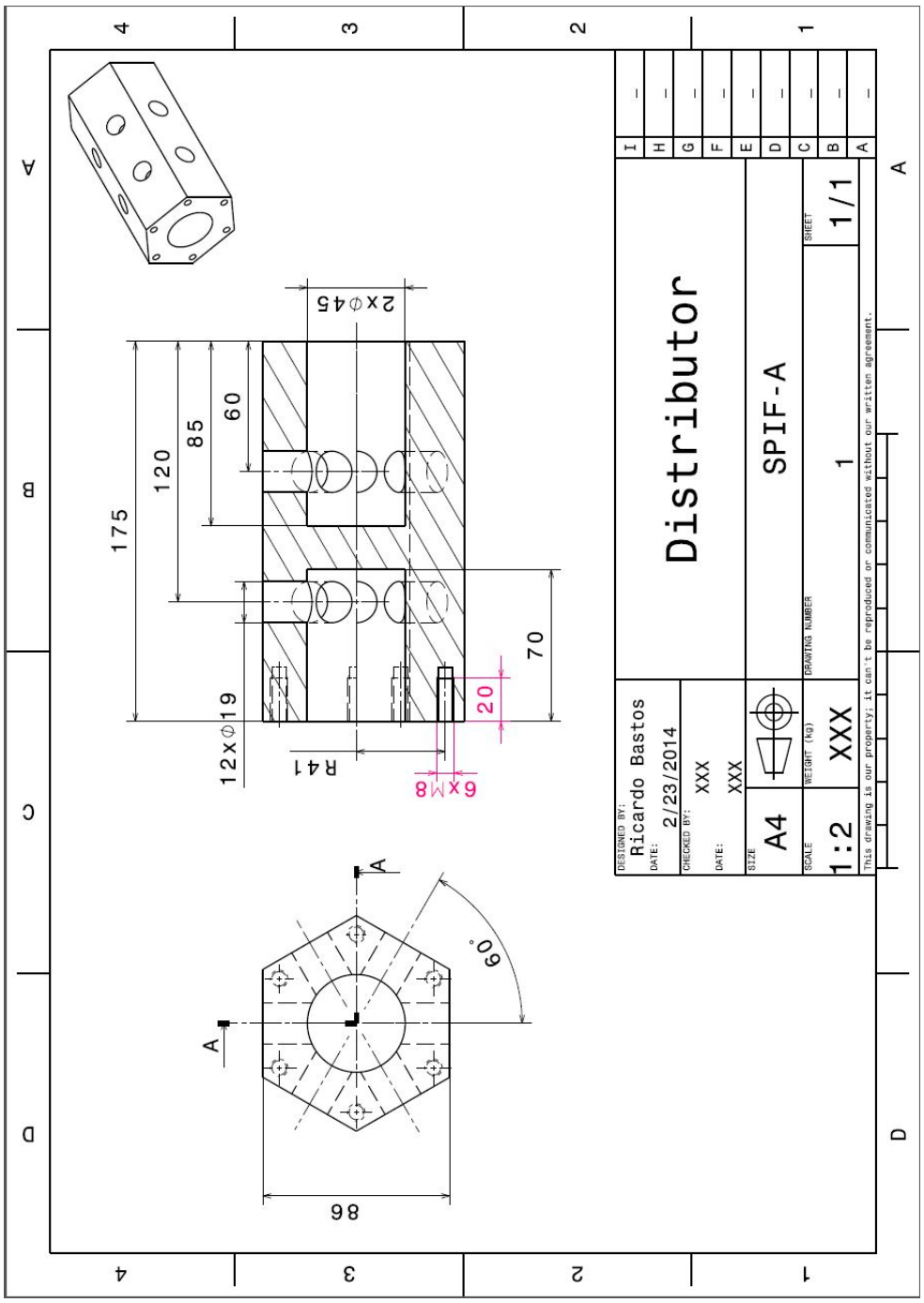
Distributor
SPIF-A
DESIGNED BY: Ricardo Bastos
DATE: 2/23/2014
CHECKED BY: XXX
DATE: XXX
SIZE A4
SCALE 1:2
WEIGHT (Kg) XXX
DRAWING NUMBER 1
SHEET 1/1
This drawing is our property; it can't be reproduced or communicated without our written agreement.
2xΦ45
175
120
85
60
70
20
12xΦ19
R41
6xM8
A
A
60°
98

Appendix B

Hydraulic Pump Performance Data

PVQ40 Model Series

Performance Data

Oil type: SAE 10W
Oil temperature: 82°C (180°F)
Inlet: 0 psi

Note: To obtain full flow operation of pump, pressure compensator setting must be 14 bar (200 psi) above desired operating pressure. Full flow curves were obtained with compensator settings 14 bar (200 psi) above 210 bar (3000 psi) max. rated pressure.

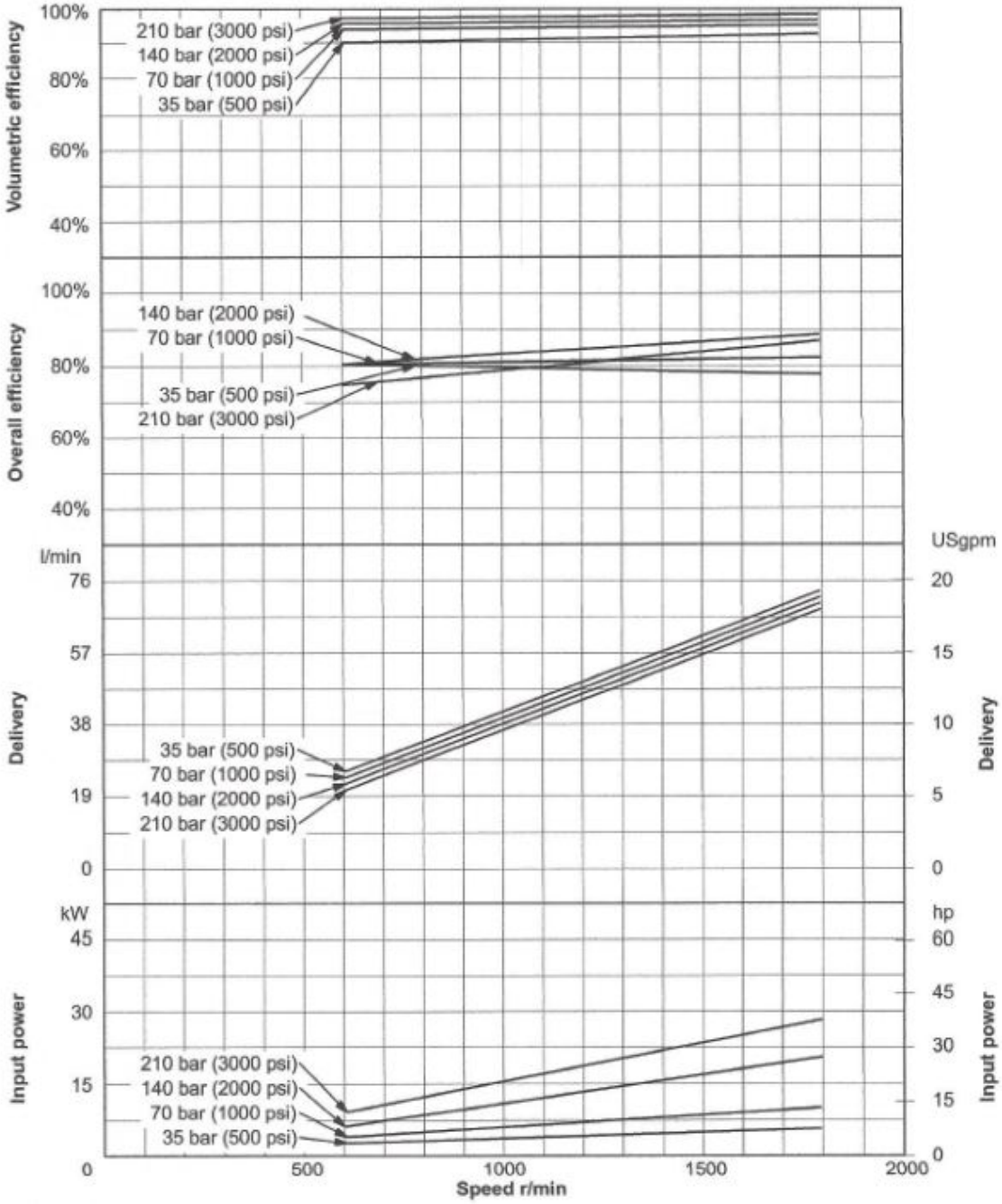

Appendix C

SPIF-A Hydraulic scheme

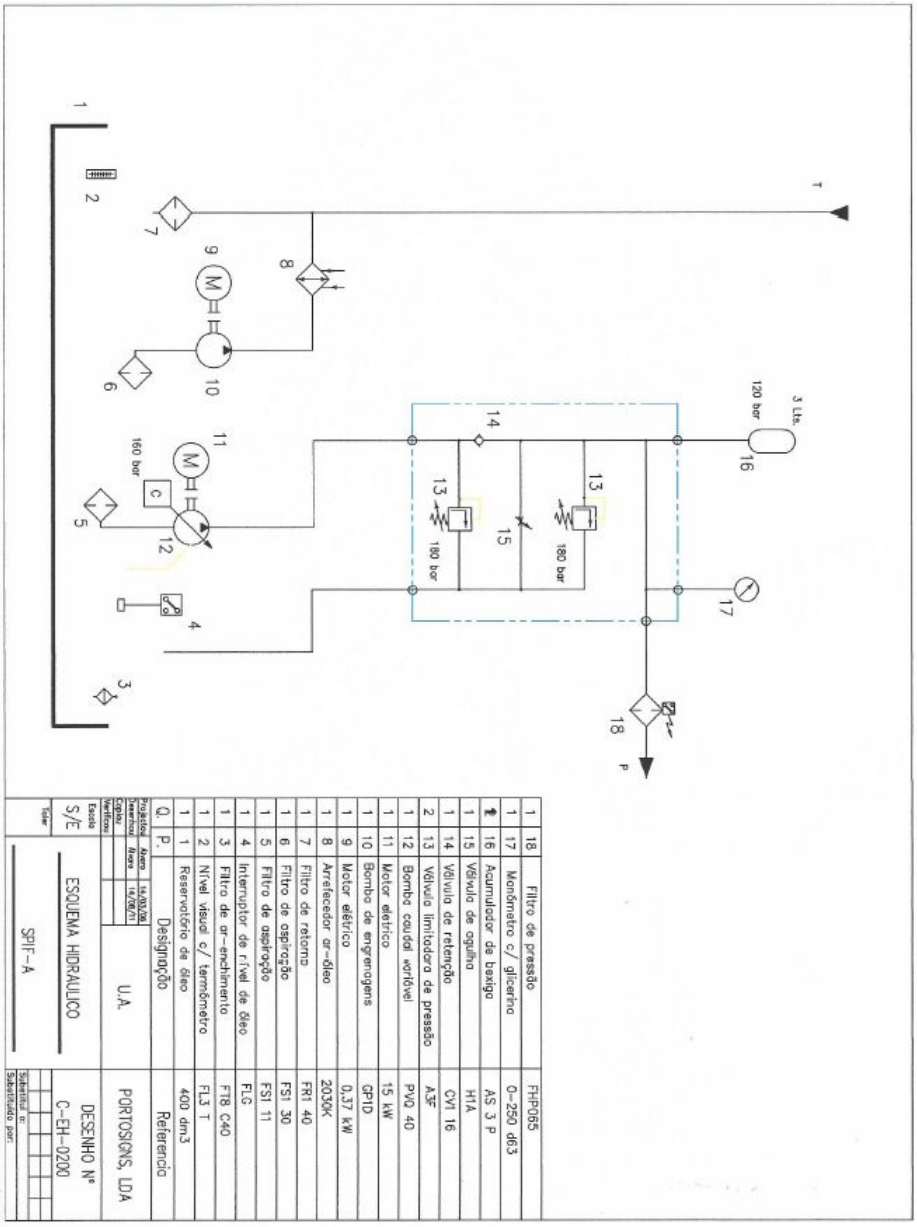

Figure C.1: Hydraulic plan regarding the new hydraulic plant.

Appendix D

PID Controller Theory

It was initially introduced by N. Minorsky in 1922 and remains the most easiest way of controlling. Mathematically simple, reliable and lightly understandable its computing complex is significantly less compared to other types of control such as fuzzy logic control. It is present in every control engineering's pocket. PID control is often combined with logic, sequential functions, selectors, and simple function blocks to build the complicated automation systems used for energy production, transportation, and manufacturing [10].

D.1 Open Loop Control

When the input is not affected by the output, the system is denominated as open loop control. In case of multiple inputs and/or multiple outputs, none of the inputs can be affected by the behavior of the outputs. As an example, if a football player shoots the ball up in the air once it left the ground the trajectory can not be modified. The ball can either fail or successfully achieve the desired target. In the figure D.1 the system to be controlled is called as plant or process. The controller's block is responsible to implement the trajectory strategy by transforming the input signal r(t) in a appropriated signal (controller signal) to be read by the plant block, therefor, the output signal y(t) can be generated. In open loop configurations the output signal entirely depends of the input signal and the plant characteristics. Regarding the given example of the football player, the ball can go higher or lower depending on the kick force, ball's weight or even the weather conditions. To obtain the desired output it is need to do some adjustments at the input signal by attempts. This type of system often faces serious problems in terms of efficiency, in some cases, the impossibility to achieve the desired output. It implies a perfect knowledge about the dynamic of the process to be controlled to build a robust controller enough to satisfy the needs. Real systems are more complex because it is inevitable to avoid external noise disturbance or perturbation (internally or externally generated) that commits the output goal.

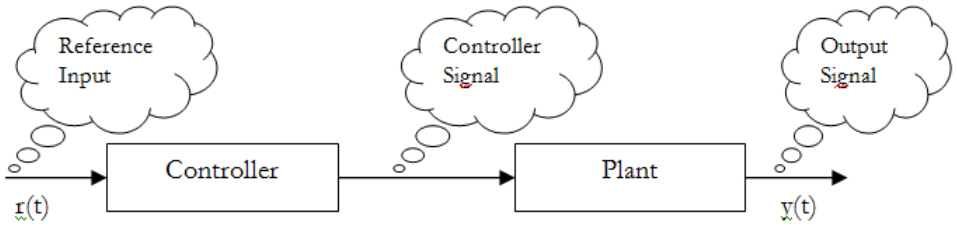

Figure D.1: Open loop control system [15].

D.2 Closed Loop Control

The problems faced in open loop controllers such as parameters variation or noise disturbance can easily be detected and solved by using a system where the input signal depends

of the output signal behavior. Here, the output signal is compared to the input signal, therefor, generating the error signal. The input signal is also known as reference signal regarding the output signal. This system is nominated as closed loop control where the output signal is algebraically added to the input signal. The feedback signal h(t), coincident with the output signal y(t), through the feedback channel is algebraically added in the sum block with the reference signal r(t) creating the error signal e(t) that will further excite the controller block. The feedback channel is often set as negative making the error signal near zero during the time. Positive feedback offers instability to the system, so that, is less used. The error signal is the difference between the desired goal or reference and the actual achieved goal. The error signal will be exactly zero if the achieved output equals the reference input. Taking the same example given in the section D.1, the football player instead of shooting the ball into the air will choose to drive the ball back to forward through the opponents by adapting the ball trajectory over time. In real systems, the feedback block is replaced with sensors that gives information to the controller about the output signal. This sensors depends on the system or application but are often used light dependent resistor (LDR), voltage dependent resistor (VDR), negative temperature coefficient (NTC) and linear variable differential transformer (LVDT).

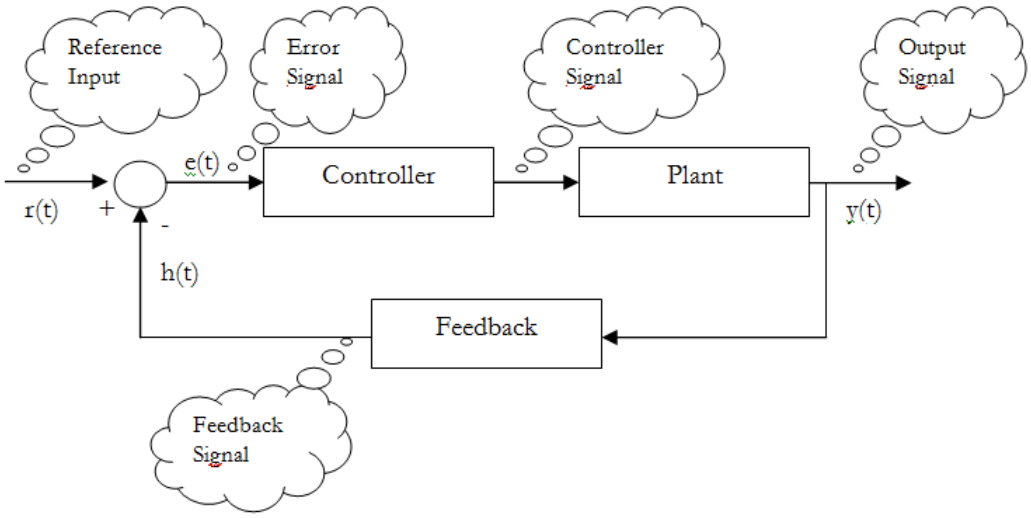

Figure D.2: Closed loop control system [15].

D.3 The Algorithm

In theory, PID controller algorithm is

$$u(t) = Ke(t) + K_i \int_0^t e(\tau)d\tau + K_d \frac{de(t)}{dt} \tag{D.1}$$

where $u(t)$ is the control signal and e is the control error ($e = r - y$) [26]. The reference signal, $r(t)$, may also be called setpoint. The control signal is the sum of the three terms presented in the equation D.1: P-term (Proportional to the error), I-term (Proportional to the integral of the error), D-term (Proportional to the derivative of the error). These terms have their own assigned gain, the proportional gain K, integral gain K_i and derivative gain K_d. The controller is also represented as

$$u(t) = K\left(e(t) + \frac{1}{T_i}\int_0^t e(t)\cdot dt + T_d\frac{de(t)}{dt}\right) \tag{D.2}$$

where T_i is the integral time and T_d is the derivative time [26]. Doing some kind of association regarding time, it is valid to say that the proportional term acts on the present value of the error, the integral represents the past value of the error and finally, the prediction of future errors based on linear extrapolation is carried out by the derivative term. Figure D.3 shows the action of this terms.

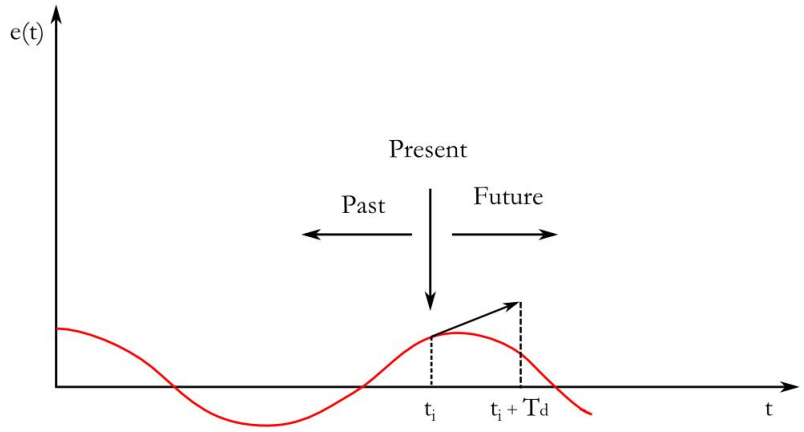

Figure D.3: PID action based on past, present and prediction of future control errors.

For K, T_i and T_d different of zero, the three modes (Proportional-Integral-Derivative) modes are grouped and so its advantages and disadvantages. This way, the controller is a forward and backwards compensator where PI action focus in low frequencies intervals and the PD action relies on high frequency zones for an improvement of steady state and transitory response of the system.

D.3.1 Proportional Action

Figure D.4 shows the response of the output signal to a unit step in the command signal for a system exclusively proportional control. In this case, the controller is given by the equation D.2 with $T_i = \infty$ and $T_d = 0$. The figure shows that steady state error is always present in controller with only proportional term. Suppose that the controller and

process have transfer functions $C(s)$ and $P(s)$, respectively. The transfer function, $H_w(s)$, regarding reference to output is [26]

$$H_w(s) = \frac{C(s)P(s)}{1 + C(s)P(s)} \tag{D.3}$$

The steady state gain with proportional control $C(s) = K$ is as follows [26]

$$H_w(0) = \frac{KP(0)}{1 + KP(0)} \tag{D.4}$$

Hence, the steady state error for a unit step is mathematically described as $1/(1+KP(0))$. The error will decrease with increasing gain, but in other hand, the system tends to be more oscillatory. The bottom graph regarding the figure D.4 shows that the initial value of the control signal is the same as the proportional gain. To avoid such steady state error, the proportional term can be tuned and changed to

$$u(t) = Ke(t) + u_b \tag{D.5}$$

where the term u_b is a bias or reset term which is adjusted for a desired steady state value, therefor, the controller performance is slightly increased [26].

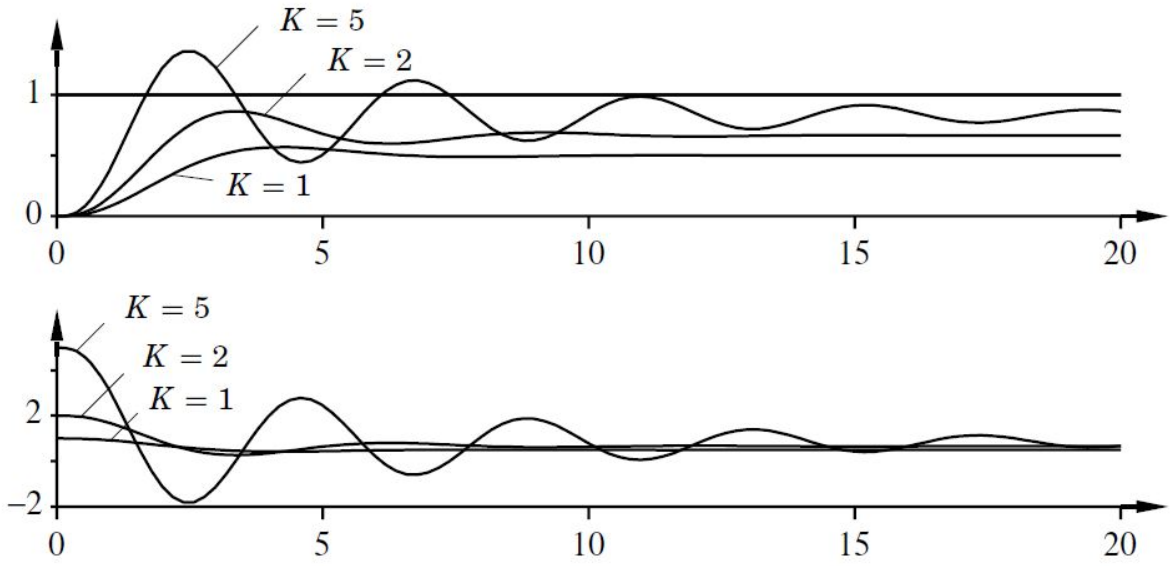

Figure D.4: Simulation of a closed-loop system with proportional control. The process transfer function is $P(s) = 1/(s+1)^3$ [26].

D.3.2 Integral Action

The main job of integral action in a controller is to guarantee that the output signal agrees with the reference signal in steady state space. Following equation D.2, the strength of integral action increases with the decreasing of integral time T_i. The figure D.6 shows that the steady state error vanish when integral term is used on the controller. Contradictory, the decreasing of T_i may tend for a sudden system oscillation. Assuming that the system is already in steady state, lets consider a constant control signal u_0 and also a constant error $e_0 \neq 0$. It follows from equation D.1 that [26]

$$u_0 = Ke_0 + K_i e_0 t \tag{D.6}$$

Notice that the first term is constant but the right term is function of time t. It creates a contradiction for a constant control signal u_0 and it forces for a null value of e_0. It follows from equation D.3 that $H_w(0) = 0$ due to the fact that with integral action, the transfer function of the controller has infinite gain at zero frequency ($C(0) = \infty$). However, it requires a linear system.

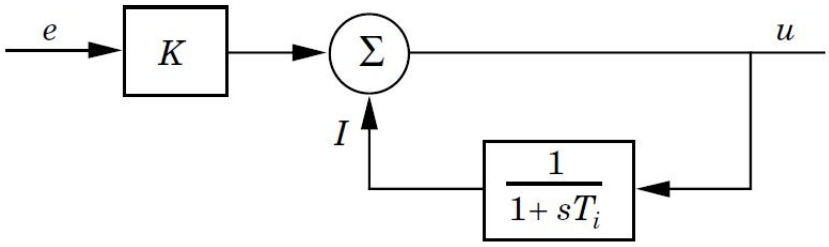

Figure D.5: Proportinal controller bias is automatically adjusted by integral implementation [26].

Integral action also automatically tunes the bias term u_b in the proportional controller described in the equation D.5. This method is is illustrated in Figure D.5 where the bias term u_b is automatically generated by a low pass filtering $(1/1 + sT_i)$ the output signal. This tuning implementation is called *automatic reset* and was one of the early inventions of integral control [26]. Analyzing again the Figure D.5, the transfer function of the system can be obtained by loop tracing. The equation D.7 [26] shows this transfer function.

$$u = Ke + \frac{1}{1 + sT_i}u \tag{D.7}$$

Solving equation D.7 regarding u becomes [26]

$$u = K\frac{1 + sT_i}{sT_i}e = K + \frac{K}{sT_i} \tag{D.8}$$

that demonstrates the transfer function of a PI controller. Integral action can be seen in Figure D.6. The case of $T_i = \infty$ represents $K_i = 0$ which is a pure proportional control that comprehend a steady state error of 50%. The steady state error is removed for small values of T_i that results in higher values of K_i. Despite the faster approach for higher integral gains, the system also tends to become more oscillatory.

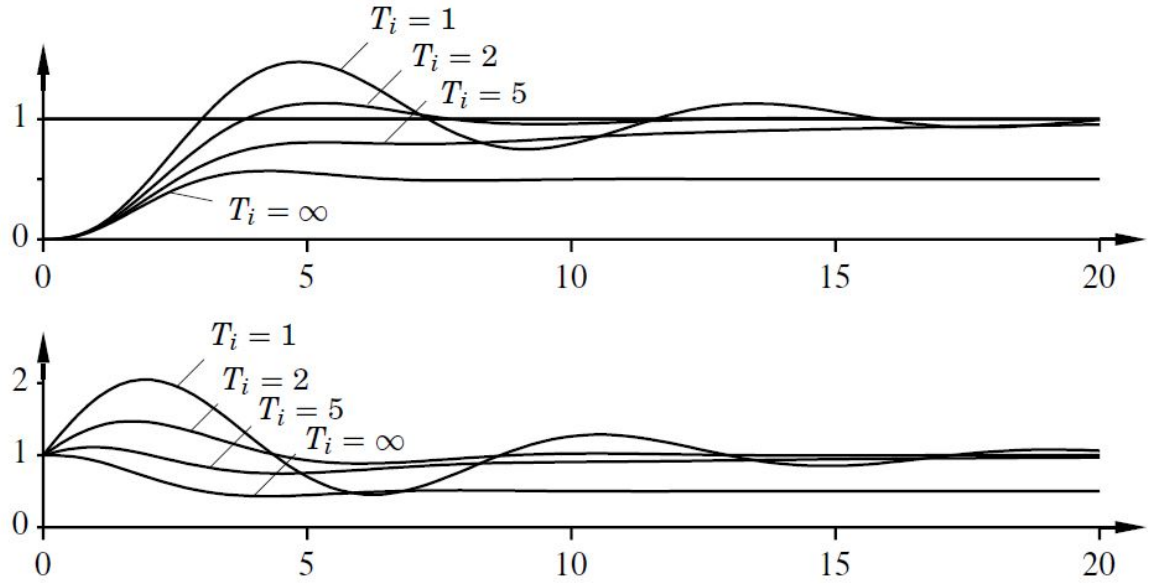

Figure D.6: Simulation of a closed-loop system with proportional and integral control. The process transfer function is $P(s) = 1/(s+1)^3$, and the controller gain is $k = 1$ [26].

D.3.3 Derivative Action

Derivative action may improve stability and rise time of the closed-loop system and it can be interpreted as providing prediction of the error by linear extrapolation over the time T_d. Doing $K_i = 0$ and follow the equation D.1, the relation between the reference and output signal is [26]

$$u(t) = Ke(t) + K_d\frac{de}{dt} = K(e(t) + T_d\frac{de}{dt}) \tag{D.9}$$

where $T_d = K_d/d$ is the derivative time. PD controller is a forward compensator and high-pass filter. Carneiro [27] shows that the action of a PD controller can be interpreted as an proportional action to the predicted value of error in $t + T_d$, as equation D.10 describes. Notice that in Figure D.7 the derivative term is benefit when it does a good prediction of the error into the future. Therefor, derivative time T_d should not be high compared to the dynamic of the error.

$$e(t + T_d) \approx T_d \frac{de(t)}{dt} + e(t) \tag{D.10}$$

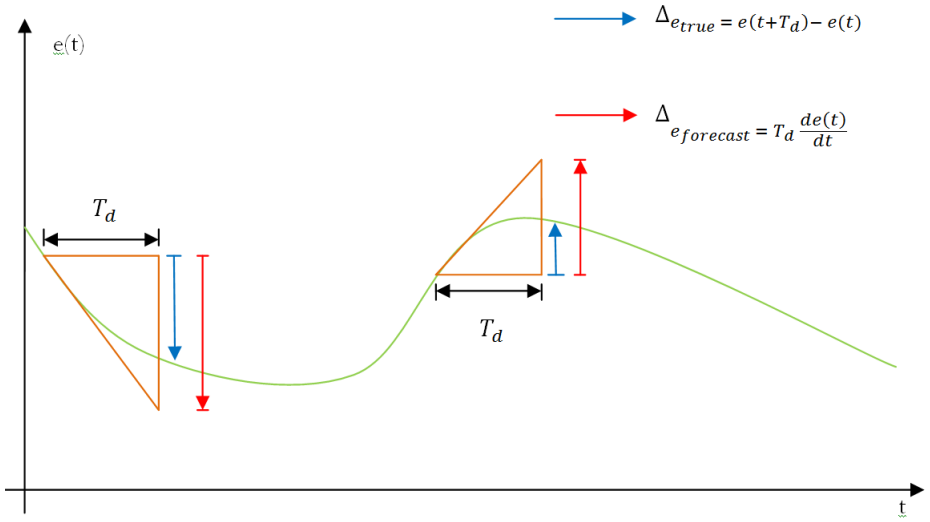

Figure D.7: Error forecast regarding the derivative term.

If the gain of the action derivative is not limited, it can reach high values enough to disturb the system provoking high and decontrolled jumps if the error has noise in high frequencies. The amplitude of derivative action depends of the noise present during the measurement of the error. The solutions goes through filtering the high frequencies of the error signal before it gets processed by the derivative term. In a controller, if the derivation action is not used the system tends to be oscillatory, in other hand, if the derivative gain is increased, the system becomes more damped. In Figure D.8 the parameters K and T_i are tuned to that the system is oscillatory and it represents the effect of adding the derivative action to the system. For T_d larger than 1 second (one sixth of the period) the derivative action seems to be effective but also for higher values of T_d the oscillation period is increased.
Filtering the derivative action is important on PID controllers to avoid excessive damping and oscillation. An disadvantage of derivative action is that an ideal derivative has very high gain for high frequency signals meaning that during the error measurement the noise will generate large variations of control signal, therefor unstable system. Replacing the term $K_d s$, see equation D.11 [26], will surge in a reduction of noise measurement on the system.

$$D_a = -\frac{K d_s}{1 + sT_f} \tag{D.11}$$

Hence, it can be faced as an ideal derivative that is filtered by a first-order system with constant T_f. Small s means a transfer function $K_d s$ and for large s is equal to K_d/T_f. This

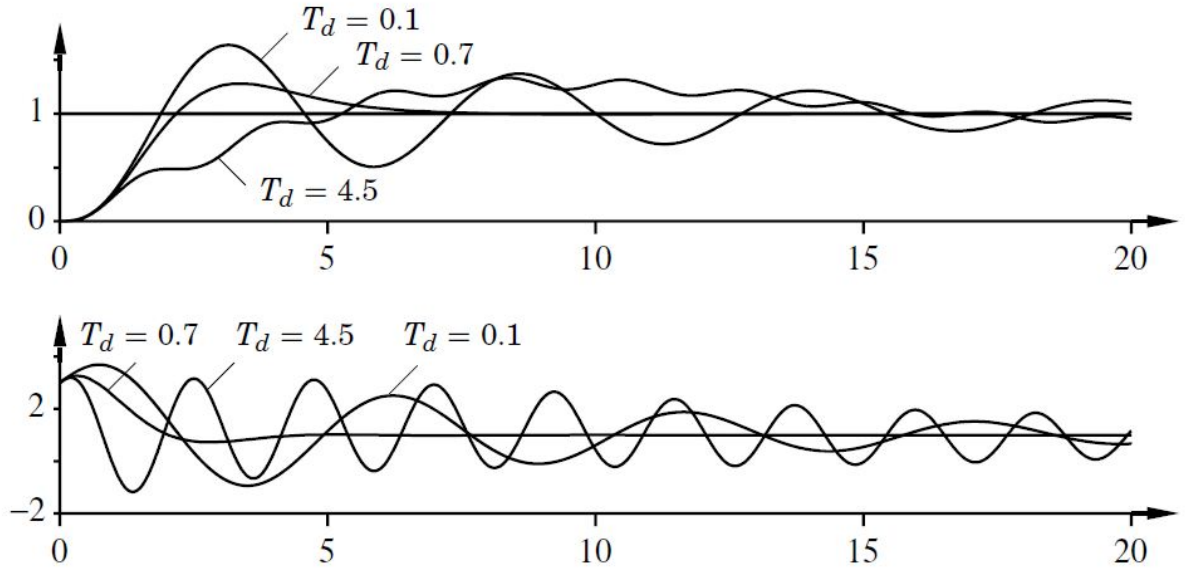

Figure D.8: Simulation of a closed-loop system with proportional and integral control. The process transfer function is $P(s) = 1/(s+1)^3$, and the controller gain is $k = 3$ and the integral time is $T_i = 2$ [26].

approach signifies a act as a derivative for low frequency measurement and as a constant gain for high frequencies. This same gain is equal to K_d/T_f and the filtering time is usually $K_d/K/N$. The range of values for N may vary, Carneiro [27] points $N \in [2, 20]$ and Carvalho [28] defends $N \in [10, 100]$. The transfer function regarding a filtered derivative is as follows [26],

$$C(s) = K\left(1 + \frac{1}{sT_i} + \frac{sT_d}{1 + s(T_d/N)}\right) \tag{D.12}$$

The refereed constant gain for high frequencies is $K(1+N)$.
Faccin [29] presents serial and parallel configuration for a PID controller, as illustrated in Figure D.9. The same author claims that the refinement of the parameters in serial configuration is simpler and more intuitive than parallel. In order hand, parallel configurations leads to best controller performances. Serial parameters can be converted in parallel form but only for cases where $T_i \geqslant 4T_d$ otherwise, K,T_i and T_d will become complex.

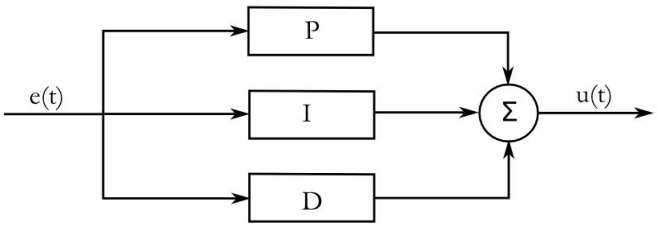

(a) Parallel configuration

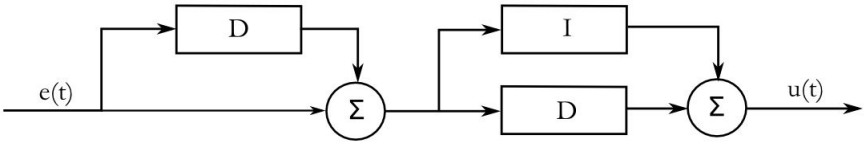

(b) Serial configuration

Figure D.9: Serial and Parallel configuration for PID controller.

D.4 Integrator Windup

Based on linear theory, many aspects of a control system can be understood. Non-linearity effects must be solved and expected in most of the existent controllers. Windup is a phenomenon which is caused by the interaction of integral action and actuator saturation, external disturbances and hardware malfunction. Every single actuator in the market as its own limitations, for instance, motor speed and valve cannot be more than fully opened or fully closed. Most of the control systems have a wide range of operating aspects that may occur a saturation of control signal, therefor, actuator reaches its limits. As soon as this happens, the feedback control loop is broken and the system basically runs in open loop because the actuator will remain on its limits independently of the process output. In a controller with integral action, the error will always be integrated and so the integral term may become very large or it "Winds Up". So it is required an opposite sign of the error for a long period of time before the system gets back to normal functioning.
Windup phenomenon is illustrated in Figure D.10 which shows the process output $y(t)$, the desired reference/setpoint $y_{sp}(t)$, output control signal $u(t)$ and the integral term behavior $I(t)$. The refereed control system is a PI controller incorporated with integrating process. Notice that the initial setpoint change is so fast and large that the output control signal $u(t)$ immediately saturates the actuator at the high limit. Therefor, the initial integral term dramatically increases and reaches its maximum at $t = 10$ towards to steady state. The output control signal remains saturated due to the large value of integral term until $t = 20$. The integral term only leaves the saturation zone and goes to lowest values when the error becomes negative for a long period of time. Notice that even for less dramatic setpoints, the control signal bounces between its limits several times. The output effect of the system is a large overshoot and a damped oscillation that literally provokes the

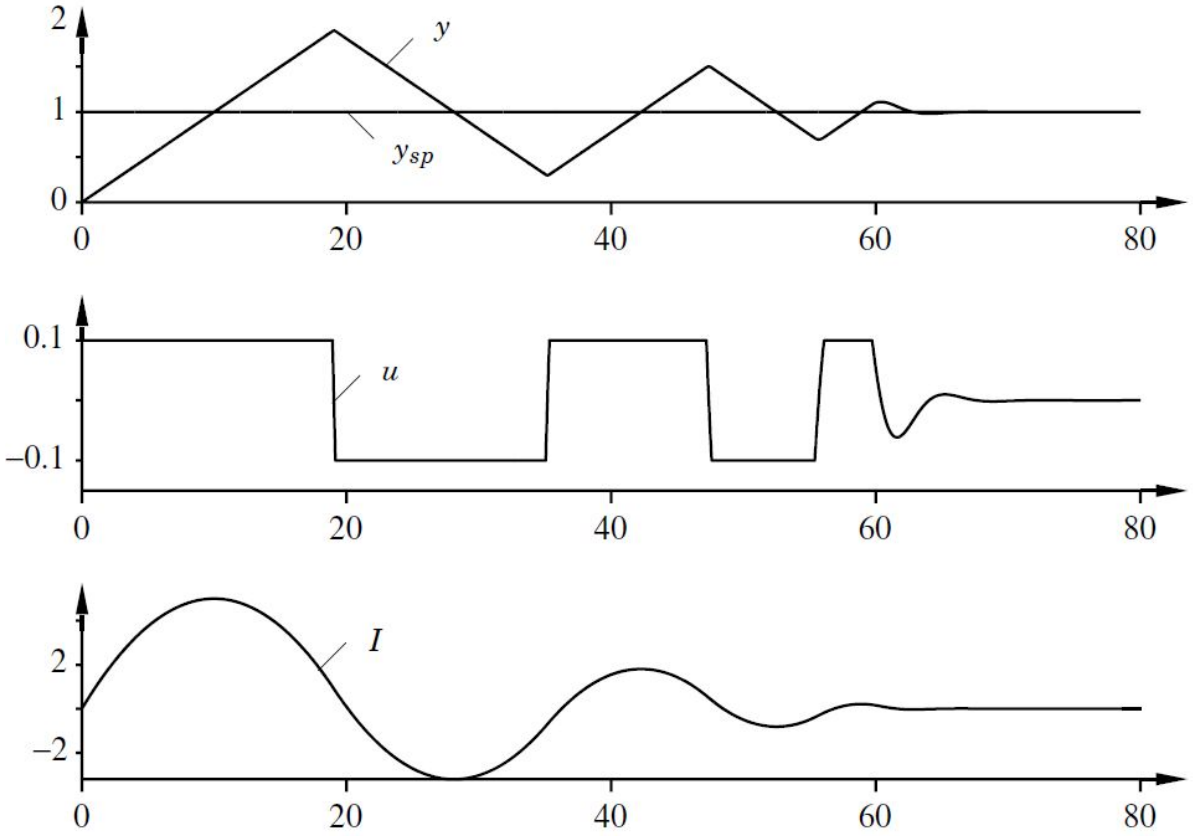

Figure D.10: Illustration of integrator windup. The diagrams shows process output $y(t)$, setpoint $y_{sp}(t)$, control signal $u(t)$ and integral part $I(t)$ [26].

actuator to flip from one extreme to the other. After a long period of time, the actuator no longer saturates and the system becomes linearly and settles.

This phenomenon of integral windup was well known to manufacturers of analog controllers who have invented several tricks and procedures to avoid or minimize the affect. Although the problem was well understood, the analog technology restrictions were always present. These tricks and procedures to avoid windup phenomenon were most of the time kept as trade secrets. This phenomenon was again merged when the controllers started to be implemented digitally and so many authors found several methods and models to avoid it. Nowadays, there are some methods to avoid integral windup such as *Setpoint Limitation*, *Incremental Algorithms* and *Back-Calculation and Tracking* described below.

Setpoint Limitation is a simple and basic implementation method that relies on introducing limiters to the setpoint variation so that the control output signal never reaches the actuators limits. In other hand, it leads to conservative bounds and poor performance and does not entirely avoid the windup caused by external disturbances, for instance, payload.

Incremental Algorithms is another way of avoiding windup effect. In early phases of

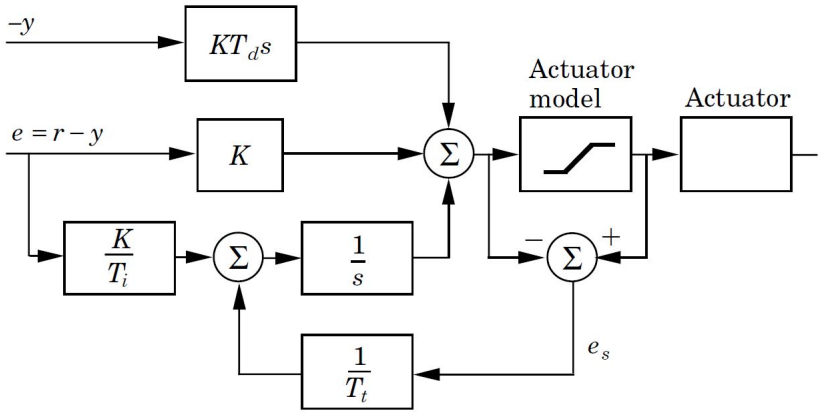

Figure D.11: PID Controller with anti-windup system based on mathematical model [26].

feedback control, the integral action was integrated with the actuator by having a motor drive directly to the valve. In this case, when the vale stops and integration also stops because it is handled automatically. Later, when digital controllers were implemented, an algorithm called *velocity algorithm* first computes the rate change of the output control signal that is then fed to the integrator either a motor directly connected to the actuator or internally implemented on the controller by software. Hence, it is easily to avoid windup phenomenon by inhibiting integration "stack" whenever the output control signal saturates. This method is now equivalent to *Back-Calculation and Tracking* that will be further described.

Back-Calculation and Tracking offers another way of avoiding integral windup phenomenon. Here, the integral term is recomputed when the output control signal saturates so that its new value gives an steady output signal at the saturation limit. At this stage, reseting the integrator is beneficial but only dynamically with a time constant T_t, see Figure D.11. This figure shows a PID controller with anti-windup system based on back-calculation. Another feedback channel is added to the controller to measure the actual output signal and forming an error signal $e_s(t)$ that is the difference between the output controller $v(t)$ and the actuator output $u(t)$. The error signal $e_s(t)$ is then fed to the input of the integrator by a gain $K_t = 1/T_t$. Obviously, if $e_s(t)$ is zero means that there is not saturation occurring on the system and it will perform as normal. However, if $e_s(t)$ is different from zero, saturation is occurring and the normal feedback path is broken because the plant input signal remains constant. Therefor, the extra feedback channel around the integrator is activated driving the integral input value towards zero. Hence, the integrator input is [26]

$$\frac{1}{T_t}e_s(t) + \frac{K}{T_i}e(t) \tag{D.13}$$

where $e(t) = r(t) - y(t)$ is the control error. So,

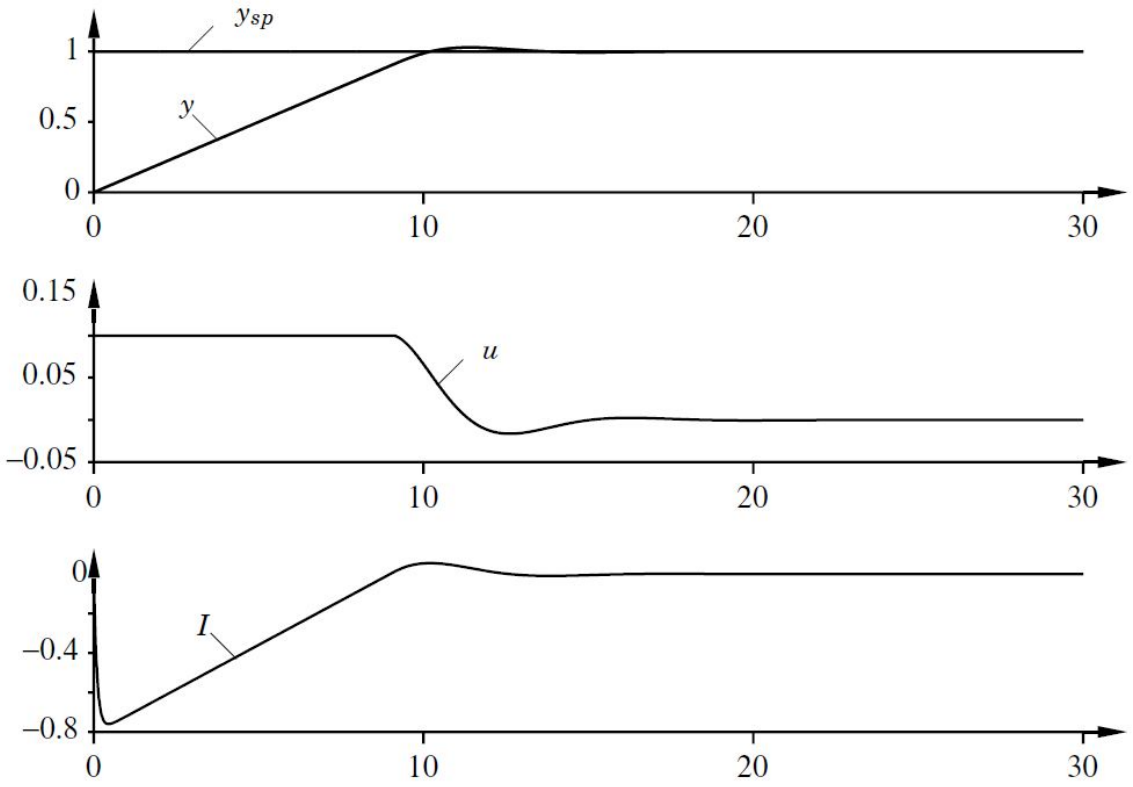

Figure D.12: Controller with anti-windup system applied to the controller in Figure D.11. The diagrams shows process output $y(t)$, setpoint $y_{sp}(t)$, control signal $u(t)$ and integral part $I(t)$ [26].

$$e_s(t) = -\frac{KT_t}{T_i}e(t) \tag{D.14}$$

in steady state [26]. Since $e_s(t) = u(t) - v(t)$, it follows

$$v(t) = v_{lim} + \frac{KT_t}{T_i}e(t) \tag{D.15}$$

where v_{lim} is the saturating value of control signal [26]. This means that the control signal reacts as soon as the error changes in time and so preventing the integrator from windup. How often and how the integral input signal changes is commanded by the feedback gain $K_t = 1/T_t$, where T_t is the time constant that determines how quickly the integral is reset.

The outcome of *Back-Calculation and Tracking* regarding the system in Figure D.11 is illustrated in Figure D.12 that clearly attenuate the effect of windup phenomenon. Notice

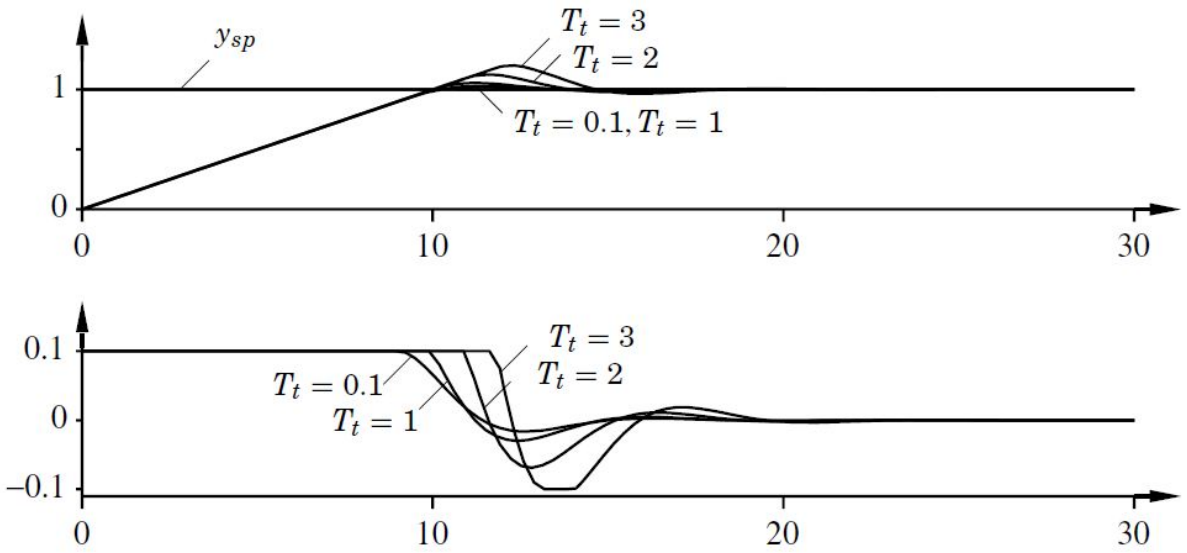

Figure D.13: Illustration of the step response of the system in Figure D.11 for different values of the tracking time constant T_t. The upper graph shows the process output $y(t)$ and the setpoint $y_{sp}(t)$ and the lower graph shows the control signal $u(t)$ [26].

that as soon as the output signal of the controller saturates, the input of the integrator is quickly reset so that $v(t) = v_{lim}$. This integral behavior is completely different from what it is illustrated in Figure D.10 with an ordinary PI controller. Regarding the Figure D.13, the effect of changing the values of tracking time constant T_t are shown. It may seen advantageous choose a small value of T_t for a quick integrator reset to achieve a better performance. But, in order hand, special care must be given when placing anti-windup systems in controllers with derivative term. If T_t is too small, spurious measured errors (Recall section D.3.3) may suddenly saturate the output control signal and so instantaneously reset the integrator action. Rule of Thumb [26] says that tracking time constant T_t should be larger than T_d and smaller than T_i, as follows in equation D.16

$$T_t = \sqrt{T_i T_d} \tag{D.16}$$

Appendix E

Fuzzy Logic Controller Theory

Fuzzy logic (FL) is widely used in machine control. Professor Lotfi A. Zadeh, for some considered the father of fuzzy logic, did the first propose of fuzzy logic in 1965 while in the University of California at Berkeley. Entitled as *Fuzzy sets*, Lotfi [36] used the following words to describe fuzzy sets

> "A fuzzy set is a closs of objects with a continuum of grades of membership. Such a set is characterized by a membership (characteristic) function which assings to each object a grade of membership ranging betweem zero and one. The notions of inclusion, union, intersection, complement, relation, convexity, etc., are extended to such sets, and various properties of these notion in the context of fuzzy sets are established. In particular, a separation theorem for convex fuzzy sets is provided without requiring that the fuzzy sets be disjoint."

The author also refers that real physical world do not have objects precisely defined criteria of membership. A good example is also described by Lotfi that class of animals clearly includes dogs, horses, birds, etc., as its members. Objects such as rocks, fluids, plants, etc. are obviously excluded. However, objects like starfish, bacteria, etc., have an ambiguous status with respect to the class of animals. The concept is the association of *fuzzy sets* to "class" ,like mentioned above, with continuum grades of membership.

Fuzzy term refers to the fact that with this logic is possible to understand concepts that may not be converted as "true" or "false" but rather as "partially true". Humans can successfully perform and mechanize tasks that can be converted to fuzzy logic and so, designing a controller. In recent years, fuzzy logic controllers (FLC) have been widely studied and used in a variety of applications. Conventional and modern control theories have managed to deal with a large of control problems by mathematically modeling the process and so solving these models to obtain control actions. However, a precise knowledge of the process to be controlled is required and its input and output parameters needs to be exactly measured. Due to the complexity and vagueness of many practical process, the non-linearity behavior and the unavailability of quantitative data regarding the input-output relationship make this analytically approach almost impossible. Fuzzy logic controllers since its discover have demonstrated and proved a large number of successful applications once the analytical models are not required. Applications such as water control quality, nuclear reactor control, automobile transmission control, aerospace (including NASA space shuttle), cameras, washing machines, robotics, power systems control and many others [38] [40]. Heske [39] argues that elevators controlled by FLC are up to 30% more efficient than conventional ones. Reality and real models are non-linear. FLC controllers are remarkable in non-linear reality due to its unique characteristics: it is intelligent, analyses and interprets the context where the process is insert, avoids any possible mathematical models of that process and it is parameterized by "linguistic variables". For a better understanding of what "linguistic variables" lets follow the given example:

> IF brake temperature IS warm AND speed IS not very fast
> THEN brake pressure IS slightly decreased.

The two input variables are the terms "brake temperature" and "speed" that have values defined as fuzzy sets. Output variable is given by the term "brake pressure" that is also defined by a fuzzy set which contains values like "static" or "slightly increased" or "slightly decreased" or others. This example can be found, for instance, in a brake system of a train that automatically controls the brake pads in function of the temperature to guarantee a good functioning of the entire braking process.

Santos [37] has described some of the FLC characteristics:

1. *Powerful capacities to deal with non-linear process.* A group of fuzzy rules can describe as refined as desired any non-linear function. FLC can produce non-linear actions for non-linear controls with high performance through *common-sense* mapping. This codification results in a good method to define a function $f(t)$ between the input $u(t)$ and output $y(t)$ regarding the *common-sense* mapping and human expertise to solve determined problem. " Thinking as human" and convert those objects into mathematical approaches (fuzzy sets) may significantly solve the non-linear effects.

2. *Conceptually easy* due to its mathematical simplicity and "natural" approach.

3. *Flexible*, at any time it is possible to change, remove or add functionality to the system.

4. *Is built by humans through its experience and mastery.* FLC is a methodology that plays with human knowledge to control the system. The expert already knows in advance the first approach to build the controller which contrast with others known control theories.

5. *Can be used along with other control techniques.* FLC is not a replacement to other control technique, but a complement. Hybrid solutions often offers best performance and robustness when analytic models comes together with human expertise.

6. *Natural language and understandable by humans.* Most of the success of FLC relies on the language bridge between the human and control methodology. "Speaks human language" FLC follows the language structure used by humans in their communication as an huge advantage. The transition among the expert and FLC is carried by high level descriptions and details regarding the human perception. There are high level computational languages like C or C++ that are closer to human natural perception. FLC is a logic that puts together and encloses the bridge between the expert and the computer.

7. *Tolerant to imprecision.* Fuzzy logic avoids any mathematical model and it is close to "human thinking" but yet very tolerate to imprecision. FLC can be modeled in a such way to avoid those inaccuracies and assure that goals are achieved with precision regarding the plant limitations. It is possible to "teach" the controller about what is "exactly right" and "estimated" and program it to chose what to do on that

circumstances. FLC is faced as if someone was "there" in real time processing as a decision maker about input-output relations.

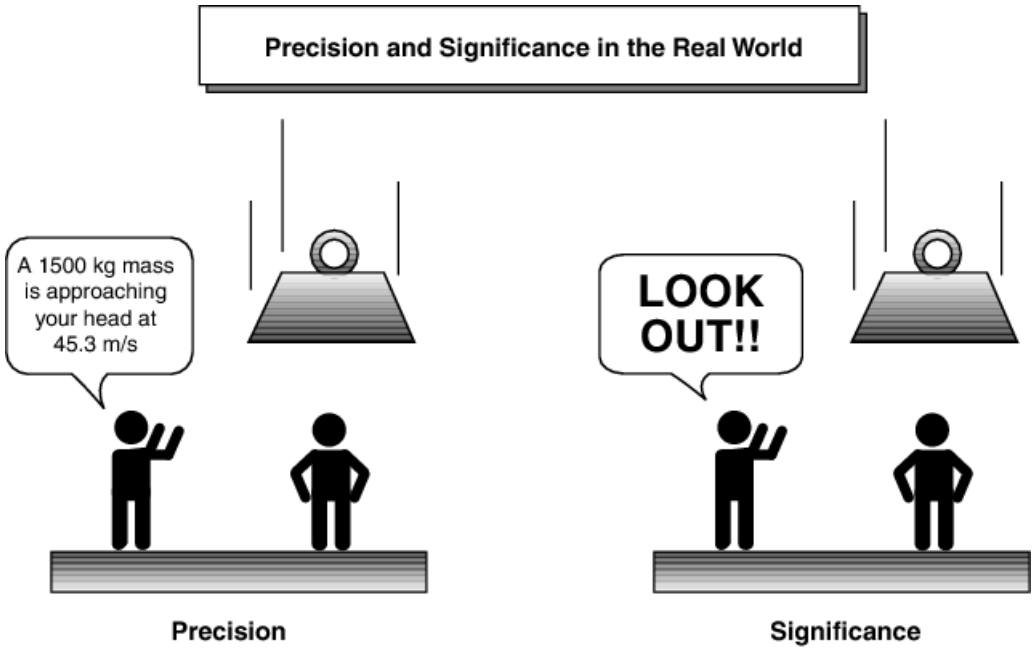

Figure E.1: Precision vs Significance [16]

Lotfi Zadeh says on his paper entitled as *Outline of a New Approach to the Analysis of Complex Systems and Decision Process* [41] that "... we employ fuzzy algorithms both consciously and subconsciously when we talk, drive a car, search for an object, tie a knot, park a car, cook a meal, find a number in a telephone directory, etc." FLC concept relies on linguistic variables based on the controller programmer. These linguistic variables are words and not numbers (see Figure E.1) that are being processed in fuzzy logic phenomenon, contrary to the known high level computational languages. Lofti on the same paper mention: "... key elements in human thinking are not numbers, but labels of fuzzy sets, that is, classes of objects in which the transition from membership to non-membership is gradual rather than abrupt." Concluding, this "intelligent control" does not substitute biological functions but emulates.

In Figure E.2 is illustrated a fuzzy logic control that incorporates 6 stages: preprocessing, fuzzification, inference engine, defuzzification and post-processing. The fuzzification block converts the crisp inputs into difuse inputs. Based on pre-defined rules, the inference engine uses those rules to produce diffuse outputs that will later be converted in crisp outputs through defuzzification process. All this stages will be further described.

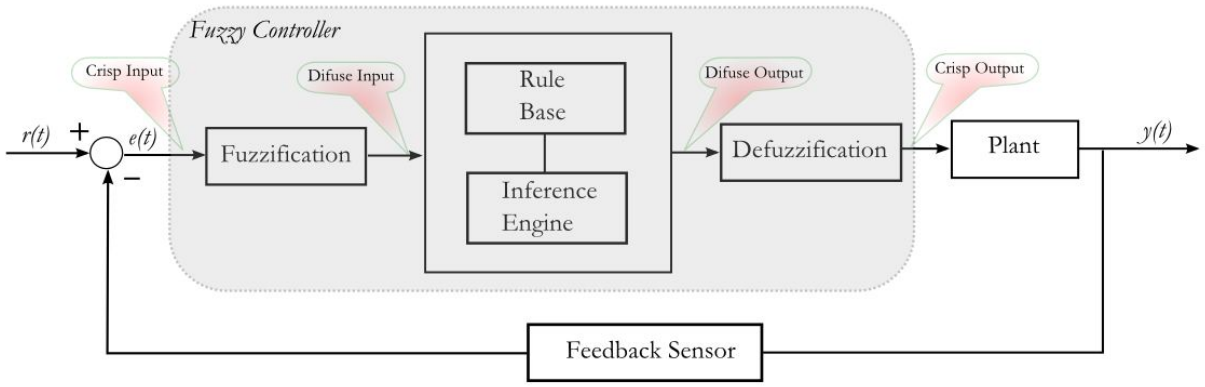

Figure E.2: Fuzzy logic controller with feedback - Example

E.1 Fuzzy Sets

Let R be a agglomerated of points (or objects), and a generic element of R denoted by r. Thus,

$$R = \{r\} \tag{E.1}$$

A *fuzzy set* (or class) C in R is featured by a *membership function* $f_C(r)$ that connects each point (object) in R a real number $N \in [0, 1]$, with the value of $f_C(r)$ at r representing the degree of membership, μ, of r in C. Near the value of $f_C(r)$ to 1, the higher the degree of membership of r in C [36].

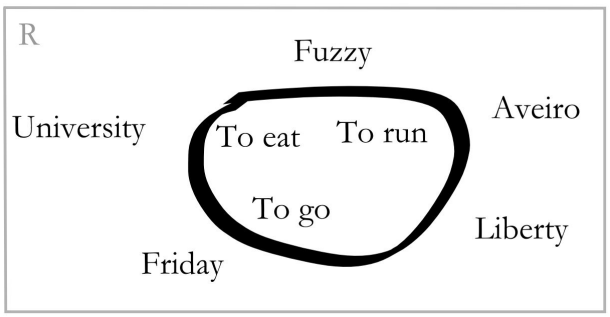

Figure E.3: Example of a space of objects R that belong to the class C of verbs.

In Figure E.3 is shown an example of a space of objects R that belong to the class C of verbs. This space of objects can be also represented in graphical form as Figure E.4 illustrates.

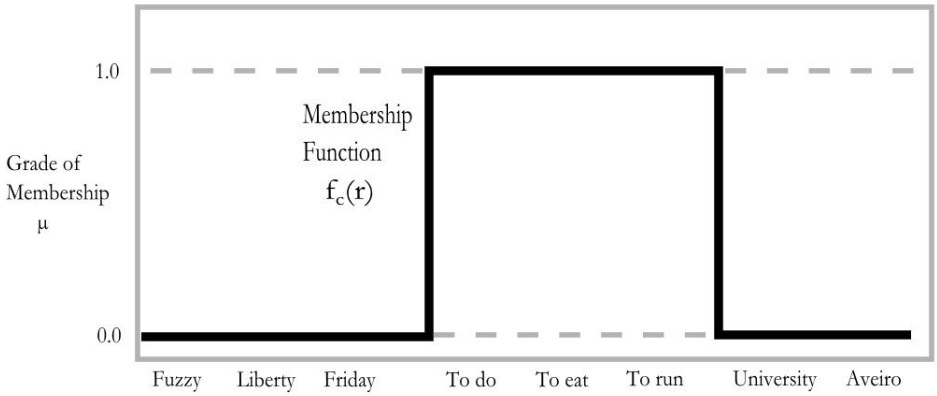

Figure E.4: Illustration of the space of objects R that belong to the class C of verbs in graphical form.

E.2 Fuzzy Linguistic Variables

A *Fuzzy linguistic variable* or as known as FLV, is a composition of one or more fuzzy sets (classes) to typify a concept or domain qualitatively. For instance, the sets "Little, Average, High" are members of the fuzzy linguistic variable Engine Efficiency, as follows

Engine Efficiency $= \{Little, Average, High\}$

E.3 Fuzzy Rules

Fuzzy logic allows to write a bunch of rules determined by the *expert* that the controller will interpret in a way to emulate and create an output value. This methodology will convert the input value in FLV regarding its membership functions. These rules are established by a set of conditions whose connection is logic and are put together into the *rules base*. A FLC controller can have the following rules:

1. IF car speed IS increased AND fuel consumption IS decreased Then engine efficiency IS High.
2. IF engine temperature IS warm AND engine torque IS low Then engine efficiency IS little.
3. IF x IS b Then $e = f(e)$.

...

n. IF <*fuzzy linguistic variable*> Then <*fuzzy linguistic variable*> .

All rules must not conflict with each other and have to make sense as if was the *expert* controlling the process by hand. There are not limit for the number of rules and it is not

mandatory to describe all possible case scenario. Obviously, higher the number of FLV's or controller inputs, the higher number of rules. Therefor, it can be used for SISO, MIMO, MISO or SIMO applications. For instance, some FLC controllers used for positioning uses error and its derivative as inputs to generate unit or multiple outputs (depending on the number of actuators). In Table E.1 is illustrated an example of a typical decision matrix based on two inputs to generate output z.

Table E.1: Representation of an imaginary example of a decision matrix.

		Input y			
		Low	Normal	High	Very High
Input x	Low	Low	High	High	High
	Normal	Low	Low	Medium	Medium
	High	Low	Low	Low	Low
	Very high	Low	Low	Low	Low

For instance, the following rules (and more) can be described regarding the decision matrix:

1. IF x IS Low AND y IS High
   THEN z IS High

2. IF x IS Very high AND y IS Normal
   THEN z IS Low

E.4 Membership Functions

Membership functions are curves that determines how each point in the input space is mapped to a degree of membership, $\mu \in [0\ 1]$. Every input value can be associated to a linguistic value. Let $f_C(r)$ be a linguistic value of a FLV r in the universe of objects C, hence $\mu(r)$ associated to $f_C(r)$ that represents $f_C(r) \in [1\ 0]$ is called degree of membership. For instance, regarding the Figure E.5, considering that "Warm" means a temperature of 90°C, it may be absurd to assume that a temperature of 89°C is "Not Warm" by following a sharp-edged function. This is an usual problem for discontinuous membership functions. To avoid this kind of problems, continuous membership functions are used so that a range of temperature can be defined as "Warm", "Not Very Warm" or "Not Warm".

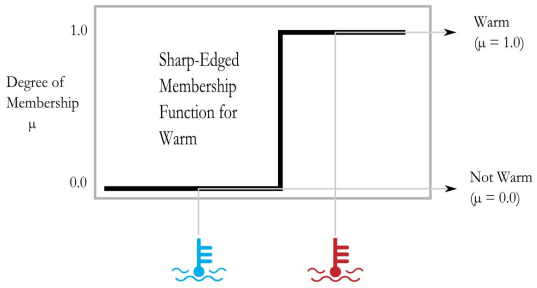

(a) Sharp-Edged membership function

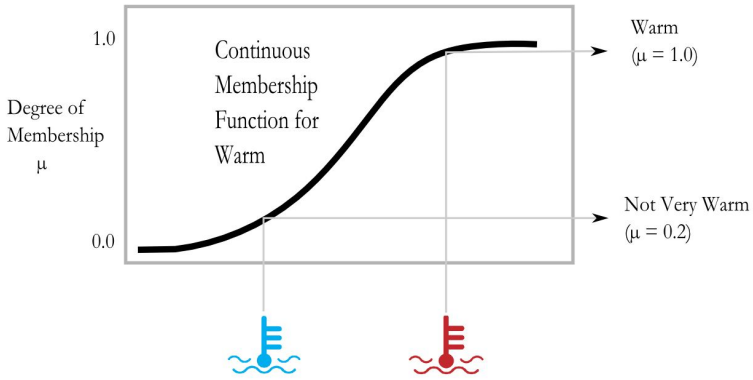

(b) Continuous membership function

Figure E.5: Continuous and discontinuous membership functions for FLV Warm.

E.5 Pre-Processing

Usually, before converting crisp inputs into diffuse outputs, it is necessary to do some adjustments or operations such as noise filtering, integration, derivation, rounding, etc. Before entering into the fuzzy logic apparatus, the signal must be "cleaned" so that best performance and best results can be obtain disregarding any possibilities of instability. Here, the input is always a crisp numerical value limited to the universe of discourse of the input variable.

E.6 Fuzzification

Crisp inputs after the pre-processing procedure belong to the universe of discourse, let's say $u_i \in \Theta_i$, $i \in \mathbb{Z}_+^*$. Fuzzification process transforms each input u_i into a value regarding its membership function that are defined to a certain range of u_i, hence, the degree of membership $\mu(u_i)$ is determined. Let $\Theta_i \rightarrow \Theta_i^Z$ be the universe of discourse of all possible diffuse values defined in Θ_i. The crisp input u_i fits a group of diffused values Z_i through an operator A (as shown in equation E.2 and E.3) what will generate a grade of membership $\mu_{Z_i}(x) \in \Theta_i^Z$, regarding the membership function $f_i(x)$, as follows in equation E.4,

$$A : \Theta_i \rightarrow \Theta_i^Z \tag{E.2}$$

$$A(u_i) = Z_i \tag{E.3}$$

$$\mu_{Z_i}(x) = f_i(x) \tag{E.4}$$

The membership function $f_i(x)$ is ,in many cases, a piecewise function. In Figure E.6, for an crisp input $u_i = 85°C$ based on the rule "Temperature IS Warm" and regarding the membership function $f_i(x)$ for FLV "Warm" , the result of the fuzzification is $\mu_{Z_i}(x) = 0.9$.

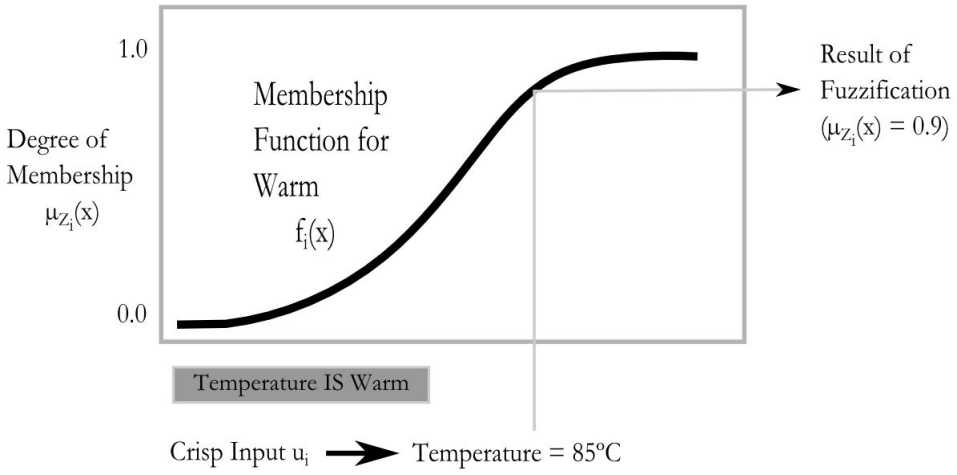

Figure E.6: Example of fuzzification system for Warm membership function.

E.7 Fuzzy Inference Engine

Fuzzy inference engine/system (FIS) is responsible for processing decisions to the given problem and act accordingly. FIS is a way of mapping an input space to an output space using fuzzy logic. Here, FIS tries to formalize the reasoning process of human language by means of fuzzy logic through "IF-THEN" rules. The most used inference system is the known Mamdani type (see section E.8 for more information). Its simple structure of "min-max" operations confers best performance and computation.
FIS generally involves two stages:

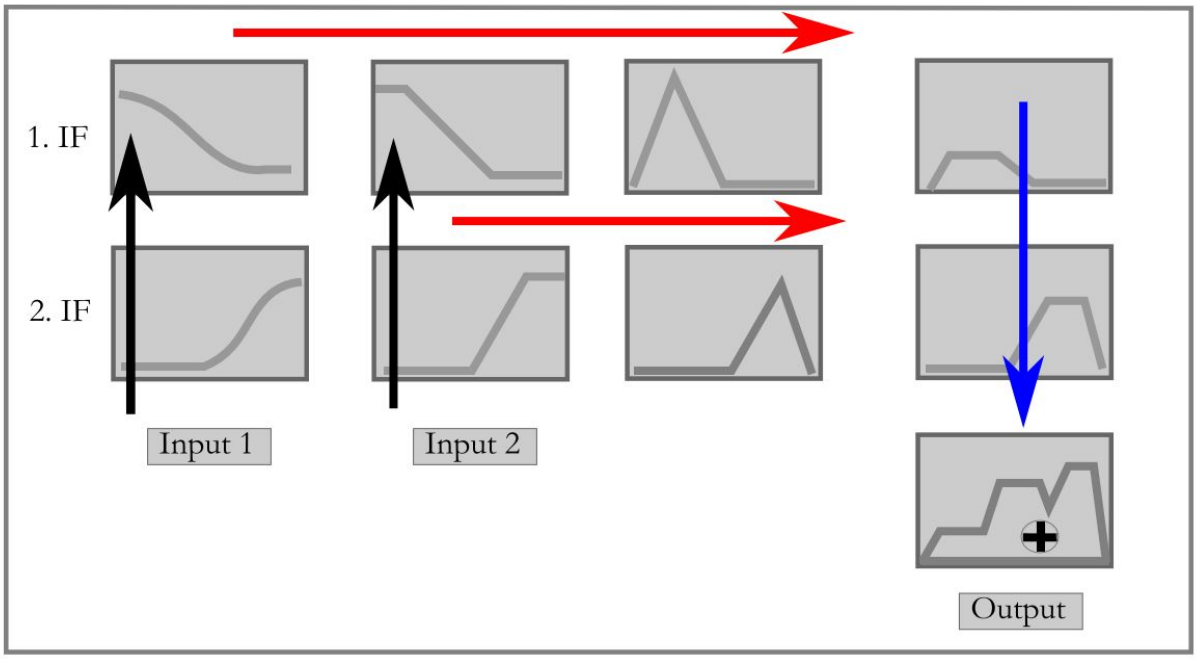

Figure E.7: Fuzzy inference system diagram.

1. A database which defines the memberships functions of the fuzzy sets used in the fuzzy rules. Known as "matching", the relevance of each rule for a determined input u_i is determined.

2. A decision-making unit which performs inference operations on the rules. Defined as "inference step" stage, uses the input u_i value and the information from the database to generate conclusions.

The inference is further divided into two stages that applies two methods:

1. *Implication Method* specifies how a FLC scales the membership functions of an output linguistic variable based on the rule weight of the corresponding rule. The rule weight is the truth value of the aggregated rule antecedent multiplied by the degree of membership that is defined by the rule. In Figure E.7, this method is illustrated by the red arrows.

2. *Aggregation Method*, denoted by the blue arrow, is the final decision based on the testing of all rules which collects all results from the implication method in a diffuse result (aggregated output fuzzy set). Hence, the diffuse result will be further head for defuzzification process.

E.8 Types of Fuzzy Inference Systems

There are two types of fuzzy inference systems,

- Mamdani
- Sugeno

These two types of fuzzy inference systems vary in how the outputs are determined. Mamdani's method is the most commomly used in FLC controllers. It was proposed in 1975 by Ebrahim Mamdani [42], based on Lotfi Zadeh's 1973 paper on fuzzy algorithms for complex systems and decision processes [41], as an attempt to control a steam engine. There is a fuzzy set for each output variable that needs defuzzification. It enhances the efficiency of the defuzzification process because it simplifies the computation required by finding the centroid of a two dimensional function through weighted average of a few data points. Sugeno method relies on integrating across two dimensional functions to find the centrioid, which is more heavy to compute. Also, Sugeno type can be used to model any inference system in which the output membership functions are either linear or constant [43]. In section E.3, the first and second rules follows the Mamdani type of inference system and the third one Sugeno type, just as an example.

E.9 Defuzzification

Defuzzification is the last stage of an FLC. The input of for defuzzification process is a fuzzy set (the output of the aggregation method) and the output is a single number denoted by crisp output. Here, the decisions made by the inference system needs to be converted in control actions. The aggregate fuzzy set is a group of fuzzy information recommended by the inference engine which using defuzzification methods such as centroid, bisector, middle of maximum, largest of maximum and smallest of maximum is possible to transform that amount of fuzzy information in crisp values, in this case, to the hydraulic actuators. Despite the large number of possible methods, perhaps the most used and popular one is the centroid defuzzification method - center of gravity (COG). Wang et al. [44] determined the centroid point ($\bar{x_0}$,$\bar{y_0}$) of a fuzzy number A, as follows

$$\bar{x_0}(A) = \frac{\int_{a_1}^{a_2} x f_A^L(x) + \int_{a_2}^{a_3} (xw)dx + \int_{a_3}^{a_4} x f_A^R(x)dx}{\int_{a_1}^{a_2} f_A^L(x) + \int_{a_2}^{a_3} (w)dx + \int_{a_3}^{a_4} f_A^R(x)dx} \tag{E.5}$$

$$\bar{y_0}(A) = \frac{\int_0^w y \left(g_A^R(y) - g_A^L(y)\right) dy}{\int_0^w \left(g_A^R(y) - g_A^L(y)\right) dy} \tag{E.6}$$

In Figure E.8 is illustrated an example regarding what was discussed above about FLC's concepts.

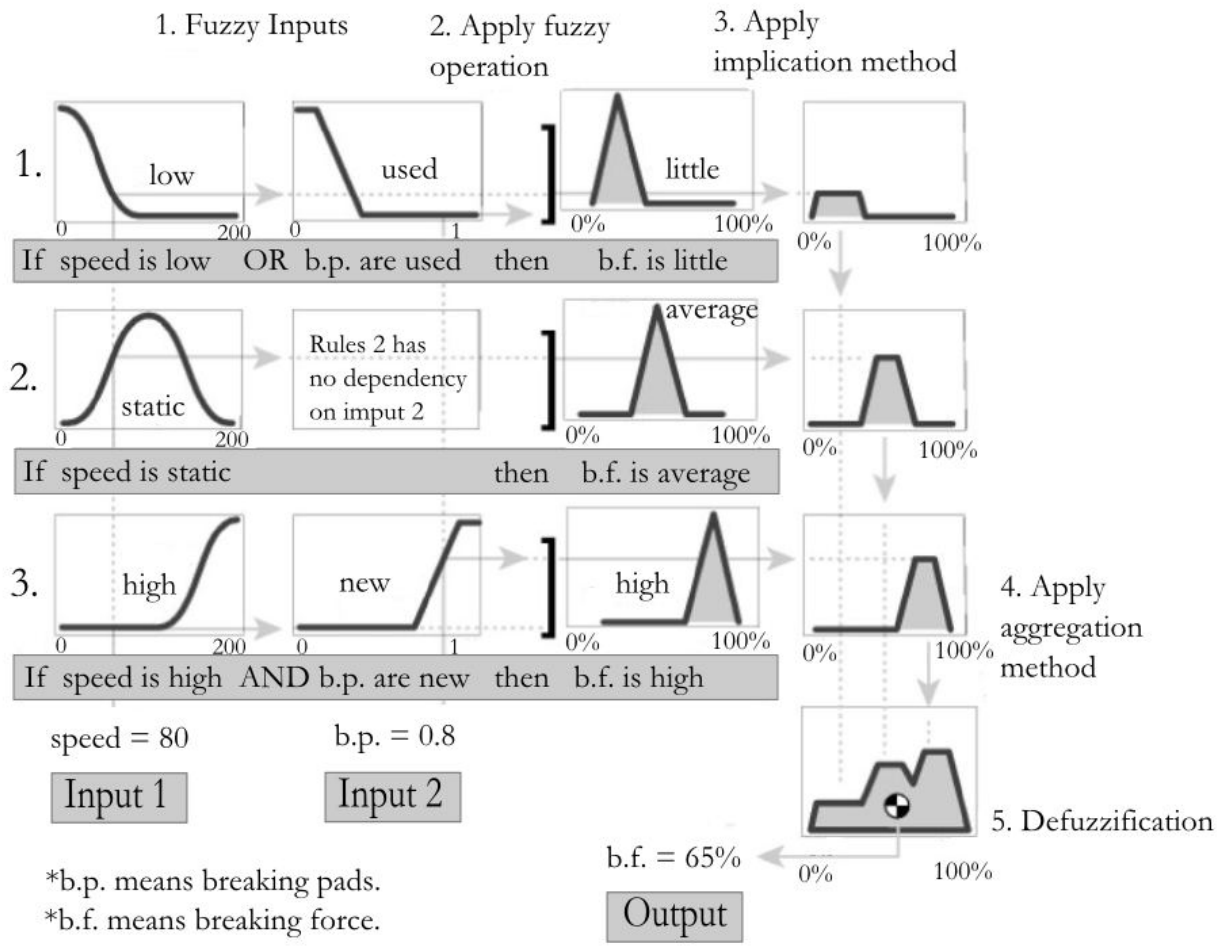

Figure E.8: Illustration of all operations in a diffuse controller regarding speed and braking pads as inputs and braking force as output.

E.10 Post-Processing

It is very likely to adapt the output signal of the fuzzy controller to the universe of discourse of the hardware or software downstream. The standard output or universe of discourse is [-1 1] and the input of the hydraulic actuator of the SPIF-A machine for this work is [-10 10] volts. Therefor, there is the need to do this adjustment that is quickly solved by applying a proportional gain.

Appendix F

Other Applications Using Parallel Platforms

Parallel manipulators are widely popular and often used for heavy duty processes. Despite less maneuverability and reduced workspace compared to serial serial robots, parallel configuration offers more reliability managing high loads with better accuracy. High machining speeds can be achieved with less vibration due to its closed chain configuration. Recently, many machining companies relies on parallel robots and study its advantages to build a product that makes possible to achieve faster machining times. Three degree-of-freedom machines are getting old and unused because the market demands complex parts that can only be achieved by six degree-of-freedom machining. So, with parallel robots it is easier, compared to serial robots, create a manipulator that can handle the tool in those different axis. There are plenty of applications for this kind of configuration, from medical assistance to milling and welding machines.

F.1 Milling Machines

F.1.1 HexaM

HexaM is a 5-Axis milling machine from Toyoda Machine Works, Ltd. It is the only parallel kinematic machine the company has. This system is a 6-PUS parallel manipulator with linear motion guides what provides actuation while the legs are of constant length. The actuators are attached to the base and the mobile part of the robot is reduced to the six legs and the mobile platform. Capable of working at high velocities and acceleration at the cost of reduced work space. The legs are made of only thin rods,thus, reducing the risk of leg interference.

Table F.1: Toyoda HexaM 5-Axis Milling Machine technical details:

Axis travels in X, Y, Z	400, 400, 350 mm
Range of tilt angle	$\pm$ 30°
Max. rates of travel in X, Y, Z	1.7 m/s each
Max. accelerations in X, Y, Z	9.8 m/s^2 each
Max. accuracy	$\pm$ 0.004 mm

Figure F.1: The HexaM 5-Axis milling machine [11].

F.1.2 Okuma Cosmo Center PM-600

Okuma's Cosmo Center PM-600 parallel mechanism machine tool to achieve high-efficiency die/mold machining that requires less polishing work and integrates operations for cutting complicated shapes. According to Okuma, it offers high-speed machining, sculptured surface machining and continuous operation [18].

Table F.2: Okuma Cosmo Center PM-600 technical details:

Axis travels in X, Y, Z	420, 420, 400 mm
Range of tilt angle	$\pm$ 25°
Max. rates of travel in X, Y, Z	100 m/min
Max. accelerations in X, Y, Z	1.5 G
Max. accuracy	$\pm$ 0.005 mm
Spindle	up to 30000 rpm

Figure F.2: The Okuma Cosmo Center PM-600 milling machine.

F.2 Manipulation, Assembly and Welding

F.2.1 Fanuc F-200iB

The F-200iB is a 6-DOF servo-driven parallel link robot designed for use in variety of manufacturing and automotive assembly process. The F-200iB is engineered for applications requiring extreme rigidity and exceptional repeatability in a compact and powerful package. This manipulator can be used for welding, part loading and positioning, nut running, vehicle lift and locate, material removal and dispense. It is also equipped with precision gear drives, fail-safe brake on each leg has 31,000 hour life at 100% duty cycle.

Table F.3: Fanuc F-200iB 6-Axis manipulator technical details.

Payload	100 Kg
Allowable bad moment at face plate	60 kgf-m
Vertical Motion Speed	300 mm/s
Horizontal Motion Speed	1500 mm/s
Repeatability	$\pm$ 0.1 mm

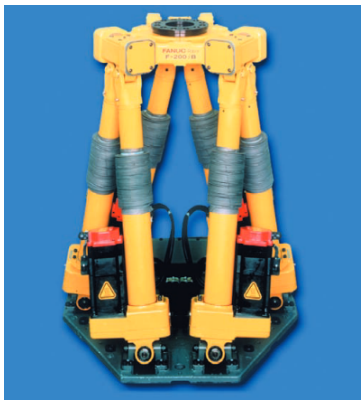

Figure F.3: Fanuc F-200iB 6-Axis manipulator [12].

F.3 Simulators

F.3.1 Advanced Concept Flight Simulator (ACFS) - NASA

The ACFS is a unique tool that was developed at Ames specifically for research with advanced aircraft. It was conceived and designed to train pilots based to the air traffic usage requirements in the 21st Century. This robot simulates a generic commercial transport aircraft and employs advanced flight systems. The cab is mounted on a 6-DOF synergistic motion system and uses side-stick controllers for aircraft control in the pitch and roll axes. It offers a 180-degree horizontal and 40-degree vertical field-of-view. Currently, the ACFS is used to simulate two aerodynamic aircraft models, a generic narrow-body transport vehicle (similar to a Boeing 757) and a C-17 transport [13].

Figure F.4: Left panel: ACFS as it looks outside. Right panel: ACFS's instruments and control panels from inside.

F.3.2 The SIMONA Research Simulator (SRS)

At Delft University of Technology, in Netherlands, along with the research simulators at the Max Planck Institute for Biological Cybernetics, a Stewart Platform was projected to build a hexapod to investigate perception and control behavior of humans in closed-loop control tasks as well as in open-loop perception experiments. Based on a MPI Stewart platform with electric actuators, SIMONA pretends to simulate it's behavior which features hydraulic actuators and a larger workspace.

Table F.4: SIMONA Research Simulator characteristics.

Range		
	Surge	2240 mm
	Sway	2062 mm
	Heave	1314 mm
	Roll	$\pm$ 25.9 deg
	Pitch	$+24.3/-23.7$ deg
	Yaw	$\pm$ 41.6 deg
Actuators		
	Type	Hydraulic
	Stroke	1.15 m
	Max. Vel	1 m/s
	Max. Acc	13 m/s^2

Figure F.5: The SIMONA Research Simulator (SRS) at Delft University of Technology [17].

F.4 Other applications

F.4.1 AMiBA - Astronomical Telescope Mount

The Array for Microwave Background Anisotropy (AMiBA) is located at the Mauna Loa weather station at an elevation of 3400 meters on Big Island, Hawaii. It targets specifically the distribution of high - redshift clusters of galaxies via the Sunyaev - Zel'dovich effect and the anisotropies in the cosmic microwave background. The design of the AMiBA mount was driven by the requirement of having a lightweight structure which can easily and quickly be dismantled and shipped to another site for a possible later relocation. The telescope is designed to meet the harsh environmental weather conditions on Mauna Loa, allowing to operate with wind speed of up to 30 ms^{-1} and operating temperature range of $-10°C$ to $30°C$.

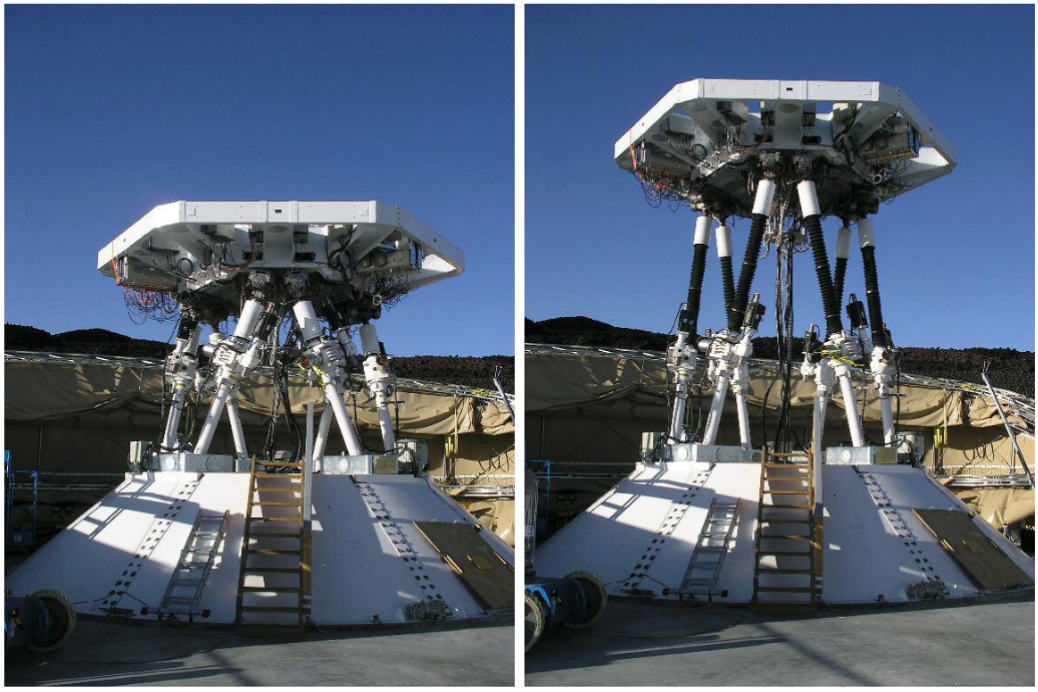

Figure F.6: Left Panel: AMiBA in stow position with fully retracted jack screws. Right Panel: AMiBA in neutral position with extended jacks to start the observation [14].

F.4.2 TREPA - Climbing robot

TREPA was developed at Miguel Hermandez University. This robot uses the six-degree-of-freedom Gough-Stewart platform. Six linear actuators are connected to a platform at their ends through universal joints. The robot is mounted around the tree and the tree trunk occupies the cylindrical void in the middle of the robot. The rings attached to the top and bottom of the robot allows to grip the tree trunk with actuated grippers that applies pressure. TREPA climbs the tree by executing four steps. First, the bottom ring grips the tree and the actuators contracted, the top ring releases its grip. With full extended actuators, the top ring gets its new position. Next, the top ring applies pressure on its grippers and grabs the tree. Once the top ring guaranties the grip, bottom ring is ready to release its grip. Finally, the actuators starts to contract the lower ring to a higher position where, afterwards, engages the tree. This process is repeated continuously.

Figure F.7: TREPA Robot for climbing a tree trunk [19].

F.4.3 Surgical Robot - Computer Aided Surgery

The Fraunhofer-Institut für Produktionstechnik und Automatisierung (IPA), Stuttgart, Germany, has realized the first functional surgical robot prototype. Its name is PI M-850 Hexapod, see Figure F.8, for micro-surgical procedures and feasibility of micro-therapy. This micro-positioning system is a hexapod, a six degree-of-freedom parallel kinematics manipulator that provides high stiffness, load capacity and accuracy than its equivalent "stacked" multi-axis positioners. This hexapod allows sub-micron precision even with high loads and serves as modular platform for different instruments, such as endoscopes, is controlled by a cockpit similar to a flight simulator. This same cockpit also enhances the surgeon's spatial understanding of the operation site, the endoscope's position and speed. This is considered a novel system and the first step for future ergonomic operating.

Figure F.8: Hexapod Surgical Robot with Endoscope and Phantom - PI M-850 Hexapod [35].

Appendix G

Other Examples of SPIF Parts

Figure G.1: A horse decal in a 1 millimeter thick aluminum sheet.

Figure G.2: Batman symbol in a 1 millimeter thick aluminum sheet.

Figure G.3: Human Face in a 1 millimeter thick aluminum sheet (Material rupture occurred - could not be finished).

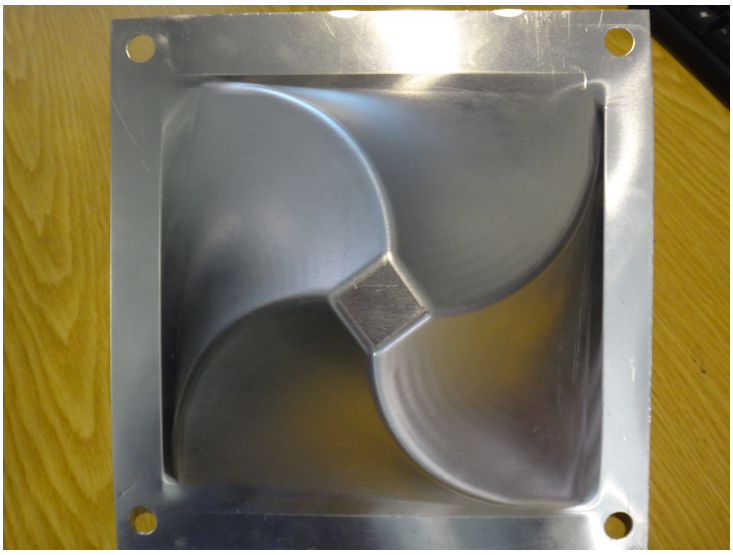

Figure G.4: 45° twisted pyramid in a 1 millimeter thick aluminum sheet.

Figure G.5: Truncated cone in a 1 millimeter thick aluminum sheet.

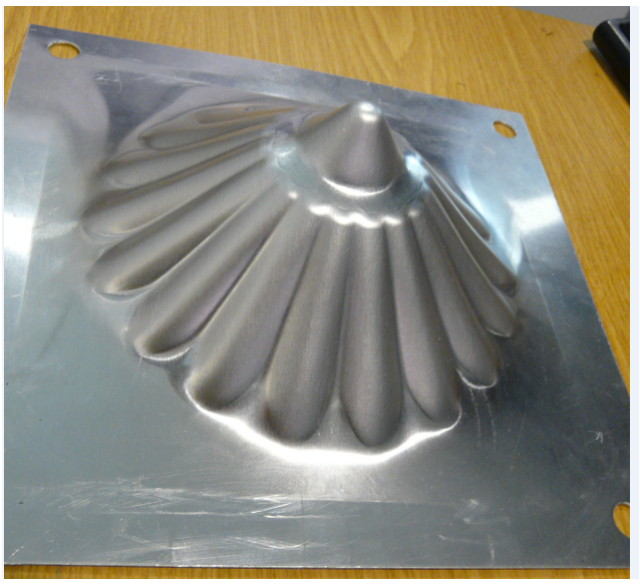

Figure G.6: Another example in a 1 millimeter thick aluminum sheet.